

Point-by-point response to review comments on manuscript acp-2017-582 “Quantifying black carbon light absorption enhancement by a novel statistical approach”

By Cheng Wu et al.

We thank the two anonymous reviewers for their constructive comments to improve the manuscript. Our point-by-point responses to the review comments are listed below. Changes to the manuscript are marked in blue in the revised manuscript. The marked manuscript is submitted together with this response document.

Anonymous Referee #1

R1-Q1. This paper proposed a new approach to characterize the light absorption enhancement of BC and reported its application to the observed results based on an aethalometer and a thermo-optical carbon analyzer in Pearl River Delta area. This manuscript includes sufficient originality, and the topic seems to fit the journal. However, there are several concerns on the accuracy of the light absorption measurements, definition of E_{abs} , and discussions on the observed optical properties. I believe that the points below should be addressed before considering the publication in ACP.

Author’s Response: Thanks for the very insightful and detailed comments. Please see below for point-by-point response to reviewers’ comments.

General comments

R1-Q2. 1) Accuracy of the aethalometer measurements. Although the authors used the correction scheme reported by Weingartner et al. (2003) to correct the artifacts due to aerosol loading, filter matrix and scattering effect, it is not clear that the light absorption for “coated-BC” can be accurately measured (or corrected), especially under “high RH” conditions. For example, Arnott et al (2003) reported that a filter-based photometer has large potential artifacts above 80% RH. The authors need to give more detailed information on accuracy of aethalometer measurements.

Author’s Response: We add the following content in section 2.1 to elaborate the factors that can affect the accuracy of Aethalometer in details.

Besides these artifacts, RH is also a source of σ_{abs} measurement uncertainty. Elevated RH is not only a driving force of increased σ_{abs} due to the hygroscopic growth of particles, but also a factor affecting ambient σ_{abs} measurements. Previous studies found σ_{abs} by PAS exhibit a systematic decrease when $RH > 70\%$ (Arnott et al., 2003; Kozlov et al., 2011). Water evaporation was found as the major cause for the biased PAS σ_{abs} measurements under high RH (Raspet et al., 2003; Lewis et al., 2009; Langridge et al., 2013). Filter-based measurements are also affected under high RH conditions. For example, Arnott et al. (2003) observed erratic responses by particle soot absorption photometer (PSAP) as RH changed. The main reason is traced to the hydrophilic cellulose membrane, which serves to reinforce the quartz filter used in PSAP. The fibers can swell and shrink as RH changes, causing unwanted light attenuation signal. The PTFE-coated glass-fiber tape has become available since 2012 for the recent model of Aethalometer to minimize the RH interference (Magee-Scientific, 2017). A study by Schmid et al. (2006) reported dependency of PSAP σ_{abs} on RH, but found negligible effect of RH on Aethalometer performance. It is also worth noting that RH in the Aethalometer optical chamber may be lower than the ambient RH due to the

slightly elevated temperature inside the instrument. The magnitude of RH difference was found similar between different instruments: 20% for the Aethalometer (Schmid et al., 2006) and 15% for the nephelometer (Guyon et al., 2004). The RH in the Aethalometer optical chamber was not measured in this study. We expected its level to be slightly lower than the ambient RH. Cappa et al. (2008) found σ_{abs} measurements by PSAP and PAS maintained a high linearity even under high RH conditions (65-91%). Inter-comparison studies demonstrated that with proper corrections, Aethalometer σ_{abs} measurements agree well with those by PAS (Ajtai et al., 2011). During the inter-comparison study of an Aethalometer (AE-16) and a PAS in Guangzhou (Wu et al., 2009), good correlation was found ($R^2=0.96$) as shown in Figure S1. These comparison results imply that the Aethalometer results are linearly correlated with PAS measurements and RH has a limited interference on Aethalometer measurements.

The Aethalometer measurements correlated well with the PAS results during a field campaign in Guangzhou as evidenced by the high R^2 (0.96) shown in Figure R-1. The ambient RH during the comparison period ranged from 20% to 95%. Since the PAS inlet was equipped with a dryer while Aethalometer was sampling without a dryer, the high R^2 proved that RH did not affect the correlation between Aethalometer and PAS. The results proved that Aethalometer can achieve comparable precision of PAS for hourly resolution data. We add tests in section 4.1 to evaluate the robustness of MRS against systematic biases. The results show that MRS is insensitive to systematic biases and details can be found in the response to R2-Q5.

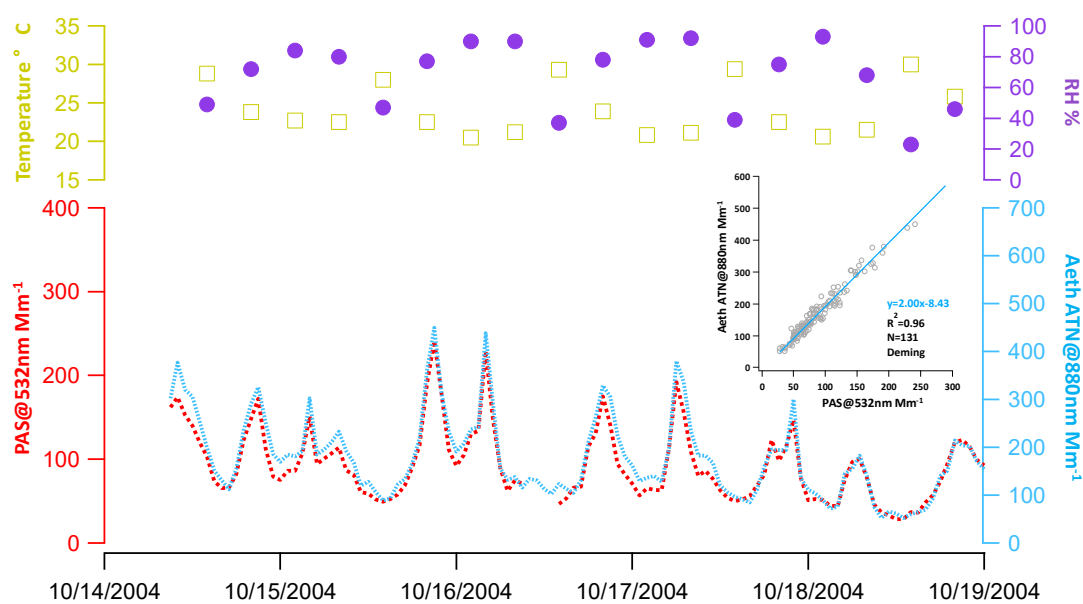


Figure R-1. Comparison of collocated Aethalometer and PAS at Guangzhou (Oct 2004). Both PAS and Aethalometer (AE-16) were equipped with $PM_{2.5}$ inlets. RH of the sampled air was controlled to be <45% for PAS. Aethalometer sampling was conducted without RH control.

R1-Q3. 2) Definitions of the MAE_p and E_{abs} The MAE_p obtained by the method in this study is MAE value for primary emission source. I think that the MAE_p , which was obtained in this study, includes the effects of “lensing effect” due to co-emitted OC. Therefore, the definition of E_{abs} values should be

different with the E_{abs} in the previous studies, at least, using TD technique. Detailed explanation on this point should be added.

Author's Response: Thanks for raising this point, which we did not make it clear in our manuscript. Yes, we agree with the reviewer that the nature of $\text{MAE}_{\text{p,TD}}$ is different from MAE_{p} at emission source. The following contents are added to clarify this point.

In introduction:

It's also worth noting that MAE_{p} by the TD approach is different from the MAE_{p} at the emission source. First, the morphology of thermally denuded BC particles (compact aggregates) is different from that of freshly emitted BC particles (chain-like aggregates). Second, most of the coatings is removed with the TD denuded soot particles, but freshly emitted soot particles usually come with a thin coating of OC formed from condensation of OC vapors as the temperature drops from engine to the ambient air. As a result, the MAE_{p} by TD approach is expected to be lower than the MAE_{p} of emission source. In this sense, the TD approach may not be a perfect "time machine" to reverse the aging process for E_{abs} determination.

In section 4.1:

As mentioned in section 1, the definition of MAE_{p} by the TD approach is different from the MAE_{p} of emission source. The TD MAE_{p} is expected to be slightly lower than the MAE_{p} of emission source. Therefore, the corresponding E_{abs} are slightly different and it should be cautioned when comparing MRS-derived E_{abs} with E_{abs} by the TD approach and Mie simulations.

R1-Q4. 3) The effect of biomass burning

3-1) Lines 371-374: "During the rainy season when oceanic prevailing wind dominates, BC from BB emission in Southeast Asia can reach PRD through long range transport (LRT), resulting in an elevated K^+/EC ratio and MAE_{550} , which might be a combination of a thicker coating when freshly emitted from BB sources and enhanced coating during LRT."

=> If so, I think the MAE_{p} values should be higher in summer (rainy season). Please consider about this point.

Author's Response: BB is one aerosol source affecting $\text{MAE}_{\text{p},550}$ but not the dominating source. As shown in Figure 8 in the revised manuscript, the data points are scattered and the R^2 (0.33) is relatively low. The intercept in Figure 8 represents the part of MAE that are not explained by K^+/EC ratio. To further clarify this point, we calculate K^+/EC ratio and MAE_{550} - K^+/EC regression intercept of each month, then we compare the correlation of $\text{MAE}_{\text{p},550}$ vs. K^+/EC ratio and $\text{MAE}_{\text{p},550}$ vs. K^+/EC intercept. As shown in Figure R-2, $\text{MAE}_{\text{p},550}$ has higher correlation with K^+/EC intercept ($R^2=0.58$) than with K^+/EC ratio ($R^2=0.23$). These results imply that BB is one of the contributors to the $\text{MAE}_{\text{p},550}$ variations, but unlikely to be the dominating one. As a result, in some summer months, the $\text{MAE}_{\text{p},550}$ is higher than the winter months but some months are not. Other BC sources and BB combustion conditions may affect the overall $\text{MAE}_{\text{p},550}$. The relevant content is revised as follow:

During the rainy season when oceanic wind prevails, BC from BB emission in Southeast Asia can reach PRD through long range transport (LRT), resulting in an elevated K^+/EC ratio and MAE_{550} . The Deming regression intercept (11.89) in Figure 8 represents the MAE without the BB effect. This non-BB MAE_{550} ($11.89 \text{ m}^2 \text{ g}^{-1}$) is only slightly lower than $\text{MAE}_{\text{p},550}$ ($13 \text{ m}^2 \text{ g}^{-1}$) obtained in section 4.3, implying that a large fraction of

MAE_{p,550} could not be explained by the BB source. Additional evidence was obtained through examining regression relationships of MAE_{p,550} with K⁺/EC month-by-month (Figure S17b). Correlation of monthly MAE_{p,550} vs. K⁺/EC ratio yield a R² of 0.23 (Figure S17c). In contrast, a much higher correlation (R²=0.58) was observed (Figure S17d) between MAE_{p,550} and non-BB MAE₅₅₀ (i.e., K⁺/EC intercepts from Figure S17b). These results imply that BB is one of the contributors to the MAE_{p,550} variations, but unlikely to be the dominating one.

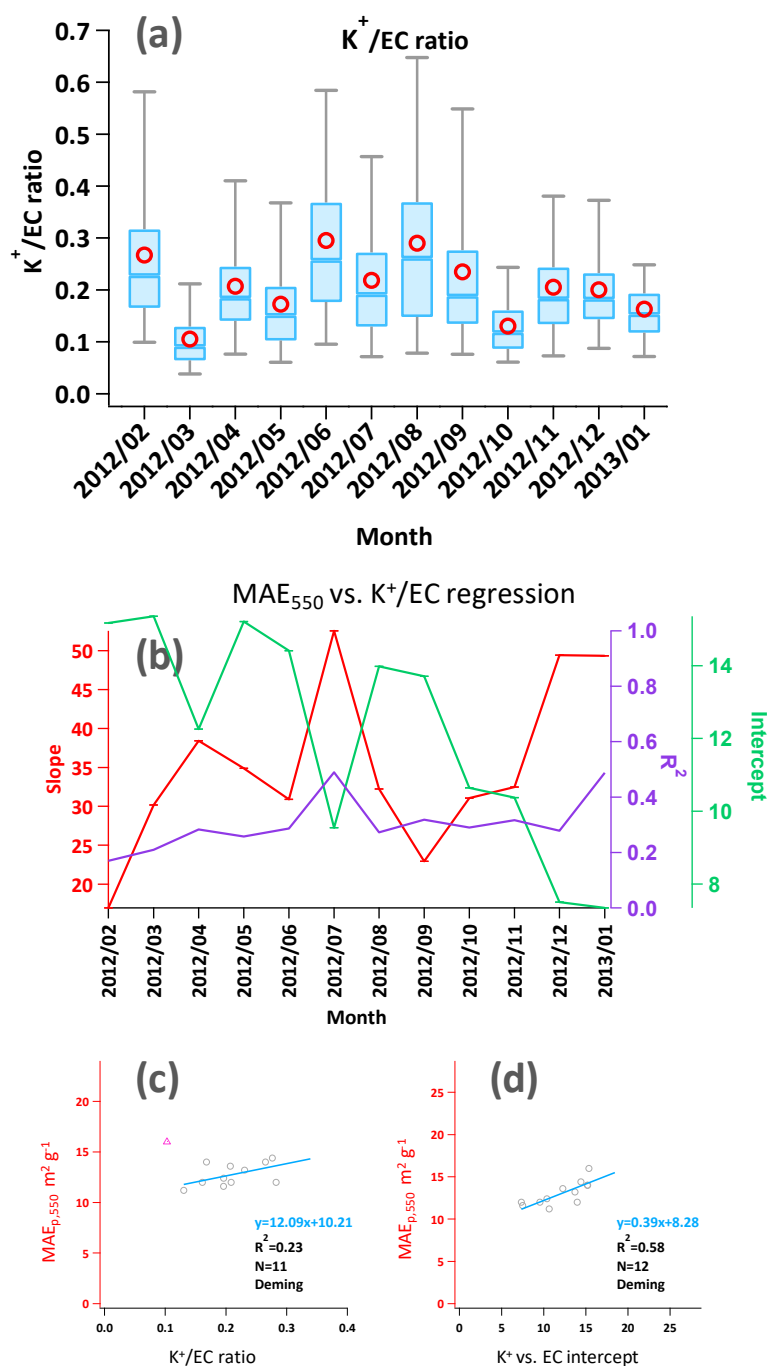


Figure R-2. (a) Monthly variations of K⁺/EC ratio from 2012 Feb to 2013 Jan at NC site. (b) Monthly regressions between MAE₅₅₀ and K⁺/EC with slope in red, intercept in green and R² in purple. (c) regressions between monthly MAE_{p,550} and K⁺/EC. (d) regression between monthly MAE_{p,550} and intercepts from (b).

R1-Q5. 3-2) Lines 384-388: “Since the monthly average AAE in wintertime didn’t exceed 1.2 (Table S3), the variations of AAE in the PRD are likely more associated with thicker coatings rather than the contribution of BrC. The results also imply that attempts on BrC absorption attribution for the PRD dataset presented in this study could be risky, considering that elevation of AAE is actually dominated by coating (Lack and Langridge, 2013).”

=> Because higher E_{abs} values were observe in summer, the coating would be thicker in summer. The suggestion that “the higher AAE in winter are likely more associated with thicker coatings” is not reasonable. Please consider about this point.

Author’s Response: The point we intend to make here is that since the seasonal variations of $AAE_{470-660}$ is small, such variations are likely induced by the coating effect as shown in the Mie simulation rather than the presence of BrC. The corresponding text is rephrased as below to improve the clarity.

Since the monthly average $AAE_{470-660}$ in wintertime did not exceed 1.2 (Table S3), the variations of $AAE_{470-660}$ in the PRD are more likely associated with coatings rather than the contribution of BrC.

R1-Q6. 4) The effect of relative humidity (RH) on optical properties As mentioned above, the authors need to show some evidences suggesting that the obtained positive correlation between $f(RH)$ (i.e., MAE) and RH is not due to the artifact of RH on aethalometer measurements. If the measurements are assumed to be accurate, the observed higher E_{abs} (and MAE) and lower AAE values in summer may be explained only by RH, considering that the RH may be higher in summer and RH for air masses from Southeast Asia. Which one of higher OC/EC ratio and higher RH do you suggest as a main contributor for observed higher E_{abs} in summer?

Author’s Response: The study by Schmid et al. (2006) found PSAP σ_{abs} shows dependency on RH, but the effect of RH on Aethalometer performance is neglectable. See our response to R1-Q2 for more detailed discussion on RH effect.

The contribution of elevated OC/EC ratio to the increase of E_{abs} might not be as important as RH in the summer time. First, the OC/EC ratios in summer is only slightly higher than other seasons (Figure R-3a). Second, as shown by the $f(OC/EC)_{MAE}$ plot (Figure R-3b), OC/EC induced MAE enhancement only occurred when $OC/EC > 4$, which corresponded to the data with the highest 20% OC/EC ratio. As a result, the OC/EC induced MAE enhancement was only important for episodes of high OC/EC hours, which have a limited temporal coverage.

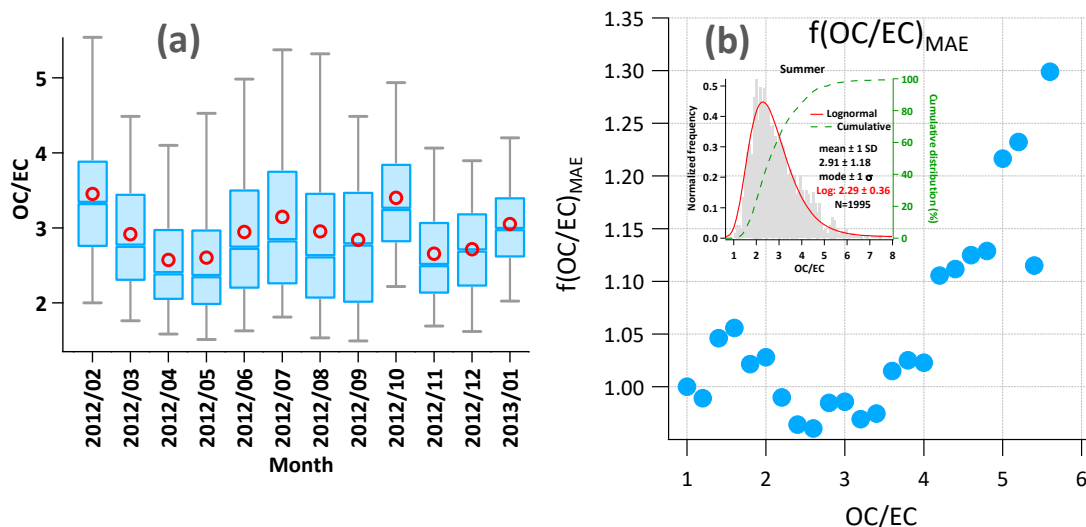


Figure R-3. (a) Monthly variations of OC/EC (b) MAE₅₅₀ enhancement as a function of OC/EC.

Specific comments

R1-Q7. 1) Line 235-236 “Thus, a BrC coating (brown shell) scenario is also considered in Mie simulation following the wavelength dependent RI suggested by Lack and Cappa (2010).” => Because the results of Mie simulation should be varied depending on the RI values given here, I recommend adding the range of RI values.

Author’s Response: Suggestion taken. The corresponding content is revised as follows:

Thus, a BrC coating (brown shell) scenario is also considered in Mie simulation following the wavelength-dependent RI suggested by Lack and Cappa (2010), which ranges from $1.55-0.059i$ (370 nm) to $1.55-0.0005i$ (950 nm).

R1-Q8. 2) Section 3.2.4, 1st paragraph. For the brown shell scenario, I think that both of lensing effect and light absorption by BrC contribute to the E_{abs} values. I recommend adding the fraction of each contribution.

Author’s Response: We agree with the reviewer on this point. Fractional contribution from BrC is discussed as shown below. The following figure is added in SI (Figure S7).

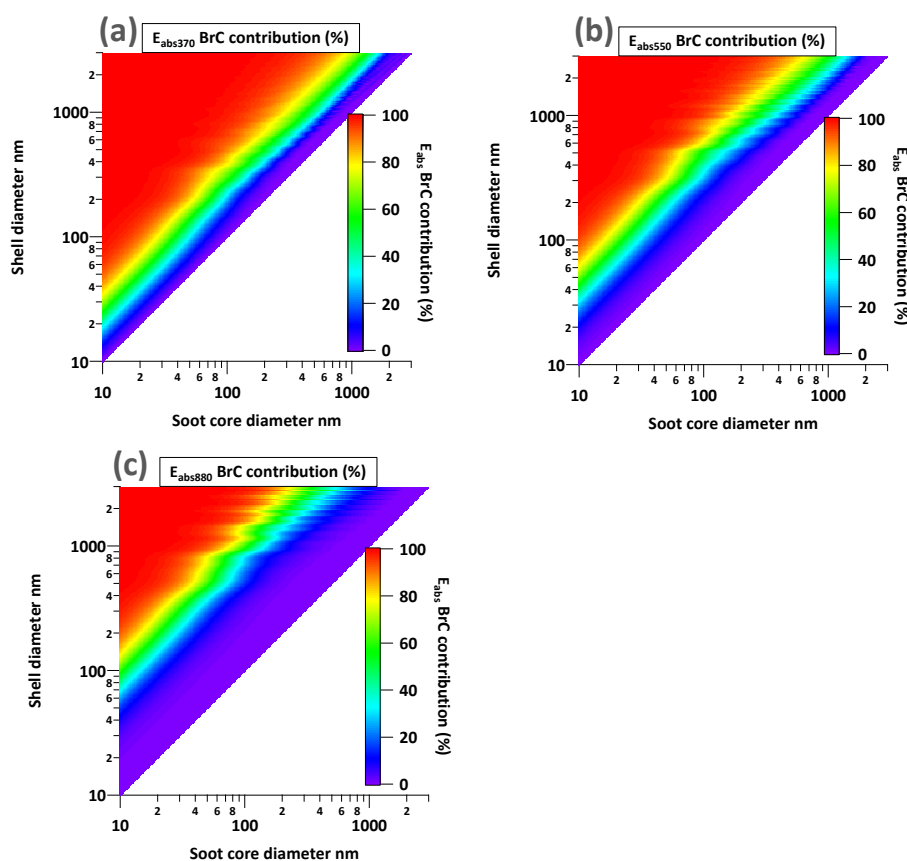


Figure R-4. Mie simulated BrC absorption contribution to total E_{abs} (lensing effect + BrC absorption) in the brown shell scenario. (a) 370 nm (b) 550 nm (c) 880 nm.

The following text is added in the revised manuscript (section 3.2.4):

The main reason behind is that in the brown shell scenario, both lensing effect and BrC absorption contribute to E_{abs} . As shown in Figure S7, the BrC absorption contribution to total E_{abs} strongly depends on coating thickness and is insensitive to soot core diameters. When the coating is relatively thin (<5 nm for $\lambda@370$ nm, <15 nm for $\lambda@550$ nm and

<40 nm for $\lambda@880$ nm), BrC absorption contribution to the total E_{abs} is less than 20%. As the coating increases to a certain level (~15 nm for $\lambda@370$ nm, ~35 nm for $\lambda@550$ nm and ~90 nm for $\lambda@880$ nm), BrC absorption contribution is comparable to the lensing effect contribution, each contributing ~50% to the total E_{abs} . When the BrC coating is sufficiently thick (>30 nm for $\lambda@370$ nm, >90 nm for $\lambda@550$ nm and >110 nm for $\lambda@880$ nm), BrC absorption dominates the E_{abs} contribution. As a result, if BrC coating is indeed present in ambient samples, a strong wavelength dependent E_{abs} could be observed, since a BrC coating of 30 nm would be enough to induce a large amount of detectable E_{abs} in the UV range.

R1-Q9. 3) Section 4.1, 2nd paragraph The annual average MAE_p value ($13 \text{ m}^2/\text{g}$) is larger than those estimated for bare BC. It may indicate that the obtained MAE_p values include the effects of “lensing effect” due to co-emitted OC, as mentioned above. If so, caution on the definition of MAE_p in each study should be taken during comparison with other studies. Also, it is better to add information on the wavelength used in each study.

Author’s Response: The authors fully agree with the reviewer that the difference in MAE_p definition should be emphasized. Following contents are added in section 4.1 to clarify this point.

MAE_p by MRS represents the MAE_p at the emission source, which is different from the MAE_p by the TD approach for two reasons. First, the morphology of thermally denuded BC particles (compact aggregates) is different from that of freshly emitted BC particles (chain-like aggregates). Second, most of the coatings are removed for TD denuded soot particles, but freshly emitted soot particles usually come with a thin coating of OC formed from condensation of OC vapors as the temperature drops from the flame to the ambient air. As a result, the MRS-derived MAE_p is expected to be higher than the MAE_p by the TD approach.

The MAE mentioned from literature was scaled to 550 nm for comparison. The following text is added to improve the clarity.

For comparison purpose, MAE measured at original wavelength and MAE scaled to 550 nm following the λ^{-1} assumption are both shown in Table S1. The MAE comparisons discussed below are MAE at 550 nm.

R1-Q10. 4) Section 4.5 How did the absorption coefficients for dry conditions determine to obtained $f(\text{RH})$?

Author’s Response: The sampled air into the Aethalometer was not dried in this study. As the sampling covered a whole year, the RH also spanned a range sufficiently large to study the RH effect. The MAE data obtained at $\text{RH}=30\%$ (as shown in Figure 9a of the revised manuscript, the starting point of the $f(\text{RH})$ curve) are used as the dry condition to calculate $f(\text{RH})$.

R1-Q11. 5) Figure 9 What do you want to suggest from 30:1 line in Fig. 9?

Author’s Response: The 30:1 line is to serve as a reference line with an integer slope that is close to the regressed slope through the origin.

References

Arnott, W. P., Moosmuller, H., Sheridan, P. J., Ogren, J. A., Rasp, R., Slaton, W. V. 2003. Photoacoustic and Filter-Based Ambient Aerosol Light Absorption Measurements: Instrument Comparisons and the Role of Relative Humidity. *J. Geophys. Res.-Atmos.*, 108: 4034–4045.

Point-by-point response to review comments on manuscript acp-2017-582 “Quantifying black carbon light absorption enhancement by a novel statistical approach”

By Cheng Wu et al.

We thank the two anonymous reviewers for their constructive comments to improve the manuscript. Our point-by-point responses to the review comments are listed below. Changes to the manuscript are marked in blue in the revised manuscript. The marked manuscript is submitted together with this response document.

Anonymous Referee #2

R2-Q1. The manuscript presents a statistical analysis of black carbon light absorption enhancement based on observations made over roughly one year using a filter-based absorption instrument and a thermal-optical analysis OC/EC analyzer. They derive the absorption enhancement (E_{abs}) from the total mass absorption efficiency measured from the ratio of the absorption and EC measurements to that estimated for bare BC particles. To determine the bare BC MAE the authors employ a method that searches for an MAE value based on an assumed independence between EC and absorption due to BC coatings. While this approach presents a potential alternative to more expensive and labor-intensive methods to examine the important topic of BC light absorption enhancement, it is not clear to me that it works based on the information presented in the manuscript. First, while it does compare E_{abs} derived using this method to previously reported values using other techniques, there is not a direct comparison between the results obtained using this technique and more established methods for the same site. As pointed out by Liu et al. (2015), the “influence of coatings on BC absorption may be source and regionally specific”, so it is difficult to draw too much confidence in the approach based on similarities with other locations. Second, it is not obvious that the measurement of EC is independent of the amount of light absorbed by BC coatings. While it is true that the mass of primary BC should be independent of coating absorption, EC is an operationally defined quantity, and depending on how coatings interact with its measurement during thermal optical analysis, could in fact have a relationship with coatings and light absorption due to coatings. For these two principle reasons I do not recommend the manuscripts publication in ACP in its current form.

Author’s Response:

- (1) A comparison would definitely be helpful for the verification of the MRS approach in the future. However, as the reviewer has pointed out, TD approach may not be a perfect “time machine” to reverse the aging process for E_{abs} determination. The definition of MAE_p by MRS is different from the MAE_p by TD. MAE_p by MRS reflect the MAE of soot particles at the emission source, while MAE_p by TD reflect the MAE of bare soot particles. First, the morphology of thermally denuded soot particles (collapsed globules) is different from the morphology of freshly emitted BC particles (fractal-like aggregates). Second, most of the coatings are removed for TD denuded soot particles, but freshly emitted soot particles usually come with a thin coating due to the temperature drop from engine to the ambient air. As a result, the MAE_p by TD approach is expected to be lower than the MAE_p of emission source retrieved by MRS. In this sense, it may be difficult to extract quantitative information through such comparisons due to the difference in MAE_p definition.
- (2) We agree with the reviewer that coating can affect EC determination by the thermal-optical analysis. Lee et al. (2007) used artificially fabricated EC samples with OC coatings to evaluate the performance of OC/EC analysis. Biases were observed but the results are linearly correlated ($R^2 > 0.9$) with the true OC and EC values. As shown in Figure R-5 and discussions in the following response to R2-Q5, the E_{abs} estimation by MRS is insensitive to systematic biases. The MRS approach mainly rely on correlation analysis, the systematic biases are not a big concern as long as the measured data correlated well with the true values.

Please see below for point-by-point response to reviewers’ comments.

General Comments

R2-Q2. RH impacts

The manuscript does not clearly state whether air was dried prior to sampling with the instruments. Section 4.5, which discusses impacts of RH on the observations, implies that it was not. The methods section states that 2.5 μm cyclones were used upstream of the Aethalometer and Sunset instruments, but does not specify a size cut for the nephelometer or MARGA instruments. If the nephelometer and MARGA instruments did not have a size cut, it is extremely difficult to compare results from those instruments to those from the AE-31 and Sunset due to potential differences from coarse mode particle contributions.

Author's Response:

Both nephelometer and MARGA are equipped with a $\text{PM}_{2.5}$ inlet to remove the coarse particles. The following text is added in section 2 to improve the clarity.

Both instruments are equipped with a $\text{PM}_{2.5}$ inlet to remove the coarse particles.

R2-Q3. If the air was not dried prior to sampling more details need to be provided regarding the effective RH for the optical instruments (AE-31 and nephelometer), which may be different from ambient RH due to temperature differences between the ambient air and the instruments. In addition, if air was sampled at near ambient RH it could have a number of complicating factors on the subsequent analysis. Filter-based absorption instruments, as the authors acknowledge, are affected by artifacts, including the scattering and shadowing of light in the filter matrix by filter fibers and particles embedded on the filter. Varying sample RH can change the filter artifacts in difficult to account for ways. For example, if hygroscopic particles are present on the filter they can swell or shrink depending on the sample RH, changing the light transmission properties of the filter, artifacts affecting the absorption measurement and possibly the absorption measurement itself depending on how RH interacts with the correction methods applied. The manuscript should include a discussion of how well the correction methods applied can account for changes arising from changes in RH. In addition, the effective size cut of the cyclone will be affected by RH in that the aerosol sampled will be different depending on how much water is associated with it. This effect may be small depending on the aerosol distribution and makeup of the light-absorbing particles, but should be addressed.

Author's Response: Thanks for the very insightful comments. We fully agree that RH could be a source of uncertainty for filter based σ_{abs} measurement. Arnott et al. (2003) found particulate soot absorption photometer (PSAP) showed erratic response as RH change. Schmid et al. (2006) observed dependency of PSAP σ_{abs} on RH, but the effect of RH on Aethalometer performance is negligible. Inter-comparison studies shown that with proper corrections, Aethalometer σ_{abs} agrees well with PAS (Ajtai et al., 2011). During the inter-comparison study of Aethalometer (AE-16) and PAS in Guangzhou (Wu et al., 2009), a good correlation was found ($R^2=0.96$) as shown in Figure R1 or Figure S1. These filed comparison results imply that Aethalometer results are linearly correlated with PAS and RH has limited effect on Aethalometer measurements. Please refer to our response to R1-Q2 for the revisions made in the manuscript.

R2-Q4. Another potential issue related to RH affects some of the results presented in Section 4.5. First, it is not clear if the RH reported is ambient RH or instrument RH. If ambient RH, it needs to be established that the RH at the location of the measurement (the filter) is also at the same RH as the ambient. In addition, it is not clear that the absorption measured on the AE-31 filter represents the absorption in the ambient air. For example, if BC becomes coated on the filter (which can happen in the presence of liquid organic aerosol (e.g. Subramanian et al., 2007) it is not clear how water uptake by those organic films might alter the absorption by particles that were not originally coated. Non-BC containing material can also take up water, alter the optical properties of the filter, and change the apparent absorption attributed to BC. Also, since the AE absorption measurement is based on the change in attenuation over time if the hygroscopic properties of particles change with time the apparent

absorption could be affected. For example, consider a situation where BC with a hygroscopic coating has been sampled onto the filter for some period of time. As the sample RH begins to decrease the water will evaporate from the filter, likely leading to a decrease in attenuation (there is a reduced enhancement of absorption, for example). At the same time consider what happens if additional BC is sampled to the filter. This acts to increase attenuation, opposing the RH effect. As a result the BC measured during this time would be underestimated (its effect on attenuation is countered to some degree by the opposing RH effect). Note that the magnitude of these impacts would be difficult to account for, in that they depend on the hygroscopicity of the material on the filter and how that material and associated water interacts in the filter matrix.

Author's Response: The RH used in this study is ambient RH. We agree with the reviewer that RH at the filter of Aethalometer is different from the ambient RH. The RH in the optical chamber of Aethalometer may be lower than the ambient RH due to the slightly elevated temperature inside the instrument. The magnitude of RH difference is similar between different instruments: 20% for the Aethalometer (Schmid et al., 2006) and 15% for the nephelometer (Guyon et al., 2004). Although the RH in the Aethalometer optical chamber was not measured in this study, its level was expected to be slightly lower than the ambient RH. Schmid et al. (2006) found PSAP σ_{abs} showed dependency on RH, but the effect of RH on Aethalometer performance was negligible. Cappa et al. (2008) found σ_{abs} by PSAP maintained high linearity with PAS even under high RH conditions (65-91%). Inter-comparison studies shown that with appropriated corrections, Aethalometer σ_{abs} agrees well with PAS (Ajtai et al., 2011). During the inter-comparison study of Aethalometer (AE-16) and PAS in Guangzhou (Wu et al., 2009), good correlation was found ($R^2=0.96$) as shown in Figure S1. These comparison results imply that Aethalometer results are linearly correlated with PAS and RH has limited interference on Aethalometer measurements.

R2-Q5. Measurement biases and impacts on the analysis Biases in filter-based absorption and OC/EC measurements are mostly associated with other materials mixed and/or co-sampled with BC/EC, so it is likely that errors in the measurements have a systematic relationship. For example, the presence of organic aerosol and organic films has been linked to both biases in filter-based measurements (e.g., Lack et al., 2008) as well as potential impacts on EC measurement via pyrolyzed carbon correction (Subramanian et al., 2007). The manuscript needs a detailed discussion of how correlations in biases between the methods affect the retrieved MAE_p values and resulting E_{abs} calculations. Since the manuscript is seeking to establish a new method this potential issue needs much more attention. Several specific comments below are related to this general concern.

Author's Response: The bead-like particles on filter fibers could interfere both Aethalometer and OC/EC measurements. Since the study by Subramanian et al. (2007) was based on source samples from low temperature BB emissions, how this bead-like particles could affect ambient measurements depends on their fractional contribution to PM_{2.5}. Cappa et al. (2008) found that the light absorption enhancement factor for the PSAP relative to the PAS due to the presence of externally mixed organic aerosols is proportional to the OA-to-soot ratio, which means this bias is systematic. We conduct two tests to investigate the effect of systematic EC and σ_{abs} bias on E_{abs} estimation. As shown in Figure R-5, the MRS approach is insensitive to systematic bias in EC and σ_{abs} measurements. Details of the tests are added in section 4.1 and also shown below.

To investigate the performance of the MRS approach in response to systematic bias in EC and σ_{abs} , two simple tests are conducted as shown in Figures S9 and S10 by adding systematic biases to σ_{abs550} and EC. Test A represents a situation when σ_{abs} is overestimated and EC is underestimated. The biased data are marked as σ'_{abs550} and EC' respectively, as shown below:

$$\sigma'_{abs550} = \sigma_{abs550} \times 2 \quad (8)$$

$$EC' = EC \times 0.7 \quad (9)$$

As a result, the average MAE_{550} changed from 18.75 to 53.58 $m^2 g^{-1}$ and MAE_p changed from 13 to 37 $m^2 g^{-1}$ (Figure S9). However, E_{abs} by ratio of averages remain the same (1.44).

In Test B, EC by different TOA protocols are compared to investigate the effect of different EC determination approaches while σ_{abs550} remains unchanged. EC by IMPROVE TOR protocol is calculated from NIOSH TOT EC following an empirical formula for suburban sites derived from a 3-year OCEC dataset in PRD (Wu et al., 2016):

$$EC_{IMP_TOR} = 2.63 \times EC_{NSH_TOT} + 0.05 \quad (10)$$

As shown in Figure S10, MAE_{550} changed from 18.75 to 7.02 $m^2 g^{-1}$ and MAE_p changed from 13 to 5 $m^2 g^{-1}$, but E_{abs} remain almost the same (1.40). Result of Test B implies that although EC is operationally defined, the discrepancy of EC between TOA protocols did not weaken the role of EC serving as a tracer for primary emissions in MRS application. These examples demonstrate that systematic biases in σ_{abs550} and EC have no effects on E_{abs} estimation by the MRS approach.

Test A

Original data

Systematically biased data

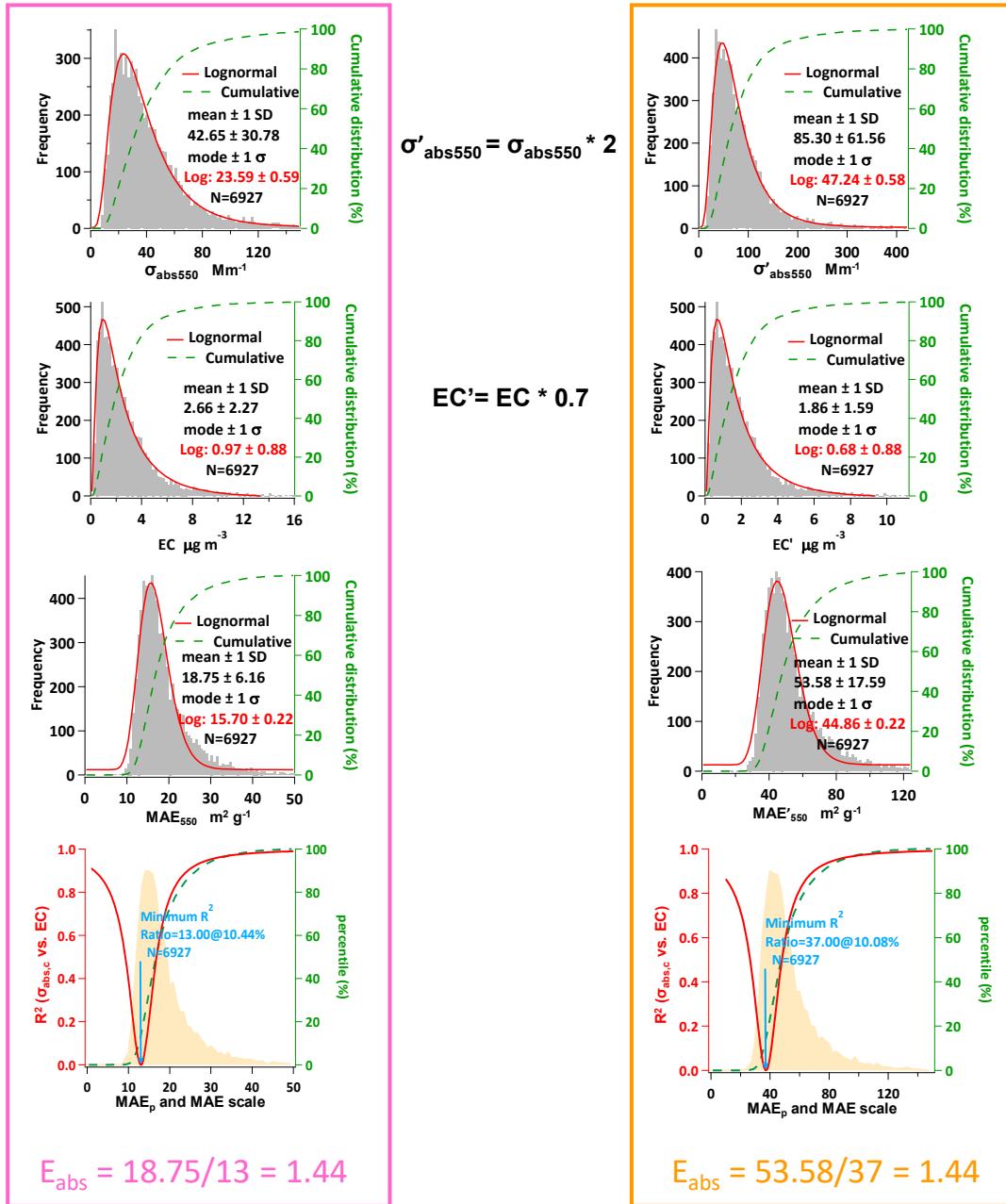


Figure R-5. Comparison of E_{abs} from original data and systematically biased data (Test A).

Specific Comments

R2-Q6. 78-80: Missing from the list of field studies is Cappa et al. (2012), which found a weak enhancement for observations in California, US.

Author's Response: Suggestion taken. Cappa et al. (2012) was added.

R2-Q7. 85: Suggest changing to “The TD approach is briefly discussed here.”

Author's Response: Revision made.

R2-Q8. 90: Some good points are raised in this discussion, but a few things are lacking. First, another major reason for use of PAS systems in the approach is that the technique does not have artifacts associated with filter-based methods for measuring light absorption, thus it provides an unambiguous measure of the light absorption coefficient in both heated and un-heated states. Also missing from the discussion is potential differences in BC core morphology being different for “fresh” versus “aged with coating removed” conditions, or in other words, the TD may not be a perfect “time machine” to reverse the aging process and determine the effects of BC aging.

Author's Response: Thanks for the suggestions. The following content is added in the main text.

As an in-situ technique, PAS eliminates the artifacts associated with filter-based methods (Weingartner et al., 2003; Coen et al., 2010) and is often considered as the reference instrument for light absorption coefficient determination (Arnott et al., 2003; Arnott et al., 2005).

It's also worth noting that MAE_p by the TD approach is different from the MAE_p at the emission source. First, the morphology of thermally denuded BC particles (compact aggregates) is different from that of freshly emitted BC particles (chain-like aggregates). Second, most of the coatings is removed with the TD denuded soot particles, but freshly emitted soot particles usually come with a thin coating of OC formed from condensation of OC vapors as the temperature drops from engine to the ambient air. As a result, the MAE_p by TD approach is expected to be lower than the MAE_p of emission source. In this sense, the TD approach may not be a perfect “time machine” to reverse the aging process for E_{abs} determination.

R2-Q9. 100-101: I realize this is not the focus of the manuscript, but it is worth noting here the logic presented here assumes a linear relationship between MAE and coated soot particle number fraction measured by SP2. This may not be the case due to limitations in the size of BC particles measured by the SP2, its ability to measure thin coatings, the potential impact of thin coatings on MA, the assumption of core-shell morphology, and the nature of the relationship between the fraction of coated particles (a parameter which ignores coating thickness, the physical driver of the absorption enhancement) and MAE.

Author's Response: The following text is added in the main text for clarification.

It is worth noting that this approach provides only a rough approximation of E_{abs} since the parameter used here (coated soot particles number fraction) ignores other main drivers of light absorption enhancement (e.g. coating thickness). As a result, this approach is only valid for a period of measurements, for which coating thickness is

relatively constant and the MAE variations are dominated by coated soot particles number fraction.

R2-Q10. 133: What does the 5% uncertainty refer to? Is this before or after corrections? Are the uncertainties in the corrections as low as 5%? Also, the manuscript gives an uncertainty of 24% for the ECOC analyzer here, but then later states (line 153) up to a factor of 5 differences in EC measured by different protocols are possible. How is this to be reconciled?

Author's Response: The 5% measurement uncertainty refers to instrument precision. An uncertainty of 24% for the ECOC analyzer is the instrument precision when NIOSH protocol is applied for TOA. The 5 times differences in EC measured by different protocols arises from inter-protocol discrepancy. It's a concept different from the instrument precision. To avoid confusion, we change the term "measurement uncertainty" to "measurement precision" throughout the manuscript.

R2-Q11. 166-169: The argument given here is only true if the errors in absorption measurement and EC mass measurement are independent and random. If some factor causes a positive bias in the filter-based absorption but a negative bias in the EC measurement they will not cancel, but instead there will be an apparent and potentially false apparent absorption enhancement. Or consider a situation where some co-sampled material affects the OC/EC split but not the filter-based absorption measurement, leading to an apparent change in E_{abs} .

Author's Response: We conduct two tests to investigate the effect of systematic EC and σ_{abs} bias on E_{abs} estimation. As shown in Figure R-5 and discussions in the response to R2-Q5, the MRS approach is insensitive to systematic bias in EC and σ_{abs} measurements.

Following contents are added in the manuscript.

In section 2.1

Systematic bias in MAE (e.g. overestimation of σ_{abs} and variability of EC mass by different TOA protocols) discussed above have little effect on E_{abs} estimation by MRS. As shown in Eq. 3, E_{abs} is the ratio of MAE_t to MAE_p or $\sigma_{abs,t}$ to $\sigma_{abs,p}$, thus most of the bias in EC mass or σ_{abs} is cancelled out during the E_{abs} calculation. More details are discussed in section 4.1.

Please refer to our response to R2-Q5 for contents added in section 4.1.

R2-Q12. 187-188: Since EC is an operationally defined parameter based on a measurement technique there is not necessarily an inherent interdependency between it and the absorption due to coatings gained following emission.

Author's Response: It is true that EC is operationally defined. But studies have shown that EC by different protocols correlate very well (Chow et al., 2001; Chow et al., 2004; Wu et al., 2012; Wu et al., 2016). The discrepancy of EC between thermal-optical analysis protocols did not weaken the role of EC to serve as a tracer for primary emission in MRS application, as shown in the Test B in the response to R2-Q5. On the other hand, extra absorption due to coating is associate with secondary process after emission. The variations of primary emission are relatively independent to the variations of secondary process.

R2-Q13. Section 3.2: The results from the Mie simulations are not a new contribution and main points drawn from the discussion could be drawn from previous studies given in the literature (e.g., Lack and Cappa, 2010; Bond et al., 2006).

Author's Response: The main purpose of including Mie simulations in this study is to help readers to understand the viability of E_{abs} and AAE from a theoretical perspective and their dependence on different core/shell diameter combinations. Citing main points from literature is one way but that could be distracting. From a reader point of view, digging the detail information from the literature might not be as convenient as reading the Mie simulations in this study. In addition, Mie simulation figures shown here are specifically plotted to support the later discussion of the measurement results. We feel that the inclusion of Mie simulations provides a smooth one-stop reading experience.

R2-Q14. 260: Should note here that the AAE observed in measurement studies also includes absorption by potentially externally mixed brown carbon particles, not just those present in the form of shells on BC particles.

Author's Response: Suggestion taken. The corresponding content has been revised as follows.

These high AAE results are consistent with the previous model study (Lack and Cappa, 2010) and could partially explain the high AAE observed in measurement studies (Kirchstetter et al., 2004; Hoffer et al., 2006), since the presence of externally mixed BrC particles also contribute to the wavelength dependent light absorption.

R2-Q15. 295: Suggest changing “concentrations” to “modes”.

Author's Response: Revision applied.

R2-Q16. 299-302: Minor point here, but the MOUDI data also reflect differences in BC core equivalent diameters measured using LII and aerodynamic diameter of BC, so we would not necessarily expect similar sizing, even for uncoated BC. Worth mentioning here, though I do not disagree with the main argument given here.

Author's Response: Thanks for the clarification. The following content is added to remind readers the difference when comparing the sizing between LII and MOUDI.

BC sizing by LII is based on volume equivalent diameter (VED), while MOUDI is based on aerodynamic diameter. As a result, these two techniques do not necessarily yield similar sizes, even for the bare soot particles. The conversion between these two types of diameters involves the knowledge of particle density and morphology (drag force).

R2-Q17. 303: Please state whether Tan et al. refer to BC only diameter or mixed particle diameter here.

Author's Response: Tan et al. refers to coated BC diameter. The corresponding content has been revised as follows to improve the clarity.

A recent closure study on BC mixing state in the PRD region suggests σ_{abs} is dominated by coated soot particles in the range of 300~400 nm (Tan et al., 2016).

R2-Q18. 314: I am curious as to why the 470 and 660 nm wavelength pairs were used to quantify AAE. Brown carbon tends to show much stronger impact at shorter wavelengths. Could the authors please include the AAE determined for the UV and 880 nm channels also measured by the AE-31?

Author's Response: The 470 and 660 nm wavelength pairs were used to represent AAE in the visible range. $AAE_{370-880}$ (1.13 ± 0.13) is added as shown in Figure S8b, which is slightly higher than $AAE_{470-660}$ (1.09 ± 0.13) shown in Figure S8a.

R2-Q19. 321: I assume MAE_p should be $MAE_{p,550}$ based on Table 1?

Author's Response: Thanks for pointing out. Revision made.

R2-Q20. 325-328: The Cappa et al. observation showing weak enhancement should also be included in this summary.

Author's Response: Suggestion taken. Cappa et al. (2012) was added.

R2-Q21. 355: Use of “significantly” implies a statistically significant difference between the clusters. Please provide uncertainty estimates and confidence levels if this is intended, or omit.

Author's Response: Results of Wilcoxon-Mann-Whitney tests are included in SI to support the statement and also shown below. Wilcoxon-Mann-Whitney tests between C1&C2, C2&C3 and C2&C4 all show $P < 0.01$, indicating that the mean of C2 is significantly higher than C1, C3 and C4.

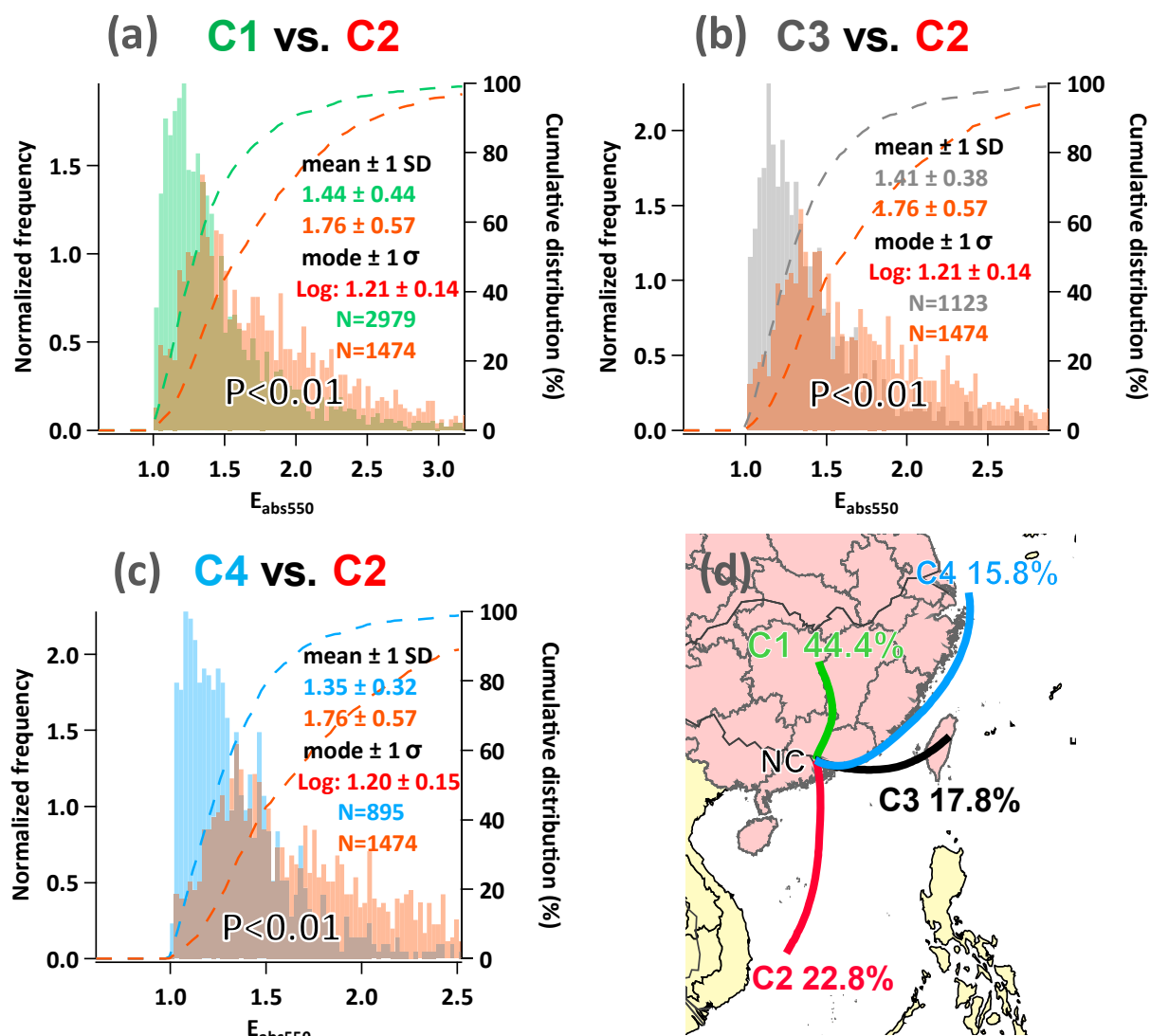


Figure R-6 Frequency distributions of E_{abs550} by different air mass clusters.

R2-Q22. 360-361: I am curious how much the air mass trajectories were influenced by precipitation during the monsoon period/rainy season. It seems like aged/coated BC likely having higher E_{abs} would be more susceptible to removal compared to less-aged/coated BC with lower E_{abs} ?

Author's Response: It's difficult to directly evaluate the rain effect on E_{abs550} for corresponding air mass trajectories since the measurement is only conducted at the end point of air mass trajectories. Alternatively, we compare the E_{abs550} before and during rain for 49 rain events from the yearlong measurements. Precipitation of 49 rain events as well as the monthly distributions are shown in Figure R7a. As for subtropical region, precipitation events are dominated in spring and summer time. EC concentration is only 43% during rain comparing before rain. However, as shown in Figure R7c, E_{abs550} values are similar before and during rain as indicated by the unity slope. These results imply that E_{abs550} is not very sensitive to rain effect in this study.

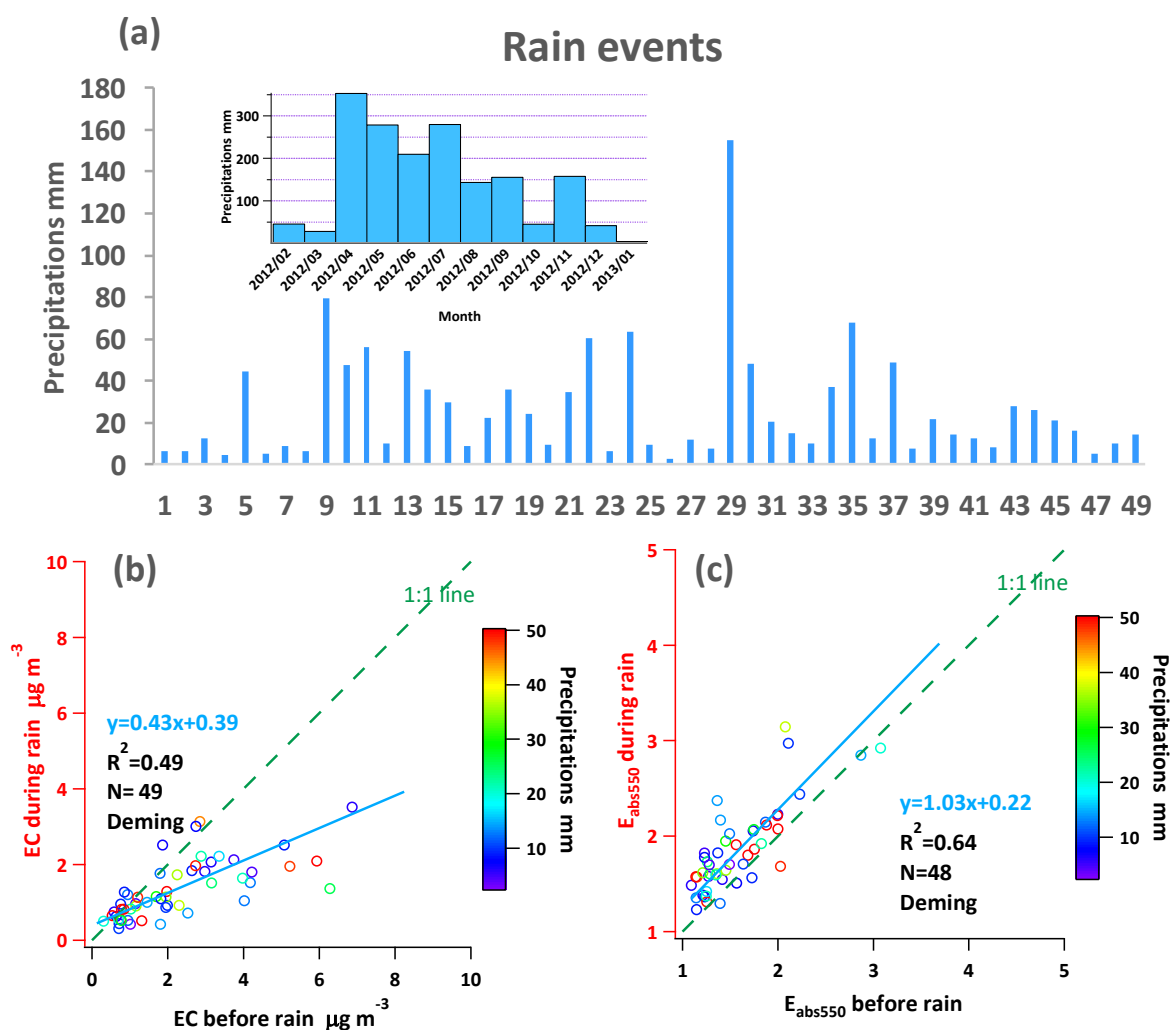


Figure R-7 Effect of precipitations. (a) Precipitations of 49 rain events and monthly distributions. (b) Scatter plot of EC before and during rain events. (c) Scatter plot of E_{abs550} before and during rain events.

R2-Q23. 375-376: Could the authors clarify the reasoning given here? First, I believe the authors mean the MAE_p determined in section 4.1, not 4.3, correct? I think this is arguing that because MAE_p is, on average, higher than the MAE observed in the absence of BB influence there must be a large amount of BB influence on BC at this location? If so, I think some caution or caveats should be included in the discussion, since the BB influence tracer is not independent of the EC measurement. Further, I would

expect there to be a much stronger effect on AAE if BB was such an important BC source, yet the later sections establish that AAE does not show a response.

Author's Response: Thanks for suggestion. The corresponding content has been revised as follows:

During the rainy season when oceanic wind prevails, BC from BB emission in Southeast Asia can reach PRD through long range transport (LRT), resulting in an elevated K^+/EC ratio and MAE_{550} . The Deming regression intercept (11.89) in Figure 8 represents the MAE without the BB effect. This non-BB MAE_{550} ($11.89 \text{ m}^2 \text{ g}^{-1}$) is only slightly lower than $MAE_{p,550}$ ($13 \text{ m}^2 \text{ g}^{-1}$) obtained in section 4.3, implying that a large fraction of $MAE_{p,550}$ could not be explained by the BB source. Additional evidence was obtained through examining regression relationships of $MAE_{p,550}$ with K^+/EC month-by-month (Figure S17b). Correlation of monthly $MAE_{p,550}$ vs. K^+/EC ratio yield a R^2 of 0.23 (Figure S17c). In contrast, a much higher correlation ($R^2=0.58$) was observed between $MAE_{p,550}$ and non-BB MAE_{550} (i.e., K^+/EC intercepts from Figure S17b). These results imply that BB is one of the contributors to the $MAE_{p,550}$ variations, but unlikely the dominating one.

R2-Q24. 381: Again I am curious as to the reasoning for selection of these wavelength pairs.

Author's Response: The 470 and 660 nm wavelength pairs were used to represent AAE in the visible range. $AAE_{370-880}$ (1.13 ± 0.13) is added as shown in Figure S8b, which is slightly higher than $AAE_{470-660}$ (1.09 ± 0.13) shown in Figure S8a.

R2-Q25. 384-386: I do not quite follow the reasoning presented here. Why does the monthly average of 1.2 suggest variations in AAE are associated with thicker coatings than BrC contribution? To me the strongest evidence of minimal BB contribution is the lack of correlation with the K^+/EC tracer. Does AAE show any correlation with E_{abs} ? The manuscript asserts AAE is dominated by coating, so there should be a relationship based on the arguments presented.

Author's Response: We fully agree that the independency between AAE and K^+/EC is the main evidence that BB is not the driving force of AAE variation. The mention of monthly AAE of 1.2 here is another evidence to support this argument. The following content is revised to improve the clarity.

These results suggest that the elevated AAE observed in the PRD wintertime is unlikely to be dominated by the BB effect. Beside the independency between $AAE_{470-660}$ and K^+/EC ratio, the measured $AAE_{470-660}$ range also implies that BB is not the major driving force of $AAE_{470-660}$ variations. The limited light absorption contribution from BrC in RPD region is observed in a recent study (Yuan et al., 2016), which suggest an upper limit of BrC contribution of 10% at 405 nm in the winter time using the AAE approach.

R2-Q26. 413-415: The refractive index of the shell also changes as it takes up water. Is this accounted for in the modeling?

Author's Response: The RI change due to water uptake is not considered in our Mie simulations.

R2-Q27. 426: This approach requires that only BC and associated coatings affect E_{abs} and AAE, but AAE can also be affected by non-BC aerosol (e.g., brown carbon or dust) that is externally mixed with BC. I am not sure how this approach can work unless there is clear evidence that there are no other light-absorbing particles or that the relative abundance does not change with season.

Author's Response: We add a section to discuss the caveats of the MRS method for E_{abs} determination. The MRS approach is a tracer based method. For a scenario that samples are strongly influenced by BrC (e.g. sample overall AAE>2), it is possible to determine the contribution of $\sigma_{abs,BrC}$ if a reliable primary BrC tracer is available. We add the following content to discuss such scenarios.

The data in this study is dominated by BC absorption that did not show much influence from BrC. However, extra care should be taken if the samples exhibit substantial BrC signature (e.g. AAE>2). Such situations are equivalent to the two-source scenarios discussed in our previous paper on the MRS method (Wu and Yu, 2016) and the major findings are described below. Two types of two-source scenarios are considered: two correlated primary sources (scenario A) and two independent primary sources (scenario B). In scenario A in which both BC and primary BrC are dominated by BB, using BC as a solo tracer to calculate the primary ratio (MAE_p) still works. In scenario B in which BC and primary BrC are independent, using BC alone to determine a single primary MAE_p could lead to a considerable bias in E_{abs} estimation. Alternatively, if a reliable primary BrC tracer is available, the corresponding $MAE_{p,BrC}$ can be determined by MRS. With the knowledge of $MAE_{p,BrC}$ and $MAE_{p,BC}$, light absorption by BC and BrC can be calculated separately and the E_{abs} can be determined using Eq. (11):

$$E_{abs} = \frac{\sigma_{abs,t}}{\sigma_{abs,p,BC} + \sigma_{abs,p,BrC}} = \frac{\sigma_{abs,t}}{MAE_{p,BC} \times EC + MAE_{p,BrC} \times BrC} \quad (11)$$

However, the implementation of Eq.11 is challenging due to the complexity in the chemical composition of BrC. For example, a recent study found that the 20 most absorbing BrC chromophores account for ~50% BrC light absorption and there is not a single compound contributing more than 10% (Lin et al., 2016), making it difficult to choose a single compound as the BrC tracer. In addition, time resolved measurement of BrC chromophores has yet to emerge. As a result, for scenario B (sample AAE>2 & primary BrC variations independent of BC), estimation of E_{abs} by MRS is not practical at this stage due to the lack of required input data. Using BC alone to determine a single primary MAE_p could lead to a considerable bias and should be avoided.

R2-Q28. Table 1, while convenient, could be omitted for length.

Author's Response: We feel that keeping table 1 in main text would be helpful for quick lookup of the abbreviations used in this study.

R2-Q29. Figures 2-4 do not add much to the manuscript, in my opinion, and could be removed for length.

Author's Response: Figure 2 is now moved to SI. As for Figure 3 and 4, they are useful to help the readers to understand how core/shell combinations can affect the variability of AAE and E_{abs} from a theoretical perspective. These two figures are used in the later discussions in section 4.5 and 4.6. Keeping these two figures will be convenient for readers to understand how observed E_{abs} and AAE can be used to infer the core/shell range from Figure 3 and 4. We believe the inclusion of the two Mie simulation figures is helpful in understand the linkage between observed AAE/ E_{abs} and core/shell ranges, especially from the cross-section plots.

R2-Q30. Figure 7: Minor, but x-axis is year and month, not just month. Replacing with “Date” would be fine.

Author’s Response: Revision made.

References:

- Bond et al. (2006) Limitations in the enhancement of visible light absorption due to mixing state, *J. Geophysical Research*, doi: 10.1029/2006JD007315
- Lack and Cappa (2010) Impact of brown and clear carbon on light absorption enhancement, single scatter albedo and absorption wavelength dependence of black carbon, *Atmospheric Chemistry and Physics*, doi: 10.5194/acp-10-4207-2010
- Lack et al. (2008) Bias in filter-based light absorption measurements due to organic aerosol loading: Evidence from ambient measurements, *Aerosol Science and Technology*, 42, doi: 10.1080/02786820802389277
- Liu et al. (2015) Enhanced light absorption by mixed source black and brown carbon particles in UK winter, *Nature Communications*, doi: 10.1038/ncomms9435
- Subramanian et al. (2007) Yellow beads and missing particles: Trouble ahead for filter-based absorption measurements, *Aerosol Science and Technology*, doi:10.1080/02786820701344589

References:

- Ajtai, T., Filep, Á., Utry, N., Schnaiter, M., Linke, C., Bozóki, Z., Szabó, G., and Leisner, T.: Inter-comparison of optical absorption coefficients of atmospheric aerosols determined by a multi-wavelength photoacoustic spectrometer and an Aethalometer under sub-urban wintry conditions, *J. Aerosol. Sci.*, 42, 859-866, 10.1016/j.jaerosci.2011.07.008, 2011.
- Arnott, W. P., Moosmuller, H., Sheridan, P. J., Ogren, J. A., Raspert, R., Slaton, W. V., Hand, J. L., Kreidenweis, S. M., and Collett, J. L.: Photoacoustic and filter-based ambient aerosol light absorption measurements: Instrument comparisons and the role of relative humidity, *J. Geophys. Res.*, 108, 2003.
- Arnott, W. P., Hamasha, K., Moosmuller, H., Sheridan, P. J., and Ogren, J. A.: Towards aerosol light-absorption measurements with a 7-wavelength Aethalometer: Evaluation with a photoacoustic instrument and 3-wavelength nephelometer, *Aerosol. Sci. Technol.*, 39, 17-29, Doi 10.1080/027868290901972, 2005.
- Cappa, C. D., Lack, D. A., Burkholder, J. B., and Ravishankara, A. R.: Bias in Filter-Based Aerosol Light Absorption Measurements Due to Organic Aerosol Loading: Evidence from Laboratory Measurements, *Aerosol. Sci. Technol.*, 42, 1022-1032, 10.1080/02786820802389285, 2008.
- Chow, J. C., Watson, J. G., Crow, D., Lowenthal, D. H., and Merrifield, T.: Comparison of IMPROVE and NIOSH carbon measurements, *Aerosol. Sci. Technol.*, 34, 23-34, 10.1080/027868201300081923, 2001.
- Chow, J. C., Watson, J. G., Chen, L. W. A., Arnott, W. P., and Moosmuller, H.: Equivalence of elemental carbon by thermal/optical reflectance and transmittance with different temperature protocols, *Environ. Sci. Technol.*, 38, 4414-4422, 10.1021/Es034936u, 2004.

Coen, M. C., Weingartner, E., Apituley, A., Ceburnis, D., Fierz-Schmidhauser, R., Flentje, H., Henzing, J. S., Jennings, S. G., Moerman, M., Petzold, A., Schmid, O., and Baltensperger, U.: Minimizing light absorption measurement artifacts of the Aethalometer: evaluation of five correction algorithms, *Atmos. Meas. Tech.*, 3, 457-474, 10.5194/amt-3-457-2010, 2010.

Guyon, P., Graham, B., Roberts, G. C., Mayol-Bracero, O. L., Maenhaut, W., Artaxo, P., and Andreae, M. O.: Sources of optically active aerosol particles over the Amazon forest, *Atmos. Environ.*, 38, 1039-1051, 10.1016/j.atmosenv.2003.10.051, 2004.

Hoffer, A., Gelencser, A., Guyon, P., Kiss, G., Schmid, O., Frank, G. P., Artaxo, P., and Andreae, M. O.: Optical properties of humic-like substances (HULIS) in biomass-burning aerosols, *Atmos. Chem. Phys.*, 6, 3563-3570, 2006.

Kirchstetter, T. W., Novakov, T., and Hobbs, P. V.: Evidence that the spectral dependence of light absorption by aerosols is affected by organic carbon, *J. Geophys. Res.*, 109, D21208, 10.1029/2004jd004999, 2004.

Kozlov, V. S., Panchenko, M. V., Tikhomirov, A. B., Tikhomirov, B. A., and Shmargunov, V. P.: Effect of relative air humidity on photoacoustic aerosol absorption measurements in the near-ground atmospheric layer, *Atmospheric and Oceanic Optics*, 24, 487, 10.1134/s1024856011050101, 2011.

Lack, D. A. and Cappa, C. D.: Impact of brown and clear carbon on light absorption enhancement, single scatter albedo and absorption wavelength dependence of black carbon, *Atmos. Chem. Phys.*, 10, 4207-4220, DOI 10.5194/acp-10-4207-2010, 2010.

Langridge, J. M., Richardson, M. S., Lack, D. A., Brock, C. A., and Murphy, D. M.: Limitations of the Photoacoustic Technique for Aerosol Absorption Measurement at High Relative Humidity, *Aerosol. Sci. Technol.*, 47, 1163-1173, 10.1080/02786826.2013.827324, 2013.

Lee, H. M., Okuyama, K., Mizohata, A., Kim, T. O., and Koyama, H.: Fabrication of reference filter for measurements of EC (elemental carbon) and OC (organic carbon) in aerosol particles, *Aerosol. Sci. Technol.*, 41, 284-294, 2007.

Lewis, K. A., Arnott, W. P., Moosmüller, H., Chakrabarty, R. K., Carrico, C. M., Kreidenweis, S. M., Day, D. E., Malm, W. C., Laskin, A., Jimenez, J. L., Ulbrich, I. M., Huffman, J. A., Onasch, T. B., Trimborn, A., Liu, L., and Mishchenko, M. I.: Reduction in biomass burning aerosol light absorption upon humidification: roles of inorganically-induced hygroscopicity, particle collapse, and photoacoustic heat and mass transfer, *Atmos. Chem. Phys.*, 9, 8949-8966, 10.5194/acp-9-8949-2009, 2009.

Lin, P., Aiona, P. K., Li, Y., Shiraiwa, M., Laskin, J., Nizkorodov, S. A., and Laskin, A.: Molecular Characterization of Brown Carbon in Biomass Burning Aerosol Particles, *Environ. Sci. Technol.*, 50, 11815-11824, 10.1021/acs.est.6b03024, 2016.

Replacement Filter Tape for the Magee Scientific Model AE33 Aethalometer®: http://www.mageesci.com/images/stories/docs/Magee_Scientific_Filter_Aethalometer_AE_Tape_Replacement_discussion.pdf, 2017.

Raspet, R., Slaton, W. V., Arnott, W. P., and Moosmüller, H.: Evaporation–Condensation Effects on Resonant Photoacoustics of Volatile Aerosols, *Journal of Atmospheric and Oceanic Technology*, 20, 685-695, 10.1175/1520-0426(2003)20<685:eceorp>2.0.co;2, 2003.

Schmid, O., Artaxo, P., Arnott, W. P., Chand, D., Gatti, L. V., Frank, G. P., Hoffer, A., Schnaiter, M., and Andreae, M. O.: Spectral light absorption by ambient aerosols influenced by biomass burning in the Amazon Basin. I: Comparison and field calibration of absorption measurement techniques, *Atmos. Chem. Phys.*, 6, 3443-3462, 2006.

Subramanian, R., Roden, C. A., Boparai, P., and Bond, T. C.: Yellow beads and missing particles: Trouble ahead for filter-based absorption measurements, *Aerosol. Sci. Technol.*, 41, 630-637, Doi 10.1080/02786820701344589, 2007.

Tan, H., Liu, L., Fan, S., Li, F., Yin, Y., Cai, M., and Chan, P. W.: Aerosol optical properties and mixing state of black carbon in the Pearl River Delta, China, *Atmos. Environ.*, 131, 196-208, 10.1016/j.atmosenv.2016.02.003, 2016.

Weingartner, E., Saathoff, H., Schnaiter, M., Streit, N., Bitnar, B., and Baltensperger, U.: Absorption of light by soot particles: determination of the absorption coefficient by means of aethalometers, *J. Aerosol. Sci.*, 34, 1445-1463, 10.1016/S0021-8502(03)00359-8, 2003.

Wu, C., Ng, W. M., Huang, J., Wu, D., and Yu, J. Z.: Determination of Elemental and Organic Carbon in PM_{2.5} in the Pearl River Delta Region: Inter-Instrument (Sunset vs. DRI Model 2001 Thermal/Optical Carbon Analyzer) and Inter-Protocol Comparisons (IMPROVE vs. ACE-Asia Protocol), *Aerosol. Sci. Technol.*, 46, 610-621, 10.1080/02786826.2011.649313, 2012.

Wu, C., Huang, X. H. H., Ng, W. M., Griffith, S. M., and Yu, J. Z.: Inter-comparison of NIOSH and IMPROVE protocols for OC and EC determination: implications for inter-protocol data conversion, *Atmos. Meas. Tech.*, 9, 4547-4560, 10.5194/amt-9-4547-2016, 2016.

Wu, C. and Yu, J. Z.: Determination of primary combustion source organic carbon-to-elemental carbon (OC/EC) ratio using ambient OC and EC measurements: secondary OC-EC correlation minimization method, *Atmos. Chem. Phys.*, 16, 5453-5465, 10.5194/acp-16-5453-2016, 2016.

Wu, D., Mao, J. T., Deng, X. J., Tie, X. X., Zhang, Y. H., Zeng, L. M., Li, F., Tan, H. B., Bi, X. Y., Huang, X. Y., Chen, J., and Deng, T.: Black carbon aerosols and their radiative properties in the Pearl River Delta region, *Sci China Ser D*, 52, 1152-1163, 10.1007/s11430-009-0115-y, 2009.

Yuan, J. F., Huang, X. F., Cao, L. M., Cui, J., Zhu, Q., Huang, C. N., Lan, Z. J., and He, L. Y.: Light absorption of brown carbon aerosol in the PRD region of China, *Atmos. Chem. Phys.*, 16, 1433-1443, 10.5194/acp-16-1433-2016, 2016.

Quantifying black carbon light absorption enhancement by a novel statistical approach

Cheng Wu^{1,2}, Dui Wu^{1,2,3}, Jian Zhen Yu^{4,5,6}

¹Institute of Mass Spectrometer and Atmospheric Environment, Jinan University, Guangzhou 510632, China

²Guangdong Provincial Engineering Research Center for on-line source apportionment system of air pollution, Guangzhou 510632, China

³Institute of Tropical and Marine Meteorology, China Meteorological Administration, Guangzhou 510080, China

⁴Division of Environment, Hong Kong University of Science and Technology, Clear Water Bay, Hong Kong, China

⁵Atmospheric Research Centre, Fok Ying Tung Graduate School, Hong Kong University of Science and Technology, Nansha, China

⁶Department of Chemistry, Hong Kong University of Science and Technology, Clear Water Bay, Hong Kong, China

Corresponding to: Cheng Wu (wucheng.vip@foxmail.com) and Jian Zhen Yu (jian.yu@ust.hk)

Abstract

Black carbon (BC) particles in the atmosphere can absorb more light when coated by non-absorbing or weakly absorbing materials during atmospheric aging, due to the lensing effect. In this study, the light absorption enhancement factor, E_{abs} , was quantified using one year's measurement of mass absorption efficiency (MAE) in the Pearl River Delta region (PRD). A new approach for calculating primary MAE (MAE_p), the key for E_{abs} estimation, is demonstrated using the Minimum Residual Squared (MRS) method, exploring the inherent source independency between BC and its coating materials. A unique feature of E_{abs} estimation by the MRS approach is its insensitivity to systematic biases in EC and σ_{abs} measurements. The annual average $E_{\text{abs}550}$ is found to be 1.50 ± 0.48 (± 1 S.D.), exhibiting a clear seasonal pattern with higher values in summer and lower in the winter. Elevated E_{abs} in the rainy summer season is likely associated with aged air masses dominating from marine origin, along with long-range transport of biomass burning influenced air masses from Southeast Asia. E_{abs}

31 induced by hygroscopic growth at elevated RH could be as high as 1.3. Core-shell Mie simulations
32 along with measured E_{abs} and Angstrom absorption exponent (AAE) constraints suggest that in the
33 PRD, the coating materials are unlikely to be dominated by brown carbon and the coating thickness is
34 higher in the rainy season than the dry season. A negative correlation is found between $AAE_{470-660}$ and
35 RH, suggesting a dominant particle size of $D_{core} = 130$ nm and D_{shell}/D_{core} range of 2 to 4.

36

37 **1 Introduction**

38 Originating from incomplete combustion, black carbon (BC) is a crucial constituent of
39 atmospheric aerosols, and is an air pollutant itself, having an adverse health impacts on humans (Suglia
40 et al., 2008). BC has also been recognized as the third most important climate forcer due to its broad
41 light absorbing capability across the UV-Vis-IR spectrum (IPCC, 2013). BC can alter the climate in a
42 variety of ways, including by direct forcing (Bond et al., 2011), affecting cloud cover (Koch and Del
43 Genio, 2010) and precipitation (Tao et al., 2012), reducing the albedo of snow and ice (Hansen and
44 Nazarenko, 2004) and causing surface dimming (Wild, 2011). The climate effects of BC can be global
45 or regional (Ramanathan and Carmichael, 2008). A recent study found BC can modify planetary
46 boundary layer meteorology, and thus enhance local pollution indirectly (Ding et al., 2016). However,
47 due to its variable optical characteristics induced during atmospheric aging, large uncertainties still
48 exist in estimating the radiative forcing from BC. Optical properties of BC can be predicted by
49 knowing the mass concentration, mixing state and size distribution, which collectively serve as the
50 cornerstone for modeling the climate effect of BC. In 3D modeling studies, to conserve computational
51 resources, the mass absorption efficiency (MAE) or mass absorption cross-section (MAC) is widely
52 used to convert black carbon mass concentration to light absorption coefficient (σ_{abs}). MAE is a
53 quantity to describe the light absorption ability per unit EC mass:

$$54 \quad MAE (m^2 g^{-1}) = \frac{\text{absorption coefficient } \sigma_{abs} (Mm^{-1})}{EC \text{ mass concentration } (\mu g m^{-3})} \quad (1)$$

55 As a fundamental input parameter, MAE has a critical impact on BC's radiative forcing
56 estimation in climate modeling studies. Mixing state is one of the governing factors affecting MAE.

57 Light absorption of soot particles is enhanced when coated with non-absorbing materials (Fuller et al.,
 58 1999) or weakly absorbing materials (Lack and Cappa, 2010) during atmospheric aging. The coating
 59 materials can focus more light onto the soot core through the lensing effect, resulting in elevated MAE
 60 (Wang et al., 2017). Strong correlations between MAE and the number/volume fraction of coated
 61 particles have been reported in urban areas like Tokyo (Naoe et al., 2009), Shenzhen (Lan et al., 2013)
 62 and Xi'an (Wang et al., 2014), implying that the elevated MAE observed at these locations was mainly
 63 due to the elevated fraction of coated of soot particles. Total absorption ($\sigma_{abs,t}$) of coated particles can
 64 be separated into two parts: primary absorption ($\sigma_{abs,p}$) due to the uncoated soot core alone, and extra
 65 absorption ($\sigma_{abs,c}$) due to lensing effect of the coating (Bond et al., 2006; Jacobson, 2006; Liu et al.,
 66 2016a) and the presence of secondarily formed brown carbon (BrC) (Lack and Cappa, 2010; Liu et al.,
 67 2016b).

$$68 \quad \sigma_{abs,t} = \sigma_{abs,p} + \sigma_{abs,c} \quad (2)$$

69 The absorption enhancement factor (E_{abs}) then can be defined as ratio of the total absorption and
 70 primary absorption coefficients or the corresponding MAE values:

$$71 \quad E_{abs} = \frac{\sigma_{abs,t}}{\sigma_{abs,p}} = \frac{MAE_t}{MAE_p} \quad (3)$$

72 Where MAE_p represents the ratio of $\sigma_{abs,p}/EC$ for uncoated soot particles, similar to the concept of
 73 the primary OC/EC ratio in the EC tracer method:

$$74 \quad MAE_p = \frac{\sigma_{abs,p}}{EC} \quad (4)$$

75 And the MAE of coated BC can be defined as:

$$76 \quad MAE_t = \frac{\sigma_{abs,t}}{EC} \quad (5)$$

77 Thus, elevated MAE induced by coating during atmospheric aging results in an E_{abs} larger than 1.

78 Previous model studies suggest that absorption by aged soot particles can be 1.5 times greater than
 79 fresh soot (Fuller et al., 1999; Bond et al., 2006). Laboratory studies have demonstrated that soot
 80 particles coated with SOA (Saathoff et al., 2003; Schnaiter et al., 2005) and sulfuric acid (Zhang et al.,
 81 2008; Khalizov et al., 2009) can increase E_{abs} . An artificial coating experiment by Shiraiwa et al. (2010)

82 found an E_{abs} of 2 for graphite particles growing in diameter from 185 to 370 nm. A laboratory study
83 by McMeeking et al. (2014) found that in the presence of BrC, light absorption enhancement is more
84 pronounced at the shorter wavelength. A recent chamber study coupling actual ambient air with seed
85 BC particles implies that the timescale for E_{abs} reaching 2.4 is only 5 hours in Beijing but 18 hours in
86 Houston (Peng et al., 2016). Field studies conducted in recent years have also substantiated enhanced
87 light absorption in Canada (Knox et al., 2009; Chan et al., 2011), US (Lack et al., 2012b), UK (Liu et
88 al., 2015) and Japan (Nakayama et al., 2014; Ueda et al., 2016). In contrast, field studies in California,
89 US (Cappa et al., 2012) found a weaker light absorption enhancement (6% on average). A recent study
90 suggests the mass ratio of non-BC content to BC particles determines the occurrence of the absorption
91 enhancement of black-carbon particles (Liu et al., 2017).

92 Two approaches are widely used to determine E_{abs} from ambient measurements. The first approach
93 removes the coating materials on particles physically using a thermal denuder (TD) (Lack et al., 2012a)
94 or by aerosol filter filtration-dissolution (AFD) (Cui et al., 2016b). The TD approach is briefly
95 discussed here. Coating materials can be removed by TD at a working temperature around 200 to
96 300 °C (depending on the charring characteristics of aerosols at the sampling site) to measure $\sigma_{\text{abs},p}$,
97 which are cycled with measurements of $\sigma_{\text{abs},t}$ (without passing through TD), allowing E_{abs} to be
98 obtained from the ratio of $\sigma_{\text{abs},t}/\sigma_{\text{abs},p}$ following Eq.3. The major advantage of the TD approach is
99 its ability to provide highly time resolved measurements (minutes). A photo-acoustic spectrometer
100 (PAS) is commonly used with TD for detection to satisfy its high time resolution demands. As an in-
101 situ technique, PAS eliminates the artifacts associated with filter-based methods (Weingartner et al.,
102 2003; Coen et al., 2010) and is often considered as the reference instrument for light absorption
103 coefficient determination (Arnott et al., 2003; Arnott et al., 2005). One limitation of the TD approach is
104 that a universal optimal operation temperature does not exist. If the temperature is too low, the coating
105 cannot be fully removed, and charring can occur if the TD temperature is too high, leading to biased
106 results. Another issue is particle loss due to TD, which can be $\sim 20\%$ and needs to be taken into account
107 (Ueda et al., 2016). It's also worth noting that MAE_p by the TD approach is different from the MAE_p
108 at the emission source. First, the morphology of thermally denuded BC particles (compact aggregates)
109 is different from that of freshly emitted BC particles (chain-like aggregates). Second, most of the

110 coatings is removed with the TD denuded soot particles, but freshly emitted soot particles usually
111 come with a thin coating of OC formed from condensation of OC vapors as the temperature drops
112 from engine to the ambient air. As a result, the MAE_p by TD approach is expected to be lower than
113 the MAE_p of emission source. In this sense, the TD approach may not be a perfect “time machine” to
114 reverse the aging process for E_{abs} determination.

115 The second approach is the MAE ratio method, which is also stated in Eq. 3. The key to this method
116 is determining an appropriate MAE_p that can represent the MAE from primary emissions. One
117 approach is to adopt the reference MAE_p from the literature but it may fail to represent the actual
118 MAE_p at a specific sampling site, since MAE_p varies temporally and spatially. For example, MAE_p of
119 diesel soot was found to be 7.1 m²g⁻¹ at 532 nm (Adler et al., 2010). A much higher MAE_p (16 m²g⁻¹
120 at 530 nm) was observed from natural gas flaring (Weyant et al., 2016). MAE_p of biomass burning
121 (BB) samples is highly varied due to a wide range of fuel types and combustion conditions (Reid et
122 al., 2005; Roden et al., 2006). A range from 6.1 to 80.8 m²g⁻¹ was reported for BB MAE_p at 550 nm
123 (Pandey et al., 2016). Without the knowledge of source contributions, it is not feasible to derive a
124 representative MAE_p for E_{abs} estimation. The other commonly used approach is to determine MAE_p
125 from the dependency of MAE on the number fraction of coated soot particles measured by SP2 (Lan
126 et al., 2013). Since MAE (y axis) is positively correlated with the number fraction of coated soot
127 particles (x axis), MAE_p can be determined by extending the regression line to x=0. It is worth noting
128 that this approach provides only a rough approximation of E_{abs} since the parameter used here (coated
129 soot particles number fraction) ignores other main drivers of light absorption enhancement (e.g.
130 coating thickness). As a result, this approach is only valid for a period of measurements, for which
131 coating thickness is relatively constant and the MAE variations are dominated by coated soot particles
132 number fraction.

133 However, the high cost of the TD-PAS system and SP2 limit the field measurement of E_{abs} around
134 the world. In addition, long-term E_{abs} measurements by a TD-PAS system and SP2 are not easily
135 achieved and rarely reported. On the other hand, an Aethalometer and RT-ECOC analyzer can be
136 effectively deployed for long term measurements and E_{abs} estimation, at a relatively lower cost. In this
137 study, based on one year of hourly MAE measurements (with the field carbon analyzer and

138 Aethalometer) at a suburban site in the Pearl River Delta (PRD) region of China, quantification of
139 MAE_p is demonstrated by a novel statistical approach, the Minimum R squared method (MRS) (Wu
140 and Yu, 2016). The aim of this study is to demonstrate the capability of E_{abs} estimation using a year-
141 long dataset from cost-effective instrumentation. The seasonal variability of MAE, AAE and E_{abs} in
142 the PRD region are characterized and their dependency on air mass origin, biomass burning and RH
143 are discussed. Abbreviations used in this study are summarized in Table 1 for a quick lookup.

144 **2 Ambient measurements**

145 Sampling was conducted from Feb 2012 to Jan 2013 at the suburban Nancun (NC) site (23° 0'11.82"N,
146 113°21'18.04"E). NC, situated on the top of the highest peak (141 m ASL) in Guangzhou's Panyu
147 district, is located at the geographic center of the PRD region, making it a representative location for
148 average atmospheric mixing characteristics of city clusters in the PRD region. Light absorption
149 measurements were performed by a 7-λ Aethalometer (AE-31, Magee Scientific Company, Berkeley,
150 CA, USA). The Aethalometer was equipped with a 2.5 μm cyclone with a sampling flow rate of 4 L
151 min⁻¹. Weingartner's algorithm (Weingartner et al., 2003) was adopted to correct the sampling artifacts
152 (aerosol loading, filter matrix and scattering effect) rooted in filter based method. A customized
153 Aethalometer data processing program (Wu, 2017a) with graphical user interface was developed to
154 perform data correction and detailed descriptions can be found in the SI (The program is available
155 from <https://sites.google.com/site/wuchengust>). Details of the Aethalometer setup and data correction
156 can be found in our previous paper (Wu et al., 2013).

157 EC mass concentrations were determined by a real time ECOC analyzer (Model RT-4, Sunset
158 Laboratory Inc., Tigard, Oregon, USA). The sunset carbon analyzer was sampling on hourly cycles at
159 a flow rate of 8 Lmin⁻¹ with a PM_{2.5} sharp-cut cyclone inlet. For each measurement hour, the first
160 45min were for sample collection and the remaining 15 min for thermal-optical analysis. OC is
161 volatilized first by step-wise temperature ramping in an oxygen-free atmosphere while in the second
162 stage EC is combusted in the presence of oxygen. Laser transmittance is applied to correct the charring
163 artifact during the OC stage.

164 Considering a measurement **precision** of 5% for the Aethalometer (Hansen, 2005) and 24% for the
165 RT-ECOC analyzer (Bauer et al., 2009), the propagated relative **precision** of E_{abs} ($E_{abs,Unc}$) is 35%
166 following Eq. S1&S2 in the SI. It should be noted that $E_{abs,Unc}$ is mainly attributed to the
167 measurement **precision** of EC by the RT-ECOC analyzer. Since the measurement **precision** of the RT-
168 ECOC analyzer estimated by Bauer et al. (2009) is obtained from field measurement at an environment
169 (EC below $1 \mu\text{g m}^{-3}$) where EC is much lower than the present study (annual average EC $2.63 \mu\text{g m}^{-3}$),
170 the $E_{abs,Unc}$ of 35% should be considered as an upper limit for the present study.

171 Light scattering was measured by an integrating nephelometer (Aurora-1000, Ecotech, Melbourne,
172 Australia). Water soluble ions were measured by MARGA (The instrument for Measuring AeRosols
173 and GAses)(ten Brink et al., 2007). **Both instruments are equipped with a PM_{2.5} inlet to remove the**
174 **coarse particles.**

175 **2.1 Uncertainties of MAE determination**

176 Two major uncertainties associated with the σ_{abs} and EC determination techniques should be taken
177 into account when comparing MAE across different studies. For the σ_{abs} determination technique,
178 photo-acoustic spectroscopy (PAS) is an in-situ technique free from filter based artifacts, but its
179 application is limited by its high cost. The filter based optical transmittance method (e.g., Aethalometer
180 and Multi Angle Absorption Photometer, MAAP) is the most widely used technique around the world,
181 but data correction is needed to minimize the bias from artifacts due to the loading effect, matrix effect
182 and scattering effect (Weingartner et al., 2003; Arnott et al., 2005; Schmid et al., 2006; Virkkula et al.,
183 2007; Coen et al., 2010; Drinovec et al., 2017; Saturno et al., 2017). **Besides these artifacts, RH is also**
184 **a source of σ_{abs} measurement uncertainty. Elevated RH is not only a driving force of increased σ_{abs}**
185 **due to the hygroscopic growth of particles, but also a factor affecting ambient σ_{abs} measurements.**
186 **Previous studies found σ_{abs} by PAS exhibit a systematic decrease when $\text{RH} > 70\%$ (Arnott et al., 2003;**
187 **Kozlov et al., 2011). Water evaporation was found as the major cause for the biased PAS σ_{abs}**
188 **measurements under high RH (Raspert et al., 2003; Lewis et al., 2009b; Langridge et al., 2013). Filter-**
189 **based measurements are also affected under high RH conditions. For example, Arnott et al. (2003)**
190 **observed erratic responses by particle soot absorption photometer (PSAP) as RH changed. The main**
191 **reason is traced to the hydrophilic cellulose membrane, which serves to reinforce the quartz filter used**
192 **in PSAP. The fibers can swell and shrink as RH changes, causing unwanted light attenuation signal.**
193 **The PTFE-coated glass-fiber tape has become available since 2012 for the recent model of**

194 Aethalometer to minimize the RH interference (Magee-Scientific, 2017). A study by Schmid et al.
195 (2006) reported dependency of PSAP σ_{abs} on RH, but found negligible effect of RH on Aethalometer
196 performance. It is also worth noting that RH in the Aethalometer optical chamber may be lower than
197 the ambient RH due to the slightly elevated temperature inside the instrument. The magnitude of RH
198 difference was found similar between different instruments: 20% for the Aethalometer (Schmid et al.,
199 2006) and 15% for the nephelometer (Guyon et al., 2004). The RH in the Aethalometer optical chamber
200 was not measured in this study. We expected its level to be slightly lower than the ambient RH. Cappa
201 et al. (2008) found σ_{abs} measurements by PSAP and PAS maintained a high linearity even under high
202 RH conditions (65-91%). Inter-comparison studies demonstrated that with proper corrections,
203 Aethalometer σ_{abs} measurements agree well with those by PAS (Ajtai et al., 2011). During the inter-
204 comparison study of an Aethalometer (AE-16) and a PAS in Guangzhou (Wu et al., 2009), good
205 correlation was found ($R^2=0.96$) as shown in Figure S1. These comparison results imply that the
206 Aethalometer results are linearly correlated with PAS measurements and RH has a limited interference
207 on Aethalometer measurements. In our study, careful corrective measures (Wu et al., 2013) are
208 conducted for the Aethalometer σ_{abs} data treatment to minimize these artifacts. But such artifacts
209 still cannot be fully eliminated.

210 For the EC determination, different thermal optical analysis (TOA) protocols can impact the
211 measurement variability and thus MAE. As shown in Table S1, MAE for the same samples at Fresno
212 varied from 6.1 to 9.3 $\text{m}^2 \text{g}^{-1}$, depending on which EC analysis protocol was applied (Chow et al.,
213 2009). Studies in the PRD found that discrepancies in measured EC by different analysis protocols
214 could be as large as a factor of 5 (Wu et al., 2012; Wu et al., 2016a), which adds to the uncertainty for
215 the MAE estimation. In addition, EC by TOA is also different from refractory BC (rBC) reported by
216 the laser induced incandescence (LII) technique (e.g. single particle soot photometer, SP2). For
217 example, two studies in Toronto (Knox et al., 2009; Chan et al., 2011) both used the PAS for σ_{abs}
218 measurement but different techniques for EC mass determination, resulting in very different MAE
219 results. LII instruments are usually calibrated with a commercially available surrogate (e.g. fullerene)
220 since direct calibration with ambient soot is not easy to achieve. Laborde et al. (2012) indicates that
221 the incandescence response of SP2 exhibits a dependency on soot type (15% between fullerene and
222 denuded diesel soot particles; 14% between biomass burning and denuded diesel soot particles). Due
223 to the absence of widely accepted reference materials for EC, the uncertainties in EC determination

224 will exist in the foreseeable future. All these uncertainties, including the uncertainty of rBC mass
225 determination by SP2, uncertainty of EC in TOA, the discrepancy between SP2 rBC and TOA EC and
226 the discrepancy of σ_{abs} between filter transmission and photo-acoustic methods, can contribute to the
227 differences in MAE listed in Table S1.

228 Systematic bias in MAE (e.g. overestimation of σ_{abs} and variability of EC mass by different
229 TOA protocols) discussed above have little effect on E_{abs} estimation by MRS. As shown in Eq. 3, E_{abs}
230 is the ratio of MAE_t to MAE_p or $\sigma_{abs,t}$ to $\sigma_{abs,p}$, thus most of the bias in EC mass or σ_{abs} is
231 cancelled out during the E_{abs} calculation. More details are discussed in section 4.1.

232 **3 Methodology**

233 **3.1 MAE_p estimation by MRS from the ambient data**

234 In this section, a new approach for MAE_p estimation is introduced for E_{abs} determination, which
235 requires the knowledge of differentiating $\sigma_{abs,p}$ and $\sigma_{abs,c}$ portions in $\sigma_{abs,t}$. The idea of
236 decoupling $\sigma_{abs,t}$ into $\sigma_{abs,p}$ and $\sigma_{abs,c}$ is conceptually similar to decoupling OC into primary OC
237 (POC) and secondary OC (SOC) in the EC tracer method as shown in Table 2. In the EC tracer method,
238 if $(OC/EC)_p$ is known, POC can be determined from OC (Turpin and Huntzicker, 1991). The role of
239 MAE_p here is similar to the role of $(OC/EC)_p$, the primary OC/EC ratio in the EC tracer method (a
240 comparison is given in Table 2). If MAE_p (average MAE from primary emission sources) is known,
241 E_{abs} can be obtained from the ratio of MAE_t/MAE_p (Eq. 3). Therefore, the key for E_{abs} estimation is to
242 derive an appropriate MAE_p. It is worth noting that MAE_p here does not represent MAE from a single
243 or specific primary emission source, instead it reflects an average and effective MAE that has taken
244 consideration of various primary emission sources. Thus, the MAE_p is conceptually analogous to
245 $(OC/EC)_p$ in the EC tracer method, in which the primary ratio reflects an overall ratio from primary
246 emission sources rather than from a single primary source.

247 The Minimum R squared method (MRS) explores the inherent independency between
248 pollutants from primary emissions (e.g., EC) and products associated with secondary formation
249 processes (e.g., SOC, $\sigma_{abs,c}$) to derive the primary ratios (e.g., $(OC/EC)_p$, MAE_p) in the EC tracer

250 method (Wu and Yu, 2016). When applying MRS for light absorption enhancement estimation, MRS
251 is used to explore the inherent independency between EC and $\sigma_{abs,c}$, which is gained during
252 atmospheric aging after emission. An example of MAE_p estimation by MRS is shown in Figure 1.
253 Firstly, the assumed MAE_p value is varied continuously in a reasonable range (0.01 to 50 m² g⁻¹ as
254 shown in Figure 1). Then at each hypothetical MAE_p, $\sigma_{abs,c}$ can be calculated by Eq. 6 (a combination
255 of Eq. 2&4) using EC and $\sigma_{abs,t}$ from ambient measurements.

$$256 \quad \sigma_{abs,c} = \sigma_{abs,t} - MAE_p \times EC \quad (6)$$

257 Accordingly, for each hypothetical MAE_p, a correlation coefficient value (R^2) of $\sigma_{abs,c}$ vs.
258 EC (i.e., $R^2(\sigma_{abs,c}, EC)$) can be obtained. The series of $R^2(\sigma_{abs,c}, EC)$ values (y axis) are then plotted
259 against the assumed MAE_p values (x axis) as shown by the red curve in Figure 1. The physical meaning
260 of this plot can be interpreted as follows. The $\sigma_{abs,p}$ is the fraction of light absorption owing to
261 primary emitted soot particles. As a result, $\sigma_{abs,p}$ is well correlated with EC mass. In contrast, the
262 $\sigma_{abs,c}$ is the fraction of light absorption gained by the lensing effect of the coating on particles after
263 emission. The variability of $\sigma_{abs,c}$ mainly depends on the coating thickness of the soot particles.
264 Consequently, $\sigma_{abs,c}$ is independent of EC mass. Since variations of EC and $\sigma_{abs,c}$ are independent,
265 the assumed MAE_p corresponding to the minimum $R^2(EC, \sigma_{abs,c})$ would then represent the most
266 statistically probable MAE_p of the tested dataset.

267 A computer program (Wu, 2017b) in Igor Pro (WaveMetrics, Inc. Lake Oswego, OR, USA)
268 was developed to facilitate MRS calculation with a user friendly graphical user interface. Another two
269 Igor Pro based computer programs Histbox (Wu, 2017c) and Scatter Plot (Wu, 2017d) are used for
270 generating histograms, box plots and scatter plots (with Deming regressions) presented in this study.
271 Detailed descriptions of these computer programs can be found in the SI and the computer programs
272 are available from <https://sites.google.com/site/wuchengust>.

273 **3.2 Mie simulation**

274 It can be informative to model a single soot particle using Mie theory (Bohren and Huffman,
275 1983) and understand the theoretical range and variability of the soot particle's optical properties.

276 Three types of mixing state are widely employed for parameterization: internal mixing, external
277 mixing and core-shell. To better represent the real situation (coating due to the aging process), a core-
278 shell model is considered in the Mie calculation (Figure S2), which is more realistic than a volume
279 mixture model (Bond et al., 2006). An aerosol optical closure study in the North China Plain (NCP)
280 found that the core-shell model can provide better performance than assuming purely internal mixing
281 and external mixing (Ma et al., 2012). A morphology study using Scanning Transmission X-ray
282 Microscopy found that core-shell is the dominating mixing state in ambient samples (Moffet et al.,
283 2016). It should be noted that the core-shell model assumption still has its own limitations. A single
284 particle soot photometer (SP2) study by Sedlacek et al. (2012) reported a negative lag time between
285 the scattering and incandescence signals in samples influenced by biomass burning, implying a near
286 surface location of soot relative to non-absorbing materials. Near surface type mixing of soot has also
287 been observed in Tokyo, but accounted for only 10% of total mixed soot containing particles (Moteki
288 et al., 2014). Considering the domination of core-shell type particles in the ambient environment, the
289 core-shell assumption in our optical model is sufficient to approximate the real situation.

290 As shown in Figure S2, fresh emitted soot particles are chain-like aggregates of small spheres
291 (30~50 nm). After the aging process, soot particles are coated with organic and inorganic materials.
292 Sufficient evidence has shown that the coating not only results in particle size growth, but also makes
293 the soot core become more compact due to its collapse (Alexander et al., 2008; Zhang et al., 2008;
294 Lewis et al., 2009a), especially under high RH conditions (Leung et al., 2017). Since the spherical like
295 core and shell favor Mie simulation, both core and shell are considered as spheres in the Mie
296 calculation.

297 To investigate the spectrum properties of soot particles, 11 wavelengths (370, 405, 470, 520,
298 532, 550, 590, 660, 781, 880 and 950 nm) are considered in calculations to cover wavelengths in the
299 most frequently used absorption measurement instruments. A refractive index (RI) of $1.85 - 0.71i$ is
300 adopted for soot core (Bond and Bergstrom, 2006) and 1.55 for non-absorbing coating (clear shell) in
301 the Mie calculation for all wavelengths. Studies suggest a group of organic matter (OM), known as
302 Brown Carbon (BrC), can absorb solar radiation at UV wavelengths (Kirchstetter et al., 2004). Thus,
303 a BrC coating (brown shell) scenario is also considered in Mie simulation following the wavelength-

304 dependent RI suggested by Lack and Cappa (2010), which ranges from 1.55-0.059i (370 nm) to 1.55-
305 0.0005i (950 nm). A modeling study by Bond et al. (2006) indicates that absorption amplification is
306 not sensitive to the RI, thus the result below is not expected to be sensitive to the RI variability. Due
307 to the spherical assumption of the BC core, a constant particle density is adopted for simplicity instead
308 of size dependent particle density. But it is worth noting that in reality, the effective density of soot
309 varies with particle size due to the morphology change during particle aging (Tavakoli and Olfert,
310 2014; Dastanpour et al., 2017). Both core diameters (D_{core}) and shell diameters (D_{shell}) are constrained
311 in the range of 10 ~ 3000 nm in the model simulations. The Mie calculations are implemented with a
312 customized program (Wu, 2017e) written in Igro Pro (WaveMetrics, Inc. Lake Oswego, OR, USA)
313 and it is available from <https://sites.google.com/site/wuchengust>. It should be noted that the core-shell
314 type mixing state of particles is still rare in 3D atmospheric models like WRF-Chem (Matsui et al.,
315 2013; Nordmann et al., 2014) due to computational cost limitation.

316 **3.2.1 Mie modeled absorption angstrom exponent (AAE)**

317 Absorption Angstrom Exponent (AAE) is a widely used parameter that describes the
318 wavelength dependence of aerosol light absorption (Moosmuller et al., 2011), which can be written
319 explicitly as

$$320 \quad AAE(\lambda_1, \lambda_2) = -\frac{\ln(\sigma_{abs,\lambda_1}) - \ln(\sigma_{abs,\lambda_2})}{\ln(\lambda_1) - \ln(\lambda_2)} \quad (7)$$

321 It is well known that ambient soot particles exhibit an AAE close to unity (Bond, 2001).
322 Modeled variability in $AAE_{470-660}$ of bare soot particles is shown in Figure S3. For soot particles with
323 $D_{\text{core}} < 200$ nm, $AAE_{470-660}$ is very close to 1 and decreases significantly for particles with $D_{\text{core}} > 200$
324 nm. Considering a typical D_{core} of fresh emitted soot particles smaller than 200 nm (Rose et al., 2006;
325 China et al., 2013), the model results confirm the frequently observed AAE close to 1 from ambient
326 measurements (Kirchstetter et al., 2004). Modeled variability in $AAE_{470-660}$ of soot particles coated by
327 non-absorbing substances (clear shell) and weakly absorbing materials (brown shell) is shown in
328 Figure 2. Elevated AAE to ~2 is observed in the clear shell scenario (Figure 2a and 3b) for the most
329 probable soot core particle sizes (<200 nm), which agrees well with a previous model study (Lack and

330 Cappa, 2010), implying that elevated AAE cannot be exclusively attributed to mixing with BrC. AAE
331 elevation is more pronounced in the brown shell scenario. For soot particles with $D_{\text{core}} < 200$ nm, brown
332 shell AAE₄₇₀₋₆₆₀ can easily reach 3 for a coating of $D_{\text{shell}}/D_{\text{core}}=3$ (Figure 2c and 2d). These high AAE
333 results are consistent with the previous model study (Lack and Cappa, 2010) and could partially
334 explain the high AAE observed in measurement studies (Kirchstetter et al., 2004; Hoffer et al., 2006),
335 since the presence of externally mixed BrC particles also contribute to the wavelength dependent light
336 absorption.

337 **3.2.2 Mie modeled single scattering albedo (SSA)**

338 Variability in modeled SSA of soot particles coated by non-absorbing substances and weakly
339 absorbing materials (e.g. BrC) is shown in Figure S4. For particles with $D_{\text{core}} < 200$ nm and $D_{\text{shell}}/D_{\text{core}}$
340 < 3 , the SSA increases gradually (up to ~ 0.9) with a thicker coating and behaves similarly between
341 clear shell and brown shell scenarios.

342 **3.2.3 Mie modeled mass absorption efficiency (MAE)**

343 MAE is a useful indicator for soot mixing state. Variability in MAE of bare soot particles as a
344 function of particle size at a wavelength of 550 nm is illustrated in Figure S5. The magnitude of MAE
345 is sensitive to the soot density assumption, especially for particles < 200 nm (Figure S5), but the overall
346 trend of particle size dependency is similar between different density scenarios. MAE peaks at a
347 particle size of 200 nm and decreases dramatically for larger particles. In our MAE calculation, a soot
348 density of 1.9 g cm^{-3} is adopted, as suggested by Bond and Bergstrom (2006). The purpose of adopting
349 constant density is to simplify the MAE calculation. It should be noted that the effective density of
350 soot core is highly variable in ambient environments. For example, a study in Beijing (Zhang et al.,
351 2016b) found a value of 1.2 g cm^{-3} . A recent chamber study found the effective density of soot can
352 evolve from 0.43 to 1.45 g cm^{-3} during aging as coated by m-Xylene oxidation products (Guo et al.,
353 2016). A study by a single-particle aerosol mass spectrometer in Guangzhou found the effective
354 density of soot increased with particle size in the range of 400 to 1600 nm (Zhang et al., 2016a). The
355 MAE of coated particles from different core/shell diameter combinations are shown in Figure S6. For

356 thickly coated particles, the MAE in the clear shell scenario varied as $D_{\text{shell}}/D_{\text{core}}$ increased, but the
357 MAE of brown shell scenario increased quasi-monotonously with $D_{\text{shell}}/D_{\text{core}}$.

358 **3.2.4 Mie modeled light absorption enhancement factor (E_{abs})**

359 E_{abs} is a better indicator for soot mixing state than MAE since it does not rely on the soot density
360 assumption and is more suitable for comparing Mie simulations with ambient measurements. Modeled
361 variability in E_{abs} of soot particles coated by non-absorbing substances and weakly absorbing materials
362 (e.g. BrC) is shown in Figure 3a and 3c respectively. E_{abs} is not only sensitive to the core/shell diameter
363 combination, but also behaves very differently on the clear and brown shell assumptions. For the clear
364 shell scenario, when $D_{\text{coat}}/D_{\text{core}} < 2$, E_{abs} does not exceed 2 for particles with different soot core sizes,
365 but for the same $D_{\text{coat}}/D_{\text{core}}$, a larger soot core size yields a higher E_{abs} (Figure 3b, cross-sections of
366 Figure 3a). If $D_{\text{coat}}/D_{\text{core}} > 2$, E_{abs} could be 3 to 5 for particles with a soot core smaller than 200 nm, but
367 for particles with a soot core larger than 200 nm, the E_{abs} is limited to ~ 2 as shown in Figure 3b. For
368 the brown shell scenario, E_{abs} increased quasi-monotonically with $D_{\text{coat}}/D_{\text{core}}$, and this trend is similar
369 for different soot core sizes (Figure 3d). **The main reason behind is that in the brown shell scenario,**
370 **both lensing effect and BrC absorption contribute to E_{abs} . As shown in Figure S7, the BrC absorption**
371 **contribution to total E_{abs} strongly depends on coating thickness and is insensitive to soot core diameters.**
372 **When the coating is relatively thin (< 5 nm for $\lambda@370$ nm, < 15 nm for $\lambda@550$ nm and < 40 nm for**
373 **$\lambda@880$ nm), BrC absorption contribution to the total E_{abs} is less than 20%. As the coating increases to**
374 **a certain level (~ 15 nm for $\lambda@370$ nm, ~ 35 nm for $\lambda@550$ nm and ~ 90 nm for $\lambda@880$ nm), BrC**
375 **absorption contribution is comparable to the lensing effect contribution, each contributing $\sim 50\%$ to**
376 **the total E_{abs} . When the BrC coating is sufficiently thick (> 30 nm for $\lambda@370$ nm, > 90 nm for $\lambda@550$**
377 **nm and > 110 nm for $\lambda@880$ nm), BrC absorption dominates the E_{abs} contribution. As a result, if BrC**
378 **coating is indeed present in ambient samples, a strong wavelength dependent E_{abs} could be observed,**
379 **since a BrC coating of 30 nm would be enough to induce a large amount of detectable E_{abs} in the UV**
380 **range. Another major difference between the clear and brown shell scenarios is that, for thickly coated**
381 **particles (e.g. $D_{\text{coat}}/D_{\text{core}} > 2$), the brown shell can yield a much higher E_{abs} than the clear shell.**

382 Both primary soot size distribution and coating thickness can affect the absorption
383 enhancement of ambient BC particles. Ambient measurements by LII found soot particle number and
384 mass modes peaking at 110 nm and 220 nm, respectively, in the PRD (Huang et al., 2011b). A study
385 in Shanghai found similar results (70 nm for number concentrations and 200 nm for mass
386 concentrations)(Gong et al., 2016). Considering that the LII technique is specific for BC mass
387 determination which is independent of BC mixing state, the size distribution reported by LII can
388 represent the size distribution of the BC core. A study using a Micro Orifice Uniform Deposit Impactor
389 (MOUDI) found a EC mass size distribution in the PRD exhibiting three modes peaking at ~300, ~900
390 and ~5000 nm (Yu et al., 2010), implying a substantial coating of BC particles, and a diameter
391 amplification of 3. BC sizing by LII is based on volume equivalent diameter (VED), while MOUDI is
392 based on aerodynamic diameter. As a result, these two techniques do not necessarily yield similar sizes,
393 even for the bare soot particles. The conversion between these two types of diameters involves the
394 knowledge of particle density and morphology (drag force). A recent closure study on BC mixing state
395 in the PRD region suggests σ_{abs} is dominated by coated soot particles in the range of 300~400 nm
396 (Tan et al., 2016). Considering the dominant BC core distribution measured by SP2 (110 nm), the
397 upper limit of E_{abs} in the PRD is roughly estimated as ~2 for the clear shell scenario (Figure 3b).

398 4 Results and discussions

399 4.1 Annual measurement statistics

400 The frequency distribution (log-normal) of σ_{abs550} is shown in Figure 4a, with an annual average (± 1
401 S.D.) of $42.65 \pm 30.78 \text{ Mm}^{-1}$. A log-normal distribution is also found in the EC mass concentration
402 (Figure 4b), with an annual average of $2.66 \pm 2.27 \mu\text{g m}^{-3}$. Figure 4c demonstrates the yearlong
403 frequency distribution of MAE_{550} at the NC site. The annual average MAE_{550} is $18.75 \pm 6.16 \text{ m}^2 \text{ g}^{-1}$ and
404 the peak (± 1 S.D.) of the lognormal fit is $15.70 \pm 0.22 \text{ m}^2 \text{ g}^{-1}$. A good correlation is observed between
405 σ_{abs} and EC mass ($R^2=0.92$) as shown in Figure 4d, and the color coding indicates a MAE dependency
406 on RH (the RH effect will be discussed in section 4.5). Annual average $AAE_{470-660}$ is 1.09 ± 0.13 (Figure
407 S8a), indicating that soot is the dominant absorbing substance in the PRD and the brown shell scenario

408 shown in the Mie simulation is unlikely to be important. Annual mean SSA₅₂₅ is 0.86±0.05 (Figure
 409 S8c), similar to previous studies in the PRD (Jung et al., 2009; Wu et al., 2009). For comparison
 410 purpose, MAE measured at original wavelength and MAE scaled to 550 nm following the λ^{-1}
 411 assumption are both shown in Table S1. The MAE comparisons discussed below are MAE at 550 nm.
 412 MAE₅₅₀ by previous studies at various locations was found to cover a wide range, from 5.9 to 61.6 m²
 413 g⁻¹. Annual average observed MAE₅₅₀ at NC (18.75 m² g⁻¹) is higher than many studies shown in Figure
 414 5, e.g., Shenzhen (Lan et al., 2013), Beijing (Yang et al., 2009), Mexico city (Doran et al., 2007) and
 415 Fresno (Chow et al., 2009).

416 As shown in Figure 1, the annual average MAE_{p,550} estimated by MRS is 13 m² g⁻¹. MAE_p by
 417 MRS represents the MAE_p at the emission source, which is different from the MAE_p by the TD
 418 approach for two reasons. First, the morphology of thermally denuded BC particles (compact
 419 aggregates) is different from that of freshly emitted BC particles (chain-like aggregates). Second, most
 420 of the coatings are removed for TD denuded soot particles, but freshly emitted soot particles usually
 421 come with a thin coating of OC formed from condensation of OC vapors as the temperature drops from
 422 the flame to the ambient air. As a result, the MRS-derived MAE_p is expected to be higher than the
 423 MAE_p by the TD approach. The estimated MAE_{p,550} is higher than a previous study in Guangzhou
 424 (7.44 m² g⁻¹) (Andreae et al., 2008), but comparable to Xi'an (11.34 m² g⁻¹) (Wang et al., 2014) and
 425 Toronto (9.53~12.57 m² g⁻¹) (Knox et al., 2009). The annual average E_{abs550} by MRS following Eq. 3
 426 is estimated to be 1.50±0.48 (mean ± 1 S.D.).

427 It should be noted that the E_{abs} estimation approach demonstrated here is insensitive to the MAE
 428 bias (e.g. overestimation of σ_{abs} and variability of EC mass by different TOA protocols) discussed in
 429 section 2.1, because bias in EC mass or σ_{abs} is cancelled out in the E_{abs} calculation (Eq. 3), since E_{abs}
 430 is the ratio of $\sigma_{abs,t}$ to $\sigma_{abs,p}$. To investigate the performance of the MRS approach in response to
 431 systematic bias in EC and σ_{abs} , two simple tests are conducted as shown in Figures S9 and S10 by
 432 adding systematic biases to σ_{abs550} and EC. Test A represents a situation when σ_{abs} is overestimated
 433 and EC is underestimated. The biased data are marked as σ'_{abs550} and EC' respectively, as shown
 434 below:

$$435 \quad \sigma'_{abs550} = \sigma_{abs550} \times 2 \quad (8)$$

$$436 \quad EC' = EC \times 0.7 \quad (9)$$

437 As a result, the average MAE₅₅₀ changed from 18.75 to 53.58 m² g⁻¹ and MAE_p changed from 13 to 37
438 m² g⁻¹ (Figure S9). However, E_{abs} by ratio of averages remain the same (1.44).

439 In Test B, EC by different TOA protocols are compared to investigate the effect of different EC
440 determination approaches while σ_{abs550} remains unchanged. EC by IMPROVE TOR protocol is
441 calculated from NIOSH TOT EC following an empirical formula for suburban sites derived from a 3-
442 year OCEC dataset in PRD (Wu et al., 2016a):

$$443 \quad EC_{IMP_TOR} = 2.63 \times EC_{NSH_TOT} + 0.05 \quad (10)$$

444 As shown in Figure S10, MAE₅₅₀ changed from 18.75 to 7.02 m² g⁻¹ and MAE_p changed from 13 to 5
445 m² g⁻¹, but E_{abs} remain almost the same (1.40). Result of Test B implies that although EC is
446 operationally defined, the discrepancy of EC between TOA protocols did not weaken the role of EC
447 serving as a tracer for primary emissions in MRS application. These examples demonstrate that
448 systematic biases in σ_{abs550} and EC have no effects on E_{abs} estimation by the MRS approach.

449 As mentioned in section 1, the definition of MAE_p by the TD approach is different from the
450 MAE_p of emission source. The TD MAE_p is expected to be slightly lower than the MAE_p of emission
451 source. Therefore, the corresponding E_{abs} are slightly different and it should be cautioned when
452 comparing MRS-derived E_{abs} with E_{abs} by the TD approach and Mie simulations. The E_{abs} could vary
453 by location, depending on the coating thickness and size distribution of the primary aerosols. After
454 undergoing atmospheric aging, the E_{abs} can be increased during transport from emission source to rural
455 areas. The magnitude of the E_{abs} found at the NC site is comparable to other locations such as Boulder
456 (Lack et al., 2012a) (1.38), London (Liu et al., 2015) (1.4), Shenzhen (Lan et al., 2013) (1.3), Yuncheng
457 (Cui et al., 2016b) (2.25), Jinan (Chen et al., 2017) (2.07) and Nanjing (Cui et al., 2016a) (1.6) and is
458 higher than studies in California (Cappa et al., 2012) (1.06), as listed in Table 3. Spectrum E_{abs} are
459 calculated from 370 to 950 nm as shown in Figure S11. E_{abs} in the PRD exhibits a weak wavelength
460 dependence, with slightly higher E_{abs} at the shorter wavelength (e.g. E_{abs370} = 1.55) and is relatively
461 lower in the IR range (e.g. E_{abs950} = 1.49).

462 **4.2 Monthly characteristics of MAE, AAE and SSA**

463 Monthly variations of MAE_{550} at the NC site are shown in Figure 6a and Table S2, revealing distinct
464 patterns of higher MAE_{550} in summer and lower in winter. On the other hand, $AAE_{470-660}$ is lower in
465 summer and higher in winter (Figure 6b and Table S3). Monthly SSA_{525} varied from 0.83 to 0.90
466 without a clear seasonal pattern, as shown in Figure S12 and Table S4. $MAE_{p,550}$ estimation for
467 individual months is shown in Figure 6a (the purple line) and monthly E_{abs550} is calculated accordingly
468 following Eq. 3 (Figure 6c). E_{abs550} shows clear seasonal variations, with higher values from April to
469 August (1.52~1.97 as shown in Table S5) and relatively lower values from September to March
470 (1.24~1.49). The highest enhancement is found in August (1.97). Factors affecting variation of E_{abs550}
471 are discussed in the following sections, including air mass origin, biomass burning and RH.

472 **4.3 The effect of air mass origin**

473 It's of interest to understand the seasonal variations of optical properties in the PRD. Hourly backward
474 trajectories for the past 72 hours were calculated using NOAA's HYSPLIT (Hybrid Single Particle
475 Lagrangian Integrated Trajectory, version 4) model (Draxier and Hess, 1998) from Feb 2012 to Jan
476 2013 as shown in Figure S13. Cluster analysis was conducted using MeteoInfo (Wang, 2014). By
477 examining the total spatial variance (TSV), the number of clusters was determined to be four as shown
478 in Figure S14. Cluster 1 (C1) represents continental air masses from the north, accounting for 44.4%
479 of total trajectories. C2 (22.8%) represents marine air masses coming from the South China Sea. C3
480 represents air masses from the east (Taiwan island). C4 (15.8%) represents transitional air masses
481 coming from the east coastline of China. As shown in Figure 7, E_{abs550} from C2 (1.78) is higher than
482 other clusters (1.30 – 1.42). Further Wilcoxon-Mann-Whitney tests show that E_{abs550} from C2 is
483 significantly higher than E_{abs550} from C1, C3 and C4 (Figure S15), implying that particles from the
484 South China Sea cluster is likely more aged than other clusters. Air mass origin in the PRD is
485 dominated by C2 from Apr to Aug (Figure S16a) as a result of the South China Sea monsoon in the
486 rainy season. In contrast, the dry season is ruled by continental air masses from the north (C1) due to
487 the influence of the northeast monsoon. E_{abs550} from C2 varied from 1.67 to 2.19, but was always

488 higher than $E_{\text{abs}550}$ from C1 and C3 during the rainy season (Figure S16b). As a result, the domination
489 of aged air mass from the vast ocean is one of the reasons for the much higher $E_{\text{abs}550}$ found in the rainy
490 season.

491 **4.4 The effect of biomass burning**

492 Biomass burning (BB) and vehicular emission are the two major sources of soot particles. BC
493 from biomass burning emission, depending on the fuel type and burning condition, may have a higher
494 OC/EC ratio and a thicker coating, resulting in a higher MAE than vehicular emission (Shen et al.,
495 2013; Cheng et al., 2016). In this study, the influence of BB on optical properties is investigated using
496 the K^+/EC ratio as a BB indicator. As shown in Figure 8, MAE_{550} is positively correlated with the
497 K^+/EC ratio, which exhibits a clear seasonal pattern that is higher in the rainy season and lower in the
498 dry season (Figure S17a). Southeast Asia has the highest fire emission density globally due to the high
499 biofuel consumption along with frequent fire activity in this region (Aouizerats et al., 2015), making
500 Southeast Asia a large contributor to BC emissions (Jason Blake, 2014). During the rainy season when
501 oceanic wind prevails, BC from BB emission in Southeast Asia can reach PRD through long range
502 transport (LRT), resulting in an elevated K^+/EC ratio and MAE_{550} . The Deming regression intercept
503 (11.89) in Figure 8 represents the MAE without the BB effect. This non-BB MAE_{550} ($11.89 \text{ m}^2 \text{ g}^{-1}$) is
504 only slightly lower than $\text{MAE}_{\text{p},550}$ ($13 \text{ m}^2 \text{ g}^{-1}$) obtained in section 4.3, implying that a large fraction of
505 $\text{MAE}_{\text{p},550}$ could not be explained by the BB source. Additional evidence was obtained through
506 examining regression relationships of $\text{MAE}_{\text{p},550}$ with K^+/EC month-by-month (Figure S17b).
507 Correlation of monthly $\text{MAE}_{\text{p},550}$ vs. K^+/EC ratio yield a R^2 of 0.23 (Figure S17c). In contrast, a much
508 higher correlation ($R^2=0.58$) was observed (Figure S17d) between $\text{MAE}_{\text{p},550}$ and non-BB MAE_{550} (i.e.,
509 K^+/EC intercepts from Figure S17b). These results imply that BB is one of the contributors to the
510 $\text{MAE}_{\text{p},550}$ variations, but unlikely the dominating one.

511 Many studies have found that BB influenced samples exhibit elevated AAE due to the presence
512 of wavelength dependent light absorbing substances like BrC and HUmic-Like Substances (HULIS)
513 (Kirchstetter et al., 2004; Hoffer et al., 2006; Sandradewi et al., 2008; Herich et al., 2011; Pokhrel et
514 al., 2017). It is of interest to investigate whether elevated AAE observed in the PRD during the dry

515 season is associated with BB influence. As shown in Figure S18, $AAE_{370-470}$ and $AAE_{470-660}$ did not
516 correlate with the BB indicator, K^+/EC ratio. These results suggest that the elevated AAE observed in
517 the PRD wintertime is unlikely to be dominated by the BB effect. Beside the independency between
518 $AAE_{470-660}$ and K^+/EC ratio, the measured $AAE_{470-660}$ range also implies that BB is not the major
519 driving force of $AAE_{470-660}$ variations. The limited light absorption contribution from BrC in RPD
520 region is observed in a recent study (Yuan et al., 2016) , which suggest an upper limit of BrC
521 contribution of 10% at 405 nm in the winter time using the AAE approach. As discussed in our Mie
522 simulation (section 3.1) and a previous study (Lack and Cappa, 2010), coating of non-absorbing
523 materials onto soot particles can increase AAE up to 2. Since the monthly average $AAE_{470-660}$ in
524 wintertime did not exceed 1.2 (Table S3), the variations of $AAE_{470-660}$ in the PRD are more likely
525 associated with coatings rather than the contribution of BrC. The results also imply that attempts on
526 BrC absorption attribution for the PRD dataset presented in this study could be risky, considering that
527 elevation of AAE is actually dominated by coating (Lack and Langridge, 2013).

528 **4.5 The effect of relative humidity (RH) on optical properties**

529 Soot particles are relatively hydrophobic when freshly emitted, but tend to gain hygroscopicity
530 during atmospheric aging. Hygroscopic growth of coated laboratory generated model BC was reported
531 by McMeeking et al. (2011). Growth of ambient BC particle size by a factor of 1.4-1.6 under high RH
532 has been observed in a UK study (Liu et al., 2013). Located in the subtropical zone, RH plays an
533 important role on aerosol optical properties in the PRD region. The yearlong measurements at the NC
534 site provide a unique opportunity to investigate the effect of RH on aerosol optical properties, since
535 most existing ad hoc studies in the PRD only last for months. Liquid water content (LWC) was
536 calculated using the E-AIM (model 2) thermodynamic model (Clegg et al., 1998). As shown in Figure
537 S19, LWC on average accounted for a significant fraction (44%) of non-EC $PM_{2.5}$ mass, making it an
538 important component of $PM_{2.5}$ mass and due to high RH in the PRD. Previously, hygroscopic growth
539 was only considered for particle scattering in the IMPROVE formula for chemically resolved light
540 extinction budget studies. In this study $f(RH)$ of MAE was obtained from yearlong measurements as
541 shown in Figure 9a for $RH = 30 \sim 100\%$ and color coded for LWC. It clearly shows that MAE_{550}

542 measured in NC is positively correlated with RH and the enhancement can be fitted by a polynomial
543 equation. When RH is close to 100%, the LWC can account for 70% of PM_{2.5} mass. The maximum
544 $f(\text{RH})$ can reach 1.3, which is higher than the value found in Beijing (1.2) (Wu et al., 2016b), **but lower**
545 **than a numerical study (1.35) (Nessler et al., 2005)**. These results reveal that a large contribution of
546 E_{abs} is coming from high LWC under high RH in the PRD region. Because RH has a clear diurnal
547 pattern, it can affect the diurnal pattern of E_{abs} in the PRD. Since the RH effect on E_{abs} is rarely
548 considered in existing climate models, the inclusion of RH effect can reduce the uncertainty for
549 assessing BC's climate effect.

550 The $\text{AAE}_{470-660}$ dependency on RH is shown in Figure 9b. When RH is low (e.g. 30%), the
551 $\text{AAE}_{470-660}$ is around 1.25 and decreases to 1.10 as RH increases to 50%. $\text{AAE}_{470-660}$ remains around
552 1.12 when RH is 50-70%. Then $\text{AAE}_{470-660}$ decreases again when RH is higher than 70% and can reach
553 1 when RH is close to 100%. Since a higher RH results in hygroscopic growth and larger particle
554 diameters, the negative correlation between $\text{AAE}_{470-660}$ and RH provides a clue on soot particles'
555 primary diameter and mixing state. As shown in the Mie simulation in Figure 2b, for a particle with
556 D_{core} of 130 nm and $D_{\text{shell}}/D_{\text{core}}$ of 2 to 4, $\text{AAE}_{470-660}$ decreases as the coating increases, and the decrease
557 tapers off when $D_{\text{shell}}/D_{\text{core}} = 3$. The D_{core} obtained here (130nm) is comparable with D_{core} obtained
558 from SP2 measurements (110nm) in the PRD (Huang et al., 2011a).

559 **4.6 Implications for mixing state**

560 Quantitative direct measurements of BC mixing state and coating thickness are still challenging.
561 SP2 can estimate the coating thickness using a lag-time approach or a Mie calculation approach can
562 be employed, but both methods have a limited range in coating thickness and uncertainties arise from
563 the assumptions made during the retrieval. For example, recent studies found that the mass equivalent
564 diameter of soot core measured by SP2 could be underestimated due to density assumptions (Zhang et
565 al., 2016b). Although size distribution measurement is not available in this study, clues of mixing state
566 still can be derived from bulk measurements of optical properties. As discussed in section 4.4.1,
567 elevated $E_{\text{abs}550}$ observed in the rainy season is associated with aged air masses from a marine origin.
568 To probe the possible mixing state difference between dry and rainy season, $E_{\text{abs}550}$, SSA_{525} and

569 AAE₄₇₀₋₆₆₀ are used to narrow down the possible core-shell size range as shown in Figure S20. Monthly
 570 averages with one standard deviation of AAE₄₇₀₋₆₆₀, SSA₅₂₅ and E_{abs550} are used as constraints to extract
 571 the intersecting core-shell size range from Figure 2a, Figure S4 and Figure 3a. **January and August**
 572 **data are used to represent two different scenarios: elevated AAE₄₇₀₋₆₆₀ (1.19±0.11) with lower E_{abs550}**
 573 **(1.31±0.32) in dry season and low AAE₄₇₀₋₆₆₀ (1.04±0.09) with elevated E_{abs550} (1.97±0.71) in rainy**
 574 **season.** The results show that January and August have a very different core-shell size range: in
 575 January, the core and shell range are 100 ~ 160 nm and 120 ~ 250 nm, respectively; in August, the
 576 core and shell range are 120 ~ 165 nm and 170 ~ 430 nm, respectively. This confirms again that the
 577 soot particles in the rainy season are likely to have a thicker coating than in the dry season.

578 **5 Caveats of the MRS method in its applications to ambient data**

579 The data in this study is dominated by BC absorption that did not show much influence from
 580 BrC. However, extra care should be taken if the samples exhibit substantial BrC signature (e.g.
 581 AAE>2). Such situations are equivalent to the two-source scenarios discussed in our previous paper
 582 on the MRS method (Wu and Yu, 2016) and the major findings are described below. Two types of
 583 two-source scenarios are considered: two correlated primary sources (scenario A) and two independent
 584 primary sources (scenario B). In scenario A in which both BC and primary BrC are dominated by BB,
 585 using BC as a solo tracer to calculate the primary ratio (MAE_p) still works. In scenario B in which BC
 586 and primary BrC are independent, using BC alone to determine a single primary MAE_p could lead to
 587 a considerable bias in E_{abs} estimation. Alternatively, if a reliable primary BrC tracer is available, the
 588 corresponding MAE_{p,BrC} can be determined by MRS. With the knowledge of MAE_{p,BrC} and MAE_{p,BC}, light
 589 absorption by BC and BrC can be calculated separately and the E_{abs} can be determined using Eq. (11) :

$$590 \quad E_{abs} = \frac{\sigma_{abs,t}}{\sigma_{abs,p,BC} + \sigma_{abs,p,BrC}} = \frac{\sigma_{abs,t}}{MAE_{p,BC} \times EC + MAE_{p,BrC} \times BrC} \quad (11)$$

591 However, the implementation of Eq.11 is challenging due to the complexity in the chemical
 592 composition of BrC. For example, a recent study found that the 20 most absorbing BrC chromophores
 593 account for ~50% BrC light absorption and there is not a single compound contributing more than 10%
 594 (Lin et al., 2016), making it difficult to choose a single compound as the BrC tracer. In addition, time

595 resolved measurement of BrC chromophores has yet to emerge. As a result, for scenario B (sample
596 AAE>2 & primary BrC variations independent of BC), estimation of E_{abs} by MRS is not practical at
597 this stage due to the lack of required input data. Using BC alone to determine a single primary MAE_p
598 could lead to a considerable bias and should be avoided.

599 **6 Conclusions**

600 In this study, a novel statistical approach is proposed and its application on ambient data is
601 demonstrated using one-year hourly OC and EC data coupled with Aethalometer measurements.
602 Unlike conventional E_{abs} determination approaches that require expensive instrumentation (e.g. TD-
603 PAS, VTDMA, SP2), this new approach employs widely deployed instruments (field carbon analyzer
604 and Aethalometer). The key of this new approach involves calculating MAE_p by the Minimum R
605 Squared (MRS) method (Wu and Yu, 2016). It is found that E_{abs} estimation by MRS is insensitive to
606 systematic biases in EC and σ_{abs} measurements. The annual average MAE_{p,550} estimated by MRS is
607 $13 \text{ m}^2 \text{ g}^{-1}$ and annual average MAE₅₅₀ is $18.75 \pm 6.16 \text{ m}^2 \text{ g}^{-1}$, suggesting an annual average enhancement
608 factor (E_{abs550}) of 1.50 ± 0.48 . This value is within the upper limit of E_{abs} (~ 2) by core-shell Mie
609 simulations considering the typical soot size distribution and coating thickness in the PRD.

610 Both MAE_{p,550} and E_{abs} show distinct seasonal variations, implying the complexity of soot
611 particle mixing state variations in this region. The elevated summertime E_{abs550} in the PRD is found to
612 be associated with the domination of aged air masses from the South China Sea, along with the long-
613 range transport of biomass burning influenced air masses from Southeast Asia. Hygroscopic growth
614 with elevated RH contributes to E_{abs} as well, which could be as high as 1.3. A negative correlation is
615 found between AAE₄₇₀₋₆₆₀ and RH, suggesting a dominant particle size with a D_{core} of 130 nm and
616 D_{shell}/D_{core} range of 2 to 4. Core-shell size ranges narrowed down by E_{abs550} and AAE₄₇₀₋₆₆₀ constraints
617 suggest that soot particles in the rainy season are likely to have thicker coatings than in the dry season.

618 **Data availability**

619 OC, EC, inorganic ions and σ_{abs} data used in this study are available from corresponding authors
620 upon request.

621

622 **Acknowledgements**

623 This work is supported by the National Natural Science Foundation of China (41605002, 41475004).

624 We gratefully acknowledge the Fok Ying Tung Foundation for funding to the Atmospheric Research
625 Center at HKUST Fok Ying Tung Graduate School. The authors thank Jingxiang Huang of Fok Ying
626 Tung Graduate School for the assistance in OCEC analyzer maintenance. The authors are also grateful
627 to Dr. Stephen M Griffith and Dr. Yongjie Li for the helpful comments. The authors gratefully
628 acknowledge the NOAA Air Resources Laboratory (ARL) for the provision of the HYSPLIT transport
629 and dispersion model used in this publication.

630 **References**

631

- 632 Adler, G., Riziq, A. A., Erlick, C., and Rudich, Y.: Effect of intrinsic organic carbon on the optical
633 properties of fresh diesel soot, *Proceedings of the National Academy of Sciences*, 107, 6699-6704, doi:
634 10.1073/pnas.0903311106, 2010.
- 635 Ajtai, T., Filep, Á., Utry, N., Schnaiter, M., Linke, C., Bozóki, Z., Szabó, G., and Leisner, T.: Inter-
636 comparison of optical absorption coefficients of atmospheric aerosols determined by a multi-
637 wavelength photoacoustic spectrometer and an Aethalometer under sub-urban wintry conditions, *J.*
638 *Aerosol. Sci.*, 42, 859-866, doi: 10.1016/j.jaerosci.2011.07.008, 2011.
- 639 Alexander, D. T. L., Crozier, P. A., and Anderson, J. R.: Brown carbon spheres in East Asian outflow
640 and their optical properties, *Science*, 321, 833-836, 2008.
- 641 Andreae, M. O., Schmid, O., Yang, H., Chand, D., Yu, J. Z., Zeng, L. M., and Zhang, Y. H.: Optical
642 properties and chemical composition of the atmospheric aerosol in urban Guangzhou, China, *Atmos.*
643 *Environ.*, 42, 6335-6350, doi: 10.1016/j.atmosenv.2008.01.030, 2008.
- 644 Aouizerats, B., van der Werf, G. R., Balasubramanian, R., and Betha, R.: Importance of transboundary
645 transport of biomass burning emissions to regional air quality in Southeast Asia during a high fire
646 event, *Atmos. Chem. Phys.*, 15, 363-373, doi: 10.5194/acp-15-363-2015, 2015.
- 647 Arnott, W. P., Moosmuller, H., Sheridan, P. J., Ogren, J. A., Raspet, R., Slaton, W. V., Hand, J. L.,
648 Kreidenweis, S. M., and Collett, J. L.: Photoacoustic and filter-based ambient aerosol light absorption
649 measurements: Instrument comparisons and the role of relative humidity, *J. Geophys. Res.*, 108, 2003.
- 650 Arnott, W. P., Hamasha, K., Moosmuller, H., Sheridan, P. J., and Ogren, J. A.: Towards aerosol light-
651 absorption measurements with a 7-wavelength Aethalometer: Evaluation with a photoacoustic
652 instrument and 3-wavelength nephelometer, *Aerosol. Sci. Technol.*, 39, 17-29, doi: Doi
653 10.1080/027868290901972, 2005.
- 654 Bauer, J. J., Yu, X.-Y., Cary, R., Laulainen, N., and Berkowitz, C.: Characterization of the sunset semi-
655 continuous carbon aerosol analyzer, *J. Air Waste Manage. Assoc.*, 59, 826-833, doi: 10.3155/1047-
656 3289.59.7.826, 2009.
- 657 Bohren, C. F. and Huffman, D. R.: *Absorption and scattering of light by small particles*, Wiley, New
658 York, xiv, 530 p. pp., 1983.
- 659 Bond, T. C.: Spectral dependence of visible light absorption by carbonaceous particles emitted from
660 coal combustion, *Geophys. Res. Lett.*, 28, 4075-4078, doi: Doi 10.1029/2001gl013652, 2001.
- 661 Bond, T. C. and Bergstrom, R. W.: Light absorption by carbonaceous particles: An investigative
662 review, *Aerosol. Sci. Technol.*, 40, 27-67, doi: Doi 10.1080/02786820500421521, 2006.
- 663 Bond, T. C., Habib, G., and Bergstrom, R. W.: Limitations in the enhancement of visible light
664 absorption due to mixing state, *J. Geophys. Res.*, 111, -, 2006.
- 665 Bond, T. C., Zarzycki, C., Flanner, M. G., and Koch, D. M.: Quantifying immediate radiative forcing
666 by black carbon and organic matter with the Specific Forcing Pulse, *Atmos. Chem. Phys.*, 11, 1505-
667 1525, doi: 10.5194/acp-11-1505-2011, 2011.
- 668 Cappa, C. D., Lack, D. A., Burkholder, J. B., and Ravishankara, A. R.: Bias in Filter-Based Aerosol
669 Light Absorption Measurements Due to Organic Aerosol Loading: Evidence from Laboratory
670 Measurements, *Aerosol. Sci. Technol.*, 42, 1022-1032, doi: 10.1080/02786820802389285, 2008.

671 Cappa, C. D., Onasch, T. B., Massoli, P., Worsnop, D. R., Bates, T. S., Cross, E. S., Davidovits, P.,
672 Hakala, J., Hayden, K. L., Jobson, B. T., Kolesar, K. R., Lack, D. A., Lerner, B. M., Li, S.-M., Mellon,
673 D., Nuaaman, I., Olfert, J. S., Petäjä, T., Quinn, P. K., Song, C., Subramanian, R., Williams, E. J., and
674 Zaveri, R. A.: Radiative Absorption Enhancements Due to the Mixing State of Atmospheric Black
675 Carbon, *Science*, 337, 1078-1081, doi: 10.1126/science.1223447, 2012.

676 Chan, T. W., Brook, J. R., Smallwood, G. J., and Lu, G.: Time-resolved measurements of black carbon
677 light absorption enhancement in urban and near-urban locations of southern Ontario, Canada, *Atmos.*
678 *Chem. Phys.*, 11, 10407-10432, 2011.

679 Chen, B., Bai, Z., Cui, X., Chen, J., Andersson, A., and Gustafsson, Ö.: Light absorption enhancement
680 of black carbon from urban haze in Northern China winter, *Environ Pollut*, 221, 418-426, doi:
681 10.1016/j.envpol.2016.12.004, 2017.

682 Cheng, Y., Engling, G., Moosmüller, H., Arnott, W. P., Chen, L. W. A., Wold, C. E., Hao, W. M., and
683 He, K.-b.: Light absorption by biomass burning source emissions, *Atmos. Environ.*, 127, 347-354, doi:
684 10.1016/j.atmosenv.2015.12.045, 2016.

685 China, S., Mazzoleni, C., Gorkowski, K., Aiken, A. C., and Dubey, M. K.: Morphology and mixing
686 state of individual freshly emitted wildfire carbonaceous particles, *Nat Commun*, 4, doi:
687 10.1038/ncomms3122, 2013.

688 Chow, J. C., Watson, J. G., Doraiswamy, P., Chen, L. W. A., Sodeman, D. A., Lowenthal, D. H., Park,
689 K., Arnott, W. P., and Motallebi, N.: Aerosol light absorption, black carbon, and elemental carbon at
690 the Fresno Supersite, California, *Atmos Res*, 93, 874-887, doi: DOI 10.1016/j.atmosres.2009.04.010,
691 2009.

692 Clegg, S. L., Brimblecombe, P., and Wexler, A. S.: Thermodynamic Model of the System
693 $H^+ - NH_4^+ - SO_4^{2-} - NO_3^- - H_2O$ at Tropospheric Temperatures, *The Journal of Physical Chemistry A*,
694 102, 2137-2154, doi: 10.1021/jp973042r, 1998.

695 Coen, M. C., Weingartner, E., Apituley, A., Ceburnis, D., Fierz-Schmidhauser, R., Flentje, H.,
696 Henzing, J. S., Jennings, S. G., Moerman, M., Petzold, A., Schmid, O., and Baltensperger, U.:
697 Minimizing light absorption measurement artifacts of the Aethalometer: evaluation of five correction
698 algorithms, *Atmos. Meas. Tech.*, 3, 457-474, doi: 10.5194/amt-3-457-2010, 2010.

699 Cui, F., Chen, M., Ma, Y., Zheng, J., Zhou, Y., Li, S., Qi, L., and Wang, L.: An intensive study on
700 aerosol optical properties and affecting factors in Nanjing, China, *Journal of Environmental Sciences*,
701 40, 35-43, doi: 10.1016/j.jes.2015.08.017, 2016a.

702 Cui, X., Wang, X., Yang, L., Chen, B., Chen, J., Andersson, A., and Gustafsson, Ö.: Radiative
703 absorption enhancement from coatings on black carbon aerosols, *Sci.Total.Environ.*, 551, 51-56, doi:
704 10.1016/j.scitotenv.2016.02.026, 2016b.

705 Dastanpour, R., Momenimovahed, A., Thomson, K., Olfert, J., and Rogak, S.: Variation of the optical
706 properties of soot as a function of particle mass, *Carbon*, 124, 201-211, doi:
707 10.1016/j.carbon.2017.07.005, 2017.

708 Ding, A. J., Huang, X., Nie, W., Sun, J. N., Kerminen, V. M., Petäjä, T., Su, H., Cheng, Y. F., Yang,
709 X. Q., Wang, M. H., Chi, X. G., Wang, J. P., Virkkula, A., Guo, W. D., Yuan, J., Wang, S. Y., Zhang,
710 R. J., Wu, Y. F., Song, Y., Zhu, T., Zilitinkevich, S., Kulmala, M., and Fu, C. B.: Enhanced haze
711 pollution by black carbon in megacities in China, *Geophys. Res. Lett.*, 43, 2873-2879, doi:
712 10.1002/2016GL067745, 2016.

713 Doran, J. C., Barnard, J. C., Arnott, W. P., Cary, R., Coulter, R., Fast, J. D., Kassianov, E. I., Kleinman,
714 L., Laulainen, N. S., Martin, T., Paredes-Miranda, G., Pekour, M. S., Shaw, W. J., Smith, D. F.,
715 Springston, S. R., and Yu, X. Y.: The T1-T2 study: evolution of aerosol properties downwind of
716 Mexico City, *Atmos. Chem. Phys.*, 7, 1585-1598, doi: 10.5194/acp-7-1585-2007, 2007.

717 Draxier, R. R. and Hess, G. D.: An overview of the HYSPLIT_4 modelling system for trajectories,
718 dispersion and deposition, *Aust Meteorol Mag*, 47, 295-308, 1998.

719 Drinovec, L., Gregorič, A., Zotter, P., Wolf, R., Bruns, E. A., Prévôt, A. S. H., Petit, J. E., Favez, O.,
720 Sciare, J., Arnold, I. J., Chakrabarty, R. K., Moosmüller, H., Filep, A., and Močnik, G.: The filter-
721 loading effect by ambient aerosols in filter absorption photometers depends on the coating of the
722 sampled particles, *Atmos. Meas. Tech.*, 10, 1043-1059, doi: 10.5194/amt-10-1043-2017, 2017.

723 Fuller, K. A., Malm, W. C., and Kreidenweis, S. M.: Effects of mixing on extinction by carbonaceous
724 particles, *J. Geophys. Res.*, 104, 15941-15954, 1999.

725 Gong, X., Zhang, C., Chen, H., Nizkorodov, S. A., Chen, J., and Yang, X.: Size distribution and mixing
726 state of black carbon particles during a heavy air pollution episode in Shanghai, *Atmos. Chem. Phys.*,
727 16, 5399-5411, doi: 10.5194/acp-16-5399-2016, 2016.

728 Guo, S., Hu, M., Lin, Y., Gomez-Hernandez, M., Zamora, M. L., Peng, J., Collins, D. R., and Zhang,
729 R.: OH-Initiated Oxidation of m-Xylene on Black Carbon Aging, *Environ. Sci. Technol.*, doi:
730 10.1021/acs.est.6b01272, 2016.

731 Guyon, P., Graham, B., Roberts, G. C., Mayol-Bracero, O. L., Maenhaut, W., Artaxo, P., and Andreae,
732 M. O.: Sources of optically active aerosol particles over the Amazon forest, *Atmos. Environ.*, 38, 1039-
733 1051, doi: 10.1016/j.atmosenv.2003.10.051, 2004.

734 Hansen, A. D. A.: *The Aethalometer Manual*, Berkeley, California, USA, Magee Scientific, 2005.

735 Hansen, J. and Nazarenko, L.: Soot climate forcing via snow and ice albedos, *P Natl Acad Sci USA*,
736 101, 423-428, doi: DOI 10.1073/pnas.2237157100, 2004.

737 Herich, H., Hueglin, C., and Buchmann, B.: A 2.5 year's source apportionment study of black carbon
738 from wood burning and fossil fuel combustion at urban and rural sites in Switzerland, *Atmos. Meas.*
739 *Tech.*, 4, 1409-1420, doi: DOI 10.5194/amt-4-1409-2011, 2011.

740 Hoffer, A., Gelencser, A., Guyon, P., Kiss, G., Schmid, O., Frank, G. P., Artaxo, P., and Andreae, M.
741 O.: Optical properties of humic-like substances (HULIS) in biomass-burning aerosols, *Atmos. Chem.*
742 *Phys.*, 6, 3563-3570, 2006.

743 Huang, X. F., Gao, R. S., Schwarz, J. P., He, L. Y., Fahey, D. W., Watts, L. A., McComiskey, A.,
744 Cooper, O. R., Sun, T. L., Zeng, L. W., Hu, M., and Zhang, Y. H.: Black carbon measurements in the
745 Pearl River Delta region of China, *J. Geophys. Res.*, 116, D12208, doi: 10.1029/2010jd014933, 2011a.

746 Huang, X. F., He, L. Y., Hu, M., Canagaratna, M. R., Kroll, J. H., Ng, N. L., Zhang, Y. H., Lin, Y.,
747 Xue, L., Sun, T. L., Liu, X. G., Shao, M., Jayne, J. T., and Worsnop, D. R.: Characterization of
748 submicron aerosols at a rural site in Pearl River Delta of China using an Aerodyne High-Resolution
749 Aerosol Mass Spectrometer, *Atmos. Chem. Phys.*, 11, 1865-1877, doi: 10.5194/acp-11-1865-2011,
750 2011b.

751 IPCC: Climate change 2013 : the physical science basis : Working Group I contribution to the Fifth
752 Assessment Report of the Intergovernmental Panel on Climate Change, xi, 1535 pages. pp., 2013.

753 Jacobson, M. Z.: Effects of externally-through-internally-mixed soot inclusions within clouds and
754 precipitation on global climate, *J Phys Chem A*, 110, 6860-6873, 2006.

755 Jason Blake, C.: Quantifying the occurrence and magnitude of the Southeast Asian fire climatology,
756 *Environmental Research Letters*, 9, 114018, 2014.

757 Jung, J., Lee, H., Kim, Y. J., Liu, X., Zhang, Y., Gu, J., and Fan, S.: Aerosol chemistry and the effect
758 of aerosol water content on visibility impairment and radiative forcing in Guangzhou during the 2006
759 Pearl River Delta campaign, *Journal of Environmental Management*, 90, 3231-3244, doi:
760 10.1016/j.jenvman.2009.04.021, 2009.

761 Khalizov, A. F., Xue, H. X., Wang, L., Zheng, J., and Zhang, R. Y.: Enhanced Light Absorption and
762 Scattering by Carbon Soot Aerosol Internally Mixed with Sulfuric Acid, *J Phys Chem A*, 113, 1066-
763 1074, 2009.

764 Kirchstetter, T. W., Novakov, T., and Hobbs, P. V.: Evidence that the spectral dependence of light
765 absorption by aerosols is affected by organic carbon, *J. Geophys. Res.*, 109, D21208, doi:
766 10.1029/2004jd004999, 2004.

767 Knox, A., Evans, G. J., Brook, J. R., Yao, X., Jeong, C. H., Godri, K. J., Sabaliauskas, K., and Slowik,
768 J. G.: Mass Absorption Cross-Section of Ambient Black Carbon Aerosol in Relation to Chemical Age,
769 *Aerosol. Sci. Technol.*, 43, 522-532, doi: Doi 10.1080/02786820902777207, 2009.

770 Koch, D. and Del Genio, A.: Black carbon semi-direct effects on cloud cover: review and synthesis,
771 *Atmos. Chem. Phys.*, 10, 7685-7696, 2010.

772 Kozlov, V. S., Panchenko, M. V., Tikhomirov, A. B., Tikhomirov, B. A., and Shmargunov, V. P.:
773 Effect of relative air humidity on photoacoustic aerosol absorption measurements in the near-ground
774 atmospheric layer, *Atmospheric and Oceanic Optics*, 24, 487, doi: 10.1134/s1024856011050101, 2011.

775 Laborde, M., Mertes, P., Zieger, P., Dommen, J., Baltensperger, U., and Gysel, M.: Sensitivity of the
776 Single Particle Soot Photometer to different black carbon types, *Atmos. Meas. Tech.*, 5, 1031-1043,
777 2012.

778 Lack, D. A. and Cappa, C. D.: Impact of brown and clear carbon on light absorption enhancement,
779 single scatter albedo and absorption wavelength dependence of black carbon, *Atmos. Chem. Phys.*, 10,
780 4207-4220, doi: DOI 10.5194/acp-10-4207-2010, 2010.

781 Lack, D. A., Langridge, J. M., Bahreini, R., Cappa, C. D., Middlebrook, A. M., and Schwarz, J. P.:
782 Brown carbon and internal mixing in biomass burning particles, *P Natl Acad Sci USA*, 109, 14802-
783 14807, doi: 10.1073/pnas.1206575109, 2012a.

784 Lack, D. A., Richardson, M. S., Law, D., Langridge, J. M., Cappa, C. D., McLaughlin, R. J., and
785 Murphy, D. M.: Aircraft instrument for comprehensive characterization of aerosol optical properties,
786 Part 2: black and brown carbon absorption and absorption enhancement measured with photo acoustic
787 spectroscopy, *Aerosol. Sci. Technol.*, 46, 555-568, 2012b.

788 Lack, D. A. and Langridge, J. M.: On the attribution of black and brown carbon light absorption using
789 the Ångström exponent, *Atmos. Chem. Phys.*, 13, 10535-10543, doi: 10.5194/acp-13-10535-2013,
790 2013.

791 Lan, Z.-J., Huang, X.-F., Yu, K.-Y., Sun, T.-L., Zeng, L.-W., and Hu, M.: Light absorption of black
792 carbon aerosol and its enhancement by mixing state in an urban atmosphere in South China, *Atmos.*
793 *Environ.*, 69, 118-123, doi: 10.1016/j.atmosenv.2012.12.009, 2013.

794 Langridge, J. M., Richardson, M. S., Lack, D. A., Brock, C. A., and Murphy, D. M.: Limitations of
795 the Photoacoustic Technique for Aerosol Absorption Measurement at High Relative Humidity,
796 *Aerosol. Sci. Technol.*, 47, 1163-1173, doi: 10.1080/02786826.2013.827324, 2013.

797 Leung, K. K., Schnitzler, E. G., Jäger, W., and Olfert, J. S.: Relative Humidity Dependence of Soot
798 Aggregate Restructuring Induced by Secondary Organic Aerosol: Effects of Water on Coating
799 Viscosity and Surface Tension, *Environmental Science & Technology Letters*, doi:
800 10.1021/acs.estlett.7b00298, 2017.

801 Lewis, K. A., Arnott, W. P., Moosmuller, H., Chakrabarty, R. K., Carrico, C. M., Kreidenweis, S. M.,
802 Day, D. E., Malm, W. C., Laskin, A., Jimenez, J. L., Ulbrich, I. M., Huffman, J. A., Onasch, T. B.,
803 Trimborn, A., Liu, L., and Mishchenko, M. I.: Reduction in biomass burning aerosol light absorption
804 upon humidification: roles of inorganically-induced hygroscopicity, particle collapse, and
805 photoacoustic heat and mass transfer, *Atmos. Chem. Phys.*, 9, 8949-8966, 2009a.

806 Lewis, K. A., Arnott, W. P., Moosmüller, H., Chakrabarty, R. K., Carrico, C. M., Kreidenweis, S. M.,
807 Day, D. E., Malm, W. C., Laskin, A., Jimenez, J. L., Ulbrich, I. M., Huffman, J. A., Onasch, T. B.,
808 Trimborn, A., Liu, L., and Mishchenko, M. I.: Reduction in biomass burning aerosol light absorption
809 upon humidification: roles of inorganically-induced hygroscopicity, particle collapse, and
810 photoacoustic heat and mass transfer, *Atmos. Chem. Phys.*, 9, 8949-8966, doi: 10.5194/acp-9-8949-
811 2009, 2009b.

812 Lin, P., Aiona, P. K., Li, Y., Shiraiwa, M., Laskin, J., Nizkorodov, S. A., and Laskin, A.: Molecular
813 Characterization of Brown Carbon in Biomass Burning Aerosol Particles, *Environ. Sci. Technol.*, 50,
814 11815-11824, doi: 10.1021/acs.est.6b03024, 2016.

815 Liu, D., Allan, J., Whitehead, J., Young, D., Flynn, M., Coe, H., McFiggans, G., Fleming, Z. L., and
816 Bandy, B.: Ambient black carbon particle hygroscopic properties controlled by mixing state and
817 composition, *Atmos. Chem. Phys.*, 13, 2015-2029, doi: 10.5194/acp-13-2015-2013, 2013.

818 Liu, D., Whitehead, J., Alfarra, M. R., Reyes-Villegas, E., Spracklen, D. V., Reddington, C. L., Kong,
819 S., Williams, P. I., Ting, Y.-C., Haslett, S., Taylor, J. W., Flynn, M. J., Morgan, W. T., McFiggans, G.,
820 Coe, H., and Allan, J. D.: Black-carbon absorption enhancement in the atmosphere determined by
821 particle mixing state, *Nature Geosci*, 10, 184-188, doi: 10.1038/ngeo2901, 2017.

822 Liu, F., Yon, J., and Bescond, A.: On the radiative properties of soot aggregates – Part 2: Effects of
823 coating, *Journal of Quantitative Spectroscopy and Radiative Transfer*, 172, 134-145, doi:
824 10.1016/j.jqsrt.2015.08.005, 2016a.

825 Liu, J., Lin, P., Laskin, A., Laskin, J., Kathmann, S. M., Wise, M., Caylor, R., Imholt, F., Selimovic,
826 V., and Shilling, J. E.: Optical properties and aging of light-absorbing secondary organic aerosol,
827 *Atmos. Chem. Phys.*, 16, 12815-12827, doi: 10.5194/acp-16-12815-2016, 2016b.

828 Liu, S., Aiken, A. C., Gorkowski, K., Dubey, M. K., Cappa, C. D., Williams, L. R., Herndon, S. C.,
829 Massoli, P., Fortner, E. C., Chhabra, P. S., Brooks, W. A., Onasch, T. B., Jayne, J. T., Worsnop, D. R.,
830 China, S., Sharma, N., Mazzoleni, C., Xu, L., Ng, N. L., Liu, D., Allan, J. D., Lee, J. D., Fleming, Z.
831 L., Mohr, C., Zotter, P., Szidat, S., and Prevot, A. S. H.: Enhanced light absorption by mixed source
832 black and brown carbon particles in UK winter, *Nat Commun*, 6, doi: 10.1038/ncomms9435, 2015.

833 Ma, N., Zhao, C. S., Muller, T., Cheng, Y. F., Liu, P. F., Deng, Z. Z., Xu, W. Y., Ran, L., Nekat, B.,
834 van Pinxteren, D., Gnauk, T., Mueller, K., Herrmann, H., Yan, P., Zhou, X. J., and Wiedensohler, A.:
835 A new method to determine the mixing state of light absorbing carbonaceous using the measured
836 aerosol optical properties and number size distributions, *Atmos. Chem. Phys.*, 12, 2381-2397, doi:
837 DOI 10.5194/acp-12-2381-2012, 2012.

838 Replacement Filter Tape for the Magee Scientific Model AE33 Aethalometer®:
839 http://www.mageesci.com/images/stories/docs/Magee_Scientific_Filter_Aethalometer_AE_Tape_Replacement_discussion.pdf, 2017.

841 Matsui, H., Koike, M., Kondo, Y., Moteki, N., Fast, J. D., and Zaveri, R. A.: Development and
842 validation of a black carbon mixing state resolved three-dimensional model: Aging processes and
843 radiative impact, *J. Geophys. Res.*, 118, 2304-2326, doi: 10.1029/2012JD018446, 2013.

844 McMeeking, G. R., Good, N., Petters, M. D., McFiggans, G., and Coe, H.: Influences on the fraction
845 of hydrophobic and hydrophilic black carbon in the atmosphere, *Atmos. Chem. Phys.*, 11, 5099-5112,
846 doi: 10.5194/acp-11-5099-2011, 2011.

847 McMeeking, G. R., Fortner, E., Onasch, T. B., Taylor, J. W., Flynn, M., Coe, H., and Kreidenweis, S.
848 M.: Impacts of nonrefractory material on light absorption by aerosols emitted from biomass burning,
849 *J. Geophys. Res.*, 119, 12,272-212,286, doi: 10.1002/2014JD021750, 2014.

850 Moffet, R. C., O'Brien, R. E., Alpert, P. A., Kelly, S. T., Pham, D. Q., Gilles, M. K., Knopf, D. A., and
851 Laskin, A.: Morphology and mixing of black carbon particles collected in central California during the
852 CARES field study, *Atmos. Chem. Phys.*, 16, 14515-14525, doi: 10.5194/acp-16-14515-2016, 2016.

853 Moosmuller, H., Chakrabarty, R. K., Ehlers, K. M., and Arnott, W. P.: Absorption Angstrom
854 coefficient, brown carbon, and aerosols: basic concepts, bulk matter, and spherical particles, *Atmos.*
855 *Chem. Phys.*, 11, 1217-1225, doi: DOI 10.5194/acp-11-1217-2011, 2011.

856 Moteki, N., Kondo, Y., and Adachi, K.: Identification by single-particle soot photometer of black
857 carbon particles attached to other particles: Laboratory experiments and ground observations in Tokyo,
858 *J. Geophys. Res.*, 119, 2013JD020655, doi: 10.1002/2013jd020655, 2014.

859 Nakayama, T., Ikeda, Y., Sawada, Y., Setoguchi, Y., Ogawa, S., Kawana, K., Mochida, M., Ikemori,
860 F., Matsumoto, K., and Matsumi, Y.: Properties of light-absorbing aerosols in the Nagoya urban area,
861 Japan, in August 2011 and January 2012: Contributions of brown carbon and lensing effect, *J. Geophys.*
862 *Res.*, 119, 2014JD021744, doi: 10.1002/2014JD021744, 2014.

863 Naoe, H., Hasegawa, S., Heintzenberg, J., Okada, K., Uchiyama, A., Zaizen, Y., Kobayashi, E., and
864 Yamazaki, A.: State of mixture of atmospheric submicrometer black carbon particles and its effect on
865 particulate light absorption, *Atmos. Environ.*, 43, 1296-1301, doi: 10.1016/j.atmosenv.2008.11.031,
866 2009.

867 Nessler, R., Weingartner, E., and Baltensperger, U.: Effect of humidity on aerosol light absorption and
868 its implications for extinction and the single scattering albedo illustrated for a site in the lower free
869 troposphere, *J. Aerosol. Sci.*, 36, 958-972, doi: 10.1016/j.jaerosci.2004.11.012, 2005.

870 Nordmann, S., Cheng, Y. F., Carmichael, G. R., Yu, M., Denier van der Gon, H. A. C., Zhang, Q.,
871 Saide, P. E., Pöschl, U., Su, H., Birmili, W., and Wiedensohler, A.: Atmospheric black carbon and
872 warming effects influenced by the source and absorption enhancement in central Europe, *Atmos. Chem.*
873 *Phys.*, 14, 12683-12699, doi: 10.5194/acp-14-12683-2014, 2014.

874 Pandey, A., Pervez, S., and Chakrabarty, R. K.: Filter-based measurements of UV-vis mass absorption
875 cross sections of organic carbon aerosol from residential biomass combustion: Preliminary findings
876 and sources of uncertainty, *Journal of Quantitative Spectroscopy and Radiative Transfer*, 182, 296-
877 304, doi: 10.1016/j.jqsrt.2016.06.023, 2016.

878 Peng, J., Hu, M., Guo, S., Du, Z., Zheng, J., Shang, D., Levy Zamora, M., Zeng, L., Shao, M., Wu, Y.-
879 S., Zheng, J., Wang, Y., Glen, C. R., Collins, D. R., Molina, M. J., and Zhang, R.: Markedly enhanced

880 absorption and direct radiative forcing of black carbon under polluted urban environments,
881 Proceedings of the National Academy of Sciences, 113, 4266-4271, doi: 10.1073/pnas.1602310113,
882 2016.

883 Pokhrel, R. P., Beamesderfer, E. R., Wagner, N. L., Langridge, J. M., Lack, D. A., Jayarathne, T.,
884 Stone, E. A., Stockwell, C. E., Yokelson, R. J., and Murphy, S. M.: Relative importance of black
885 carbon, brown carbon, and absorption enhancement from clear coatings in biomass burning emissions,
886 Atmos. Chem. Phys., 17, 5063-5078, doi: 10.5194/acp-17-5063-2017, 2017.

887 Ramanathan, V. and Carmichael, G.: Global and regional climate changes due to black carbon, Nat
888 Geosci, 1, 221-227, doi: Doi 10.1038/Ngeo156, 2008.

889 Raspert, R., Slaton, W. V., Arnott, W. P., and Moosmüller, H.: Evaporation–Condensation Effects on
890 Resonant Photoacoustics of Volatile Aerosols, Journal of Atmospheric and Oceanic Technology, 20,
891 685-695, doi: 10.1175/1520-0426(2003)20<685:eeceorp>2.0.co;2, 2003.

892 Reid, J. S., Eck, T. F., Christopher, S. A., Koppmann, R., Dubovik, O., Eleuterio, D. P., Holben, B. N.,
893 Reid, E. A., and Zhang, J.: A review of biomass burning emissions part III: intensive optical properties
894 of biomass burning particles, Atmos. Chem. Phys., 5, 827-849, doi: 10.5194/acp-5-827-2005, 2005.

895 Roden, C. A., Bond, T. C., Conway, S., and Pinel, A. B. O.: Emission factors and real-time optical
896 properties of particles emitted from traditional wood burning cookstoves, Environ. Sci. Technol., 40,
897 6750-6757, doi: 10.1021/es052080i, 2006.

898 Rose, D., Wehner, B., Ketzler, M., Engler, C., Voigtländer, J., Tuch, T., and Wiedensohler, A.:
899 Atmospheric number size distributions of soot particles and estimation of emission factors, Atmos.
900 Chem. Phys., 6, 1021-1031, doi: 10.5194/acp-6-1021-2006, 2006.

901 Saathoff, H., Naumann, K. H., Schnaiter, M., Schöck, W., Möhler, O., Schurath, U., Weingartner, E.,
902 Gysel, M., and Baltensperger, U.: Coating of soot and (NH₄)₂SO₄ particles by ozonolysis products of
903 α -pinene, J. Aerosol. Sci., 34, 1297-1321, doi: 10.1016/S0021-8502(03)00364-1, 2003.

904 Sandradewi, J., Prévôt, A. S. H., Weingartner, E., Schmidhauser, R., Gysel, M., and Baltensperger, U.:
905 A study of wood burning and traffic aerosols in an Alpine valley using a multi-wavelength
906 Aethalometer, Atmos. Environ., 42, 101-112, doi: 10.1016/j.atmosenv.2007.09.034, 2008.

907 Saturno, J., Pöhlker, C., Massabò, D., Brito, J., Carbone, S., Cheng, Y., Chi, X., Ditas, F., Hrabě de
908 Angelis, I., Morán-Zuloaga, D., Pöhlker, M. L., Rizzo, L. V., Walter, D., Wang, Q., Artaxo, P., Prati,
909 P., and Andreae, M. O.: Comparison of different Aethalometer correction schemes and a reference
910 multi-wavelength absorption technique for ambient aerosol data, Atmos. Meas. Tech., 10, 2837-2850,
911 doi: 10.5194/amt-10-2837-2017, 2017.

912 Schmid, O., Artaxo, P., Arnott, W. P., Chand, D., Gatti, L. V., Frank, G. P., Hoffer, A., Schnaiter, M.,
913 and Andreae, M. O.: Spectral light absorption by ambient aerosols influenced by biomass burning in
914 the Amazon Basin. I: Comparison and field calibration of absorption measurement techniques, Atmos.
915 Chem. Phys., 6, 3443-3462, 2006.

916 Schnaiter, M., Linke, C., Mohler, O., Naumann, K. H., Saathoff, H., Wagner, R., Schurath, U., and
917 Wehner, B.: Absorption amplification of black carbon internally mixed with secondary organic aerosol,
918 J. Geophys. Res., 110, -, 2005.

919 Schwarz, J. P., Spackman, J. R., Fahey, D. W., Gao, R. S., Lohmann, U., Stier, P., Watts, L. A.,
920 Thomson, D. S., Lack, D. A., Pfister, L., Mahoney, M. J., Baumgardner, D., Wilson, J. C., and Reeves,

921 J. M.: Coatings and their enhancement of black carbon light absorption in the tropical atmosphere, *J.*
922 *Geophys. Res.*, 113, -, 2008.

923 Sedlacek, A. J., Lewis, E. R., Kleinman, L., Xu, J. Z., and Zhang, Q.: Determination of and evidence
924 for non-core-shell structure of particles containing black carbon using the Single-Particle Soot
925 Photometer (SP2), *Geophys. Res. Lett.*, 39, 2012.

926 Shen, G., Chen, Y., Wei, S., Fu, X., Zhu, Y., and Tao, S.: Mass absorption efficiency of elemental
927 carbon for source samples from residential biomass and coal combustions, *Atmos. Environ.*, 79, 79-
928 84, doi: 10.1016/j.atmosenv.2013.05.082, 2013.

929 Shiraiwa, M., Kondo, Y., Iwamoto, T., and Kita, K.: Amplification of Light Absorption of Black
930 Carbon by Organic Coating, *Aerosol. Sci. Technol.*, 44, 46-54, 2010.

931 Suglia, S. F., Gryparis, A., Wright, R. O., Schwartz, J., and Wright, R. J.: Association of Black Carbon
932 with Cognition among Children in a Prospective Birth Cohort Study, *American Journal of*
933 *Epidemiology*, 167, 280-286, doi: 10.1093/aje/kwm308, 2008.

934 Tan, H., Liu, L., Fan, S., Li, F., Yin, Y., Cai, M., and Chan, P. W.: Aerosol optical properties and
935 mixing state of black carbon in the Pearl River Delta, China, *Atmos. Environ.*, 131, 196-208, doi:
936 10.1016/j.atmosenv.2016.02.003, 2016.

937 Tao, W. K., Chen, J. P., Li, Z. Q., Wang, C., and Zhang, C. D.: Impact of Aerosols on Convective
938 Clouds and Precipitation, *Rev Geophys*, 50, Rg2001, doi: Doi 10.1029/2011rg000369, 2012.

939 Tavakoli, F. and Olfert, J. S.: Determination of particle mass, effective density, mass–mobility
940 exponent, and dynamic shape factor using an aerodynamic aerosol classifier and a differential mobility
941 analyzer in tandem, *J. Aerosol. Sci.*, 75, 35-42, doi: 10.1016/j.jaerosci.2014.04.010, 2014.

942 ten Brink, H., Otjes, R., Jongejan, P., and Slanina, S.: An instrument for semi-continuous monitoring
943 of the size-distribution of nitrate, ammonium, sulphate and chloride in aerosol, *Atmos. Environ.*, 41,
944 2768-2779, doi: 10.1016/j.atmosenv.2006.11.041, 2007.

945 Turpin, B. J. and Huntzicker, J. J.: Secondary Formation of Organic Aerosol in the Los-Angeles Basin
946 - a Descriptive Analysis of Organic and Elemental Carbon Concentrations, *Atmos. Environ.*, 25, 207-
947 215, 1991.

948 Ueda, S., Nakayama, T., Taketani, F., Adachi, K., Matsuki, A., Iwamoto, Y., Sadanaga, Y., and
949 Matsumi, Y.: Light absorption and morphological properties of soot-containing aerosols observed at
950 an East Asian outflow site, Noto Peninsula, Japan, *Atmos. Chem. Phys.*, 16, 2525-2541, doi:
951 10.5194/acp-16-2525-2016, 2016.

952 Virkkula, A., Makela, T., Hillamo, R., Yli-Tuomi, T., Hirsikko, A., Hameri, K., and Koponen, I. K.:
953 A simple procedure for correcting loading effects of aethalometer data, *J. Air Waste Manage. Assoc.*,
954 57, 1214-1222, 2007.

955 Wang, Q., Huang, R., Zhao, Z., Cao, J., Ni, H., Tie, X., Zhu, C., Shen, Z., Wang, M., and Dai, W.:
956 Effects of photochemical oxidation on the mixing state and light absorption of black carbon in the
957 urban atmosphere of China, *Environmental Research Letters*, 12, 044012, 2017.

958 Wang, Q. Y., Huang, R. J., Cao, J. J., Han, Y. M., Wang, G. H., Li, G. H., Wang, Y. C., Dai, W. T.,
959 Zhang, R. J., and Zhou, Y. Q.: Mixing State of Black Carbon Aerosol in a Heavily Polluted Urban
960 Area of China: Implications for Light Absorption Enhancement, *Aerosol. Sci. Technol.*, 48, 689-697,
961 doi: 10.1080/02786826.2014.917758, 2014.

962 Wang, Y. Q.: *MeteoInfo: GIS software for meteorological data visualization and analysis*,
963 *Meteorological Applications*, 21, 360-368, doi: 10.1002/met.1345, 2014.

964 Weingartner, E., Saathoff, H., Schnaiter, M., Streit, N., Bitnar, B., and Baltensperger, U.: Absorption
965 of light by soot particles: determination of the absorption coefficient by means of aethalometers, *J.*
966 *Aerosol. Sci.*, 34, 1445-1463, doi: 10.1016/S0021-8502(03)00359-8, 2003.

967 Weyant, C. L., Shepson, P. B., Subramanian, R., Cambaliza, M. O. L., Heimbürger, A., McCabe, D.,
968 Baum, E., Stirm, B. H., and Bond, T. C.: Black Carbon Emissions from Associated Natural Gas Flaring,
969 *Environ. Sci. Technol.*, 50, 2075-2081, doi: 10.1021/acs.est.5b04712, 2016.

970 Wild, M.: Enlightening Global Dimming and Brightening, *B Am Meteorol Soc*, 93, 27-37, doi:
971 10.1175/bams-d-11-00074.1, 2011.

972 Wu, C., Ng, W. M., Huang, J., Wu, D., and Yu, J. Z.: Determination of Elemental and Organic Carbon
973 in PM_{2.5} in the Pearl River Delta Region: Inter-Instrument (Sunset vs. DRI Model 2001
974 Thermal/Optical Carbon Analyzer) and Inter-Protocol Comparisons (IMPROVE vs. ACE-Asia
975 Protocol), *Aerosol. Sci. Technol.*, 46, 610-621, doi: 10.1080/02786826.2011.649313, 2012.

976 Wu, C., Huang, X. H. H., Ng, W. M., Griffith, S. M., and Yu, J. Z.: Inter-comparison of NIOSH and
977 IMPROVE protocols for OC and EC determination: implications for inter-protocol data conversion,
978 *Atmos. Meas. Tech.*, 9, 4547-4560, doi: 10.5194/amt-9-4547-2016, 2016a.

979 Wu, C. and Yu, J. Z.: Determination of primary combustion source organic carbon-to-elemental carbon
980 (OC/EC) ratio using ambient OC and EC measurements: secondary OC-EC correlation minimization
981 method, *Atmos. Chem. Phys.*, 16, 5453-5465, doi: 10.5194/acp-16-5453-2016, 2016.

982 Wu, D., Mao, J. T., Deng, X. J., Tie, X. X., Zhang, Y. H., Zeng, L. M., Li, F., Tan, H. B., Bi, X. Y.,
983 Huang, X. Y., Chen, J., and Deng, T.: Black carbon aerosols and their radiative properties in the Pearl
984 River Delta region, *Sci China Ser D*, 52, 1152-1163, doi: 10.1007/s11430-009-0115-y, 2009.

985 Wu, D., Wu, C., Liao, B., Chen, H., Wu, M., Li, F., Tan, H., Deng, T., Li, H., Jiang, D., and Yu, J. Z.:
986 Black carbon over the South China Sea and in various continental locations in South China, *Atmos.*
987 *Chem. Phys.*, 13, 12257-12270, doi: 10.5194/acp-13-12257-2013, 2013.

988 Wu, Y., Zhang, R., Tian, P., Tao, J., Hsu, S. C., Yan, P., Wang, Q., Cao, J., Zhang, X., and Xia, X.:
989 Effect of ambient humidity on the light absorption amplification of black carbon in Beijing during
990 January 2013, *Atmos. Environ.*, 124, Part B, 217-223, doi: 10.1016/j.atmosenv.2015.04.041, 2016b.

991 Yang, M., Howell, S. G., Zhuang, J., and Huebert, B. J.: Attribution of aerosol light absorption to black
992 carbon, brown carbon, and dust in China - interpretations of atmospheric measurements during EAST-
993 AIRE, *Atmos. Chem. Phys.*, 9, 2035-2050, 2009.

994 Yu, H., Wu, C., Wu, D., and Yu, J. Z.: Size distributions of elemental carbon and its contribution to
995 light extinction in urban and rural locations in the pearl river delta region, China, *Atmos. Chem. Phys.*,
996 10, 5107-5119, doi: 10.5194/acp-10-5107-2010, 2010.

997 Yuan, J. F., Huang, X. F., Cao, L. M., Cui, J., Zhu, Q., Huang, C. N., Lan, Z. J., and He, L. Y.: Light
998 absorption of brown carbon aerosol in the PRD region of China, *Atmos. Chem. Phys.*, 16, 1433-1443,
999 doi: 10.5194/acp-16-1433-2016, 2016.

1000 Zhang, G., Bi, X., Qiu, N., Han, B., Lin, Q., Peng, L., Chen, D., Wang, X., Peng, P., Sheng, G., and
1001 Zhou, Z.: The real part of the refractive indices and effective densities for chemically segregated
1002 ambient aerosols in Guangzhou measured by a single-particle aerosol mass spectrometer, *Atmos.*
1003 *Chem. Phys.*, 16, 2631-2640, doi: 10.5194/acp-16-2631-2016, 2016a.

1004 Zhang, R. Y., Khalizov, A. F., Pagels, J., Zhang, D., Xue, H. X., and McMurry, P. H.: Variability in
1005 morphology, hygroscopicity, and optical properties of soot aerosols during atmospheric processing, P
1006 Natl Acad Sci USA, 105, 10291-10296, 2008.

1007 Zhang, Y., Zhang, Q., Cheng, Y., Su, H., Kecorius, S., Wang, Z., Wu, Z., Hu, M., Zhu, T.,
1008 Wiedensohler, A., and He, K.: Measuring the morphology and density of internally mixed black carbon
1009 with SP2 and VTDMA: new insight into the absorption enhancement of black carbon in the atmosphere,
1010 Atmos. Meas. Tech., 9, 1833-1843, doi: 10.5194/amt-9-1833-2016, 2016b.

1011

1012

1013 Table 1. Abbreviations.

1014

Abbreviation	Definition
AAE ₄₇₀₋₆₆₀	Absorption Angstrom Exponent between 470 and 660 nm
BB	Biomass burning
BrC	Brown Carbon
D _{core} , D _{shell}	Particle diameter of core/shell
E _{abs550}	Light absorption enhancement factor at 550 nm
σ_{abs550}	Light absorption coefficient at 550 nm
$\sigma_{abs,t}$	Total light absorption coefficient of a coated particle
$\sigma_{abs,p}$	Primary light absorption coefficient attributed to the soot core alone of a coated particle
$\sigma_{abs,c}$	Extra light absorption coefficient due to the lensing effect of coating on the soot core
LII	Laser induced incandescence technique for soot measurement
LWC	Liquid water content
MAE ₅₅₀	Mass absorption efficiency at 550 nm, also known as mass absorption cross-section (MAC)
MAE _{p,550}	Primary MAE of freshly emitted soot particles at 550 nm
MAAP	Multi Angle Absorption Photometer
MOUDI	Micro Orifice Uniform Deposit Impactor
MRS	Minimum R squared method
PAS	Photo acoustic spectrometer
PRD	Pearl River Delta region, China
SP2	Single particle soot photometer
SSA	Single scattering albedo
TD	Thermal denuder
TOA	Thermal optical analysis
TSV	Total spatial variance in backward trajectories cluster analysis

1015

1016 Table 2. Comparison of MRS application on $(OC/EC)_p$ (for SOC estimation) and MAE_p (for E_{abs} estimation).
 1017

	MRS in EC tracer method for SOC estimation (Wu and Yu, 2016)	MRS in EC tracer method for E_{abs} estimation (this study)
Key parameter of fresh EC particles to be determined	$\left(\frac{OC}{EC}\right)_p = \frac{POC}{EC}$	$MAE_p = \frac{O\sigma_{abs,p}}{EC}$
Input quantities for MRS from measurements	OC, EC (tracer)	$\sigma_{abs,t}$, EC (tracer)
Variable to be decoupled by the tracer	$OC = POC + SOC$ $= \left(\frac{OC}{EC}\right)_p \times EC + SOC$	$\sigma_{abs,t} = \sigma_{abs,p} + \sigma_{abs,c}$ $= \left(\frac{O\sigma_{abs,t}C}{EC}\right)_p \times EC + \sigma_{abs,c}$
Ambient measurement at its closest to fresh emissions	Minimum R^2 (SOC, EC) $SOC = OC - \left(\frac{OC}{EC}\right)_p \times EC$	Minimum R^2 ($\sigma_{abs,c}$, EC) $\sigma_{abs,c} = \sigma_{abs,t} - MAE_p \times EC$
Graph	<p>Minimum R^2 $(OC/EC)_p = 2.26$</p>	<p>Minimum R^2 $(OC/EC)_p = 13$</p>

1018

1019 Table 3. Comparison of E_{abs} between various studies.

1020

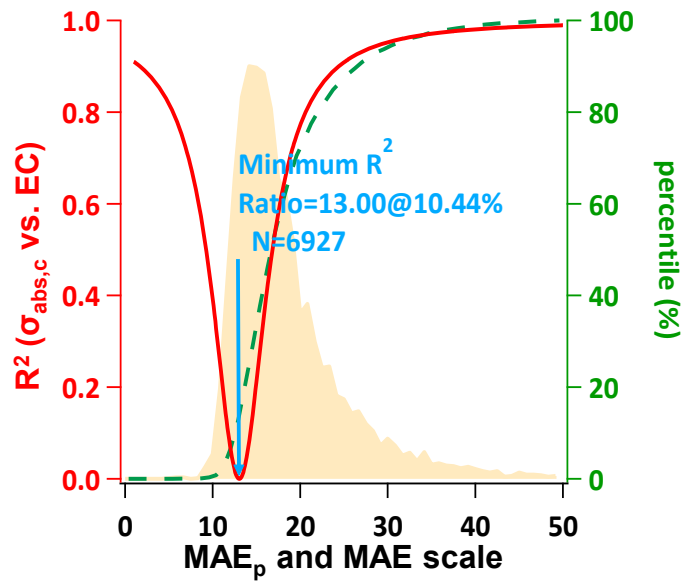
Location	Type	Sampling Duration	λ (nm)	Instrument	E_{abs}	Method	Reference
Guangzhou, China	Suburban	2012.2-2013.1	550	AE+OCEC	1.50±0.48	MAE	This study
Xi'an, China	Urban	2012.12-2013.1	870	PAS	1.8	MAE	(Wang et al., 2014)
Shenzhen, China	Urban	2011.8-9	532	PAS	1.3	MAE	(Lan et al., 2013)
Jinan, China	Urban	2014.2	678	OCEC	2.07 ± 0.72	AFD	(Chen et al., 2017)
Nanjing, China	Suburban	2012.11	532	PAS	1.6	MAE	(Cui et al., 2016a)
Boulder, USA	Forest fire	2010.9	532	PAS	1.38	TD 200°C	(Lack et al., 2012a)
London, UK	Rural	2012.2	781	PAS	1.4	TD 250°C	(Liu et al., 2015)
California, USA	Rural	2010.6	532	PAS	1.06	TD 250°C	(Cappa et al., 2012)
Noto Peninsula, Japan	Rural	2013.4-5	781	PAS	1.22	TD 300°C	(Ueda et al., 2016)
Yuncheng, China	Rural	2014.6-7	678	OCEC	2.25 ± 0.55	AFD	(Cui et al., 2016b)
San Jose, Costa Rica	Rural	2006 winter	1064	SP2	1.3	Mie+SP2	(Schwarz et al., 2008)

1021

AE: Aethalometer ; OCEC: OCEC analyzer; PAS: photo acoustic spectrometer; SP2: Single particle soot photometer; TD: Thermal denuder AFD: filter filtration-dissolution

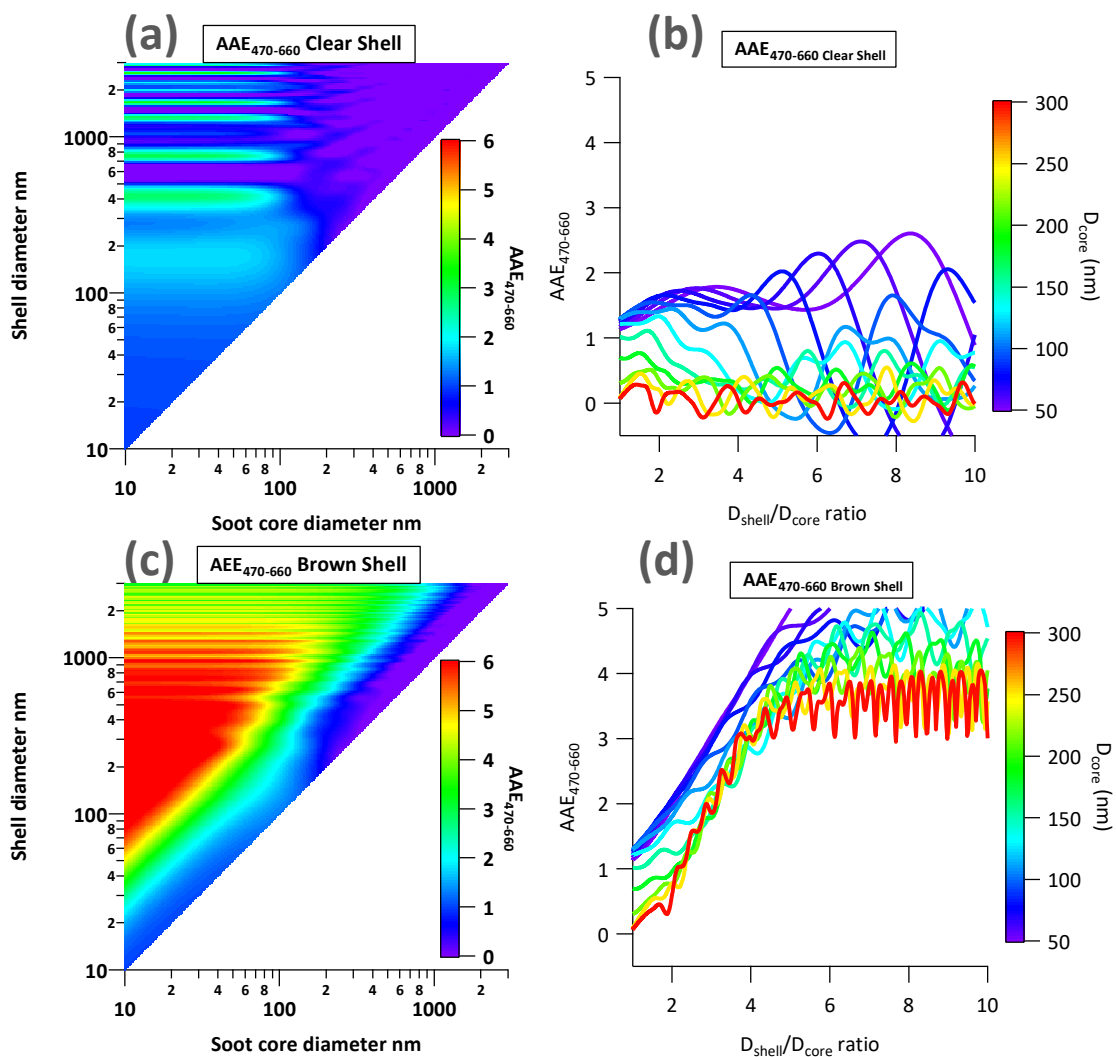
1022

1023



1024

1025 Figure 1. Minimum R squared (MRS) plot for calculating MAE_p at 550 nm. The red curve is the correlation result between
 1026 $\sigma_{abs,c}$ ($\sigma_{abs,t} - EC * MAE_p$) and EC mass. The shaded area in light tan represents the frequency distribution of observed
 1027 MAE. The dashed green line is the cumulative distribution of observed MAE.



1028

1029

1030

1031

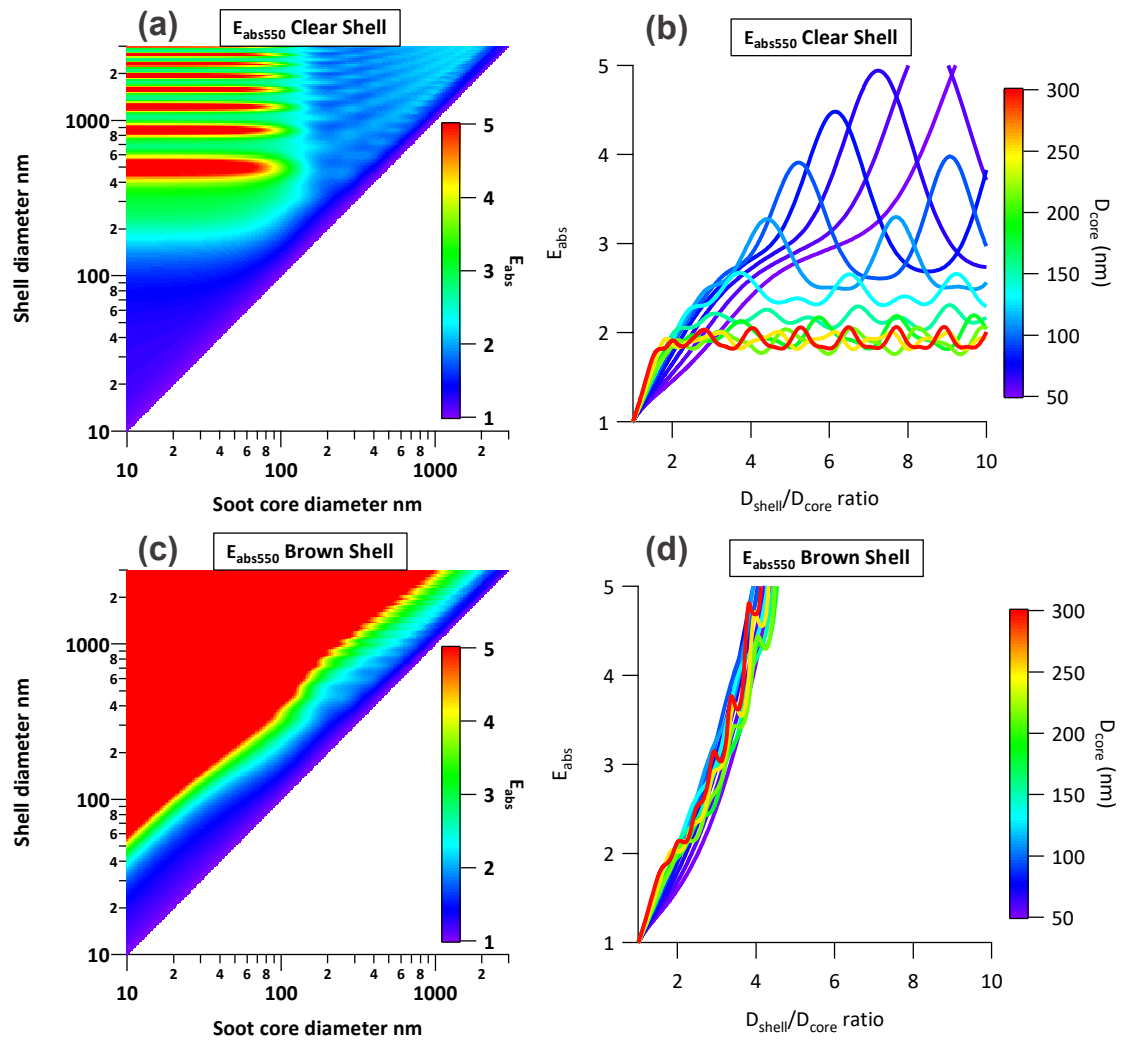
1032

1033

1034

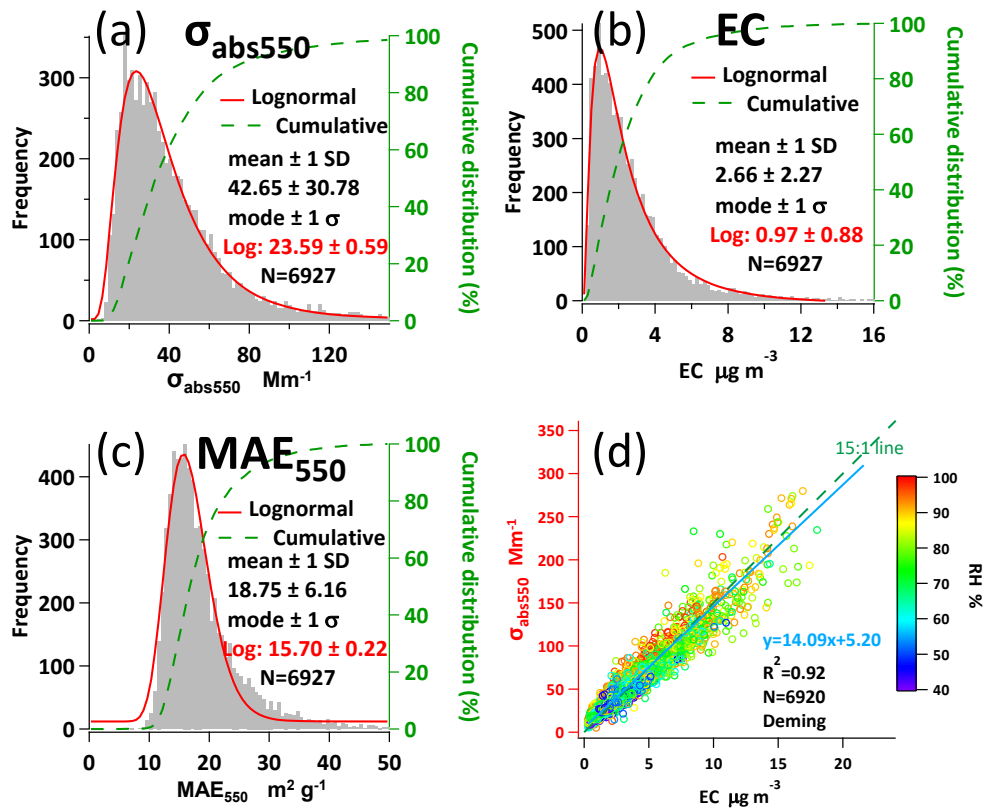
1035

Figure 2. Mie simulated size dependency of soot particles AAE₄₇₀₋₆₆₀. (a) Combination of different clear shell (y axis) and core diameters (x axis). The color coding represents the AAE₄₇₀₋₆₆₀ of a particle with specific core and clear shell size; (b) Cross-sections views of (a). The color coding represents different D_{core} in the range of 50 ~ 300 nm. (c)&(d) Similar to (a)&(b) but from the brown shell scenario.



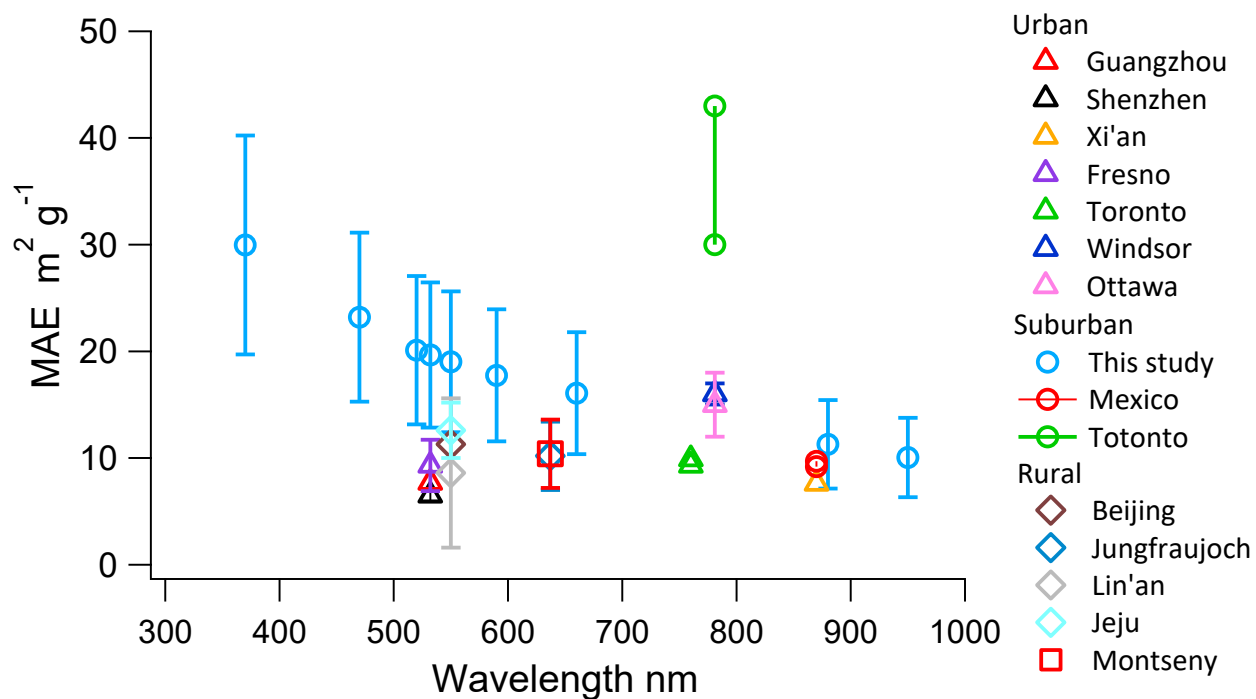
1036
 1037
 1038
 1039
 1040
 1041
 1042
 1043

Figure 3. Mie simulated size dependency of soot particles E_{abs} at wavelength 550 nm. (a) Combination of different clear shell (y axis) and core diameters (x axis). The color coding represents the E_{abs} of a particle with specific core and clear shell size; (b) Cross-sections views of (a). The color coding represents different D_{core} in the range of 50 – 300 nm. (c)&(d) Similar to (a)&(b) but from the brown shell scenario.



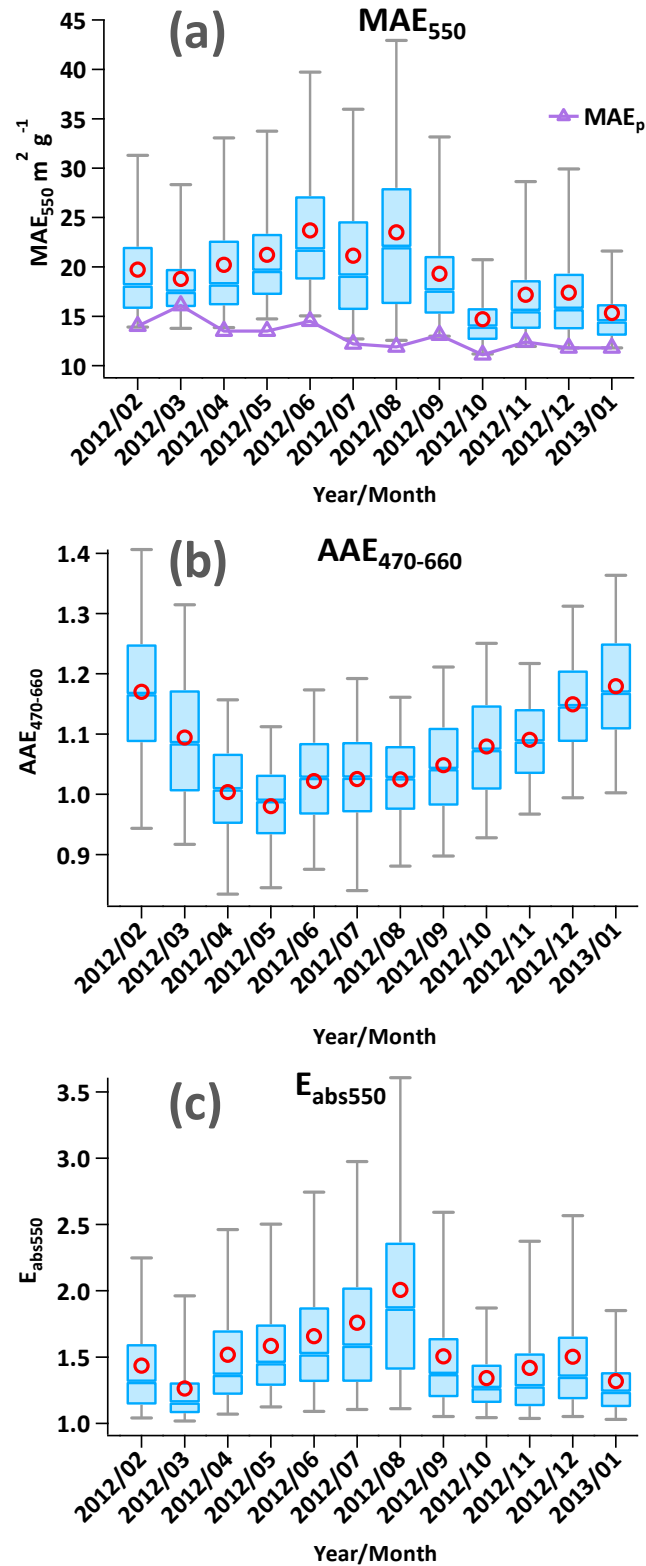
1044

1045 Figure 4. Measured annual statistics of σ_{abs550} , EC and MAE₅₅₀. (a) Annual frequency distribution of light absorption at
 1046 550 nm. The red curve represents the fitting line for a log-normal distribution. (b) Annual frequency distribution of EC
 1047 mass concentration (c) Frequency distribution of Mass absorption efficiency (MAE) at 550 nm. (d) Scatter plot of light
 1048 absorption (550 nm) and EC mass. The slope represents MAE₅₅₀. The blue regression line is by Deming regression. The
 1049 color coding represents RH.
 1050



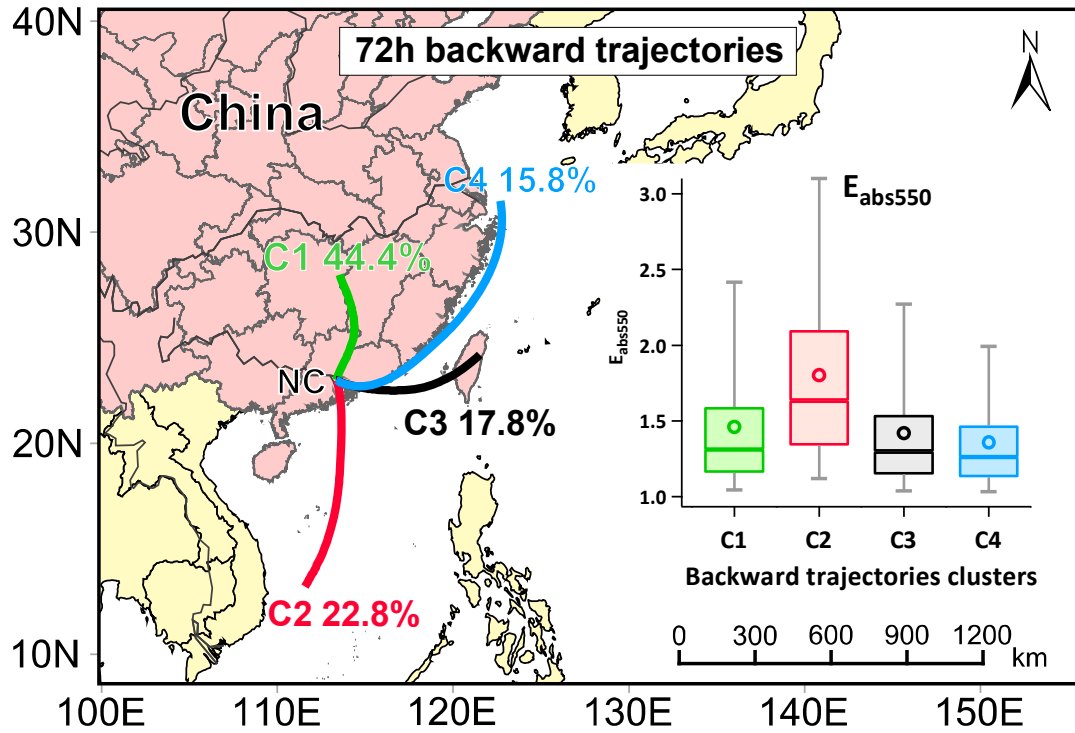
1051

1052 Figure 5. Comparison of spectral MAE measurements from this study with previous studies. Triangle, circle and rhombus
 1053 represent urban, suburban and rural respectively. Details and reference can be found in Table S1. The whiskers represent
 1054 one standard deviation.



1055

1056 Figure 6. Measured monthly variations of (a) MAE₅₅₀, the purple line represents MAE_p estimated by MRS (b) AAE₄₇₀₋₆₆₀
 1057 and (c) E_{abs550}. Red circles represent the monthly average. The line inside the box indicates the monthly median. Upper and
 1058 lower boundaries of the box represent the 75th and the 25th percentiles; the whiskers above and below each box represent
 1059 the 95th and 5th percentiles.

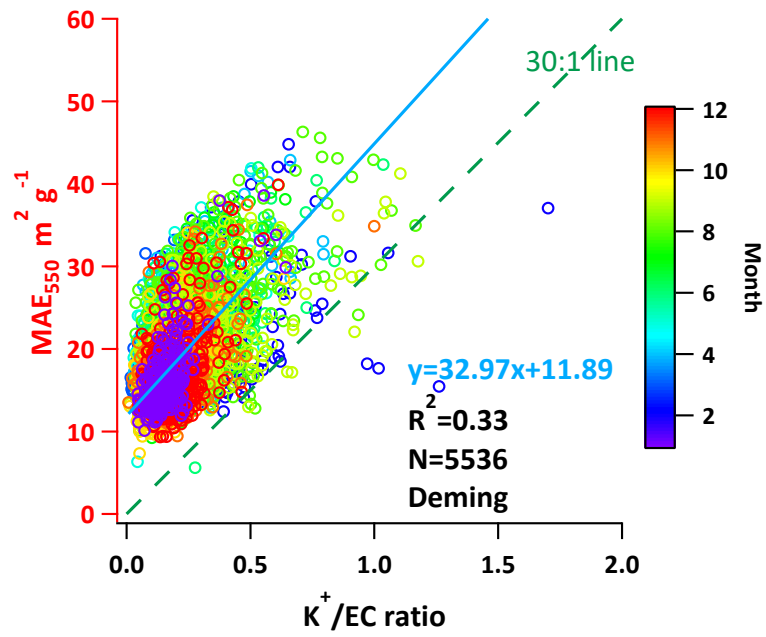


1060

1061

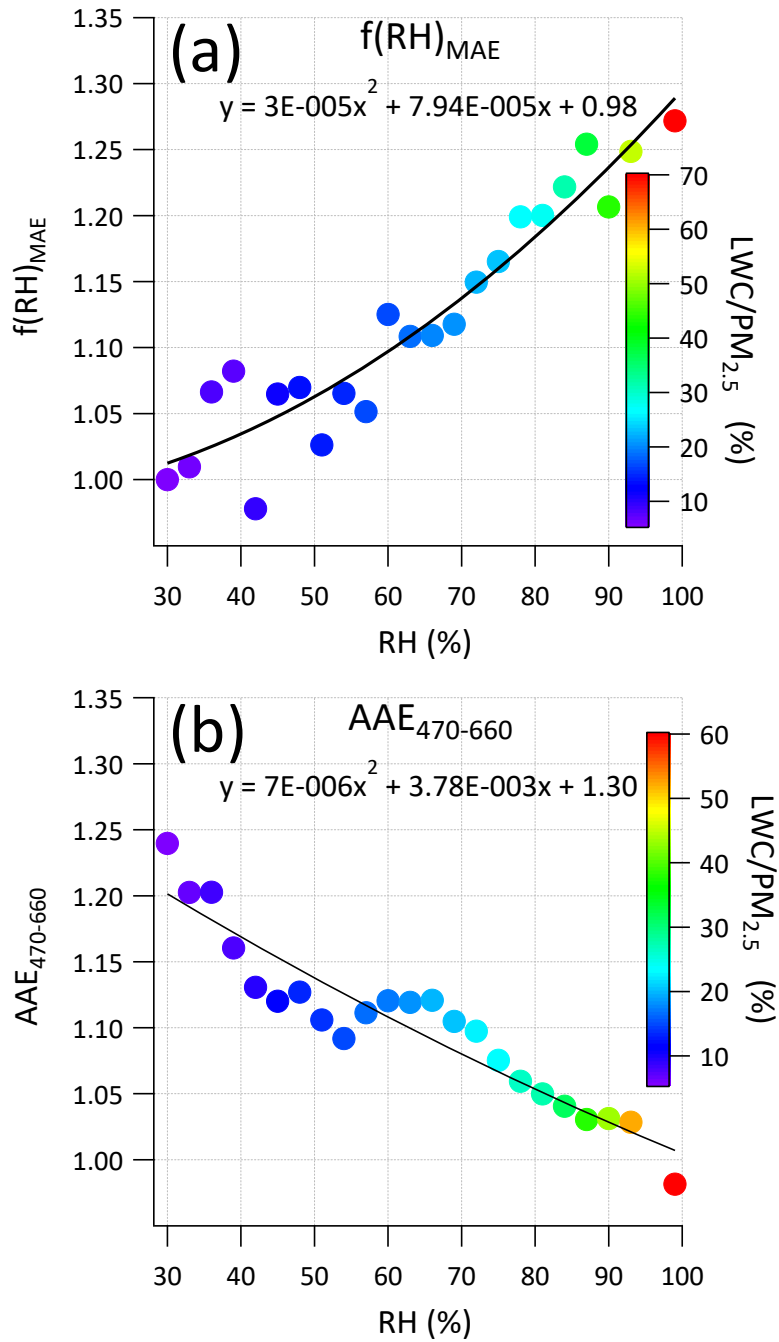
1062

Figure 7. Average backward trajectories arriving at 100 m at NC site for four clusters (2012 Feb - 2013 Jan). E_{abs550} by different clusters are shown in the box plot.



1063

1064 Figure 8. MAE₅₅₀ dependency on biomass burning indicator K^+/EC ratio. The color coding represents months. The intercept
 1065 represents MAE without biomass burning effect. The 30:1 line serves as a reference line with an integer slope that
 1066 is close to the regressed slope through the origin.



1067

1068

1069

Figure 9. Optical properties dependency on RH determined from one year's sampling data at NC site. (a) Hygroscopic growth factor ($f(RH)$) of EC MAE₅₅₀ (b) $AAE_{470-660}$ as a function of RH.

1 *Supplement of*

2 **Quantifying black carbon light absorption enhancement by**
3 **a novel statistical approach**

4

5 **Cheng Wu^{1,2}, Dui Wu^{1,2,3}, Jian Zhen Yu^{4,5,6}**

6

7 [1] Institute of Mass Spectrometer and Atmospheric Environment, Jinan University,
8 Guangzhou 510632, China

9 [2] Guangdong Provincial Engineering Research Center for on-line source apportionment
10 system of air pollution, Guangzhou 510632, China

11 [3] Institute of Tropical and Marine Meteorology, China Meteorological Administration,
12 Guangzhou 510080, China

13 [4] Division of Environment, Hong Kong University of Science and Technology, Clear Water
14 Bay, Hong Kong, China

15 [5] Atmospheric Research Centre, Fok Ying Tung Graduate School, Hong Kong University
16 of Science and Technology, Nansha, China

17 [6] Department of Chemistry, Hong Kong University of Science and Technology, Clear Water
18 Bay, Hong Kong, China

19 *Corresponding to:* Cheng Wu (wucheng.vip@foxmail.com) and Jian Zhen Yu (jian.yu@ust.hk)

20

21

22
23 This SI contains five tables and twenty-five figures.

24

25 **Uncertainty of E_{abs} estimation**

26 The uncertainty of E_{abs} estimation depends on uncertainty propagation from MAE uncertainty,
27 which can be calculated from (Harris, 2010):

$$28 \quad MAE_{Unc} = MAE \times \sqrt{\left(\frac{\sigma_{abs,Unc}}{\sigma_{abs}}\right)^2 + \left(\frac{EC_{Unc}}{EC}\right)^2} \quad S1$$

$$29 \quad E_{abs,Unc} = E_{abs} \times \sqrt{\left(\frac{MAE_{Unc}}{MAE}\right)^2 + \left(\frac{MAE_{p,Unc}}{MAE_p}\right)^2} \quad S2$$

30

31 **Descriptions of customized programs used in this study for data analysis and** 32 **visualization**

33 Several computer programs were developed to meet specific research purpose in this study. All
34 the programs are based on Igor Pro (www.wavemetrics.com) that provides a friendly GUI. Brief
35 descriptions are given below.

36

37 **MRS program (Igor Pro based)**

38 The program (Figure S21) is written in Igor Pro (WaveMetrics, Inc. Lake Oswego, OR, USA)
39 to feasible MRS calculation via a user-friendly GUI. The MRS application is not limited in
40 SOC estimation, but can also be extended to other applications (e.g. E_{abs} estimation) as long as
41 a reliable tracer is available.

42 MRS calculation can be done by different temporal cycles (batch calculation): by year, by
43 year&season, by season, by year&month, by month, by year&month&hour. Data filter is also
44 available to calculate MRS on a specific subset of data.

45 The program is available from <https://sites.google.com/site/wuchengust>.

46

47 **Mie program and source code written in Igor Pro**

48 A computer program (Figure S22) written in Igor Pro (WaveMetrics, Inc. Lake Oswego, OR,
49 USA) for Mie scattering calculation. Both BHMIE and BHCOAT (coated particles)
50 algorithms(Bohren and Huffman, 1983) are included. The program is also capable of batch
51 calculation for both algorithms. Available from <https://sites.google.com/site/wuchengust>.

52

53 **Aethalometer data processing program (Igor Pro based)**

54 This handy tool (Figure S23) can perform different corrections (e.g. Weingartner, Virkkula) on
55 Aethalometer data. Raw Aethalometer data suffers from several artifacts including filter matrix
56 effect (multiple scattering), loading effect (shadowing) and scattering effect. Careful
57 corrections are needed for reporting light absorption coefficient from attenuation measurement.
58 This Igor based program can directly import Aethalometer raw data and perform corrections
59 (algorithm can be selected by user). Results can be exported to .csv files. Extra information
60 including statistics of sensor voltage from each channel, sampling flow rate, etc are plotted for
61 a quick QA/QC check. Available from <https://sites.google.com/site/wuchengust>.

62

63 **Histbox program (Igor Pro based)**

64 A handy tool (Figure S24) to generate histogram and box plots with many powerful features.
65 Data can be sorted by different time scale and batch plotting is available. Available from
66 <https://sites.google.com/site/wuchengust>.

67

68 **Scatter plot program**

69 Scatter plot (Figure S25) is a handy tool to maximize the efficiency of data visualization in
70 atmospheric science. The program includes Deming, WODR and York algorithm for linear
71 regression, which consider uncertainties in both X and Y, that is more realistic for atmospheric
72 applications. It is Igor based, and packed with lots of useful features for data analysis and graph
73 plotting, including batch plotting, data masking via GUI, color coding in Z axis, data filtering
74 and grouping. Available from <https://sites.google.com/site/wuchengust>.

75

76

77 Reference

- 78 Andreae, M. O., Schmid, O., Yang, H., Chand, D., Yu, J. Z., Zeng, L. M., and Zhang, Y. H.:
79 Optical properties and chemical composition of the atmospheric aerosol in urban Guangzhou,
80 China, *Atmos. Environ.*, 42, 6335-6350, doi: 10.1016/j.atmosenv.2008.01.030, 2008.
- 81 Bohren, C. F. and Huffman, D. R.: *Absorption and scattering of light by small particles*, Wiley,
82 New York, xiv, 530 p. pp., 1983.
- 83 Chan, T. W., Brook, J. R., Smallwood, G. J., and Lu, G.: Time-resolved measurements of black
84 carbon light absorption enhancement in urban and near-urban locations of southern Ontario,
85 Canada, *Atmos. Chem. Phys.*, 11, 10407-10432, 2011.
- 86 Chow, J. C., Watson, J. G., Doraiswamy, P., Chen, L. W. A., Sodeman, D. A., Lowenthal, D.
87 H., Park, K., Arnott, W. P., and Motallebi, N.: Aerosol light absorption, black carbon, and
88 elemental carbon at the Fresno Supersite, California, *Atmos Res*, 93, 874-887, doi: DOI
89 10.1016/j.atmosres.2009.04.010, 2009.
- 90 Chuang, P. Y., Duvall, R. M., Bae, M. S., Jefferson, A., Schauer, J. J., Yang, H., Yu, J. Z., and
91 Kim, J.: Observations of elemental carbon and absorption during ACE-Asia and implications
92 for aerosol radiative properties and climate forcing, *J. Geophys. Res.*, 108, 8634, doi: Doi
93 10.1029/2002jd003254, 2003.
- 94 Doran, J. C., Barnard, J. C., Arnott, W. P., Cary, R., Coulter, R., Fast, J. D., Kassianov, E. I.,
95 Kleinman, L., Laulainen, N. S., Martin, T., Paredes-Miranda, G., Pekour, M. S., Shaw, W. J.,
96 Smith, D. F., Springston, S. R., and Yu, X. Y.: The T1-T2 study: evolution of aerosol properties
97 downwind of Mexico City, *Atmos. Chem. Phys.*, 7, 1585-1598, doi: 10.5194/acp-7-1585-2007,
98 2007.
- 99 Harris, D. C.: *Quantitative chemical analysis*, 8th ed., W.H. Freeman and Co., New York, 2010.
- 100 Knox, A., Evans, G. J., Brook, J. R., Yao, X., Jeong, C. H., Godri, K. J., Sabaliauskas, K., and
101 Slowik, J. G.: Mass Absorption Cross-Section of Ambient Black Carbon Aerosol in Relation
102 to Chemical Age, *Aerosol. Sci. Technol.*, 43, 522-532, doi: Doi 10.1080/02786820902777207,
103 2009.
- 104 Lack, D. A. and Cappa, C. D.: Impact of brown and clear carbon on light absorption
105 enhancement, single scatter albedo and absorption wavelength dependence of black carbon,
106 *Atmos. Chem. Phys.*, 10, 4207-4220, doi: DOI 10.5194/acp-10-4207-2010, 2010.
- 107 Lan, Z.-J., Huang, X.-F., Yu, K.-Y., Sun, T.-L., Zeng, L.-W., and Hu, M.: Light absorption of
108 black carbon aerosol and its enhancement by mixing state in an urban atmosphere in South
109 China, *Atmos. Environ.*, 69, 118-123, doi: <http://dx.doi.org/10.1016/j.atmosenv.2012.12.009>,
110 2013.
- 111 Liu, D., Flynn, M., Gysel, M., Targino, A., Crawford, I., Bower, K., Choularton, T., Jurányi,
112 Z., Steinbacher, M., Hüglin, C., Curtius, J., Kampus, M., Petzold, A., Weingartner, E.,
113 Baltensperger, U., and Coe, H.: Single particle characterization of black carbon aerosols at a
114 tropospheric alpine site in Switzerland, *Atmos. Chem. Phys.*, 10, 7389-7407, doi: 10.5194/acp-
115 10-7389-2010, 2010.
- 116 Mayol-Bracero, O. L., Gabriel, R., Andreae, M. O., Kirchstetter, T. W., Novakov, T., Ogren,
117 J., Sheridan, P., and Streets, D. G.: Carbonaceous aerosols over the Indian Ocean during the
118 Indian Ocean Experiment (INDOEX): Chemical characterization, optical properties, and
119 probable sources, *J. Geophys. Res.*, 107, 8030, doi: Doi 10.1029/2000jd000039, 2002.
- 120 Moosmuller, H., Chakrabarty, R. K., Ehlers, K. M., and Arnott, W. P.: Absorption Angstrom
121 coefficient, brown carbon, and aerosols: basic concepts, bulk matter, and spherical particles,
122 *Atmos. Chem. Phys.*, 11, 1217-1225, doi: DOI 10.5194/acp-11-1217-2011, 2011.
- 123 Naoe, H., Hasegawa, S., Heintzenberg, J., Okada, K., Uchiyama, A., Zaizen, Y., Kobayashi, E.,
124 and Yamazaki, A.: State of mixture of atmospheric submicrometer black carbon particles and

125 its effect on particulate light absorption, *Atmos. Environ.*, 43, 1296-1301, doi:
126 <https://doi.org/10.1016/j.atmosenv.2008.11.031>, 2009.
127 Pandolfi, M., Cusack, M., Alastuey, A., and Querol, X.: Variability of aerosol optical properties
128 in the Western Mediterranean Basin, *Atmos. Chem. Phys.*, 11, 8189-8203, doi: DOI
129 10.5194/acp-11-8189-2011, 2011.
130 Thompson, J. E., Hayes, P. L., Jimenez, K. A. J. L., Zhang, X., Liu, J., Weber, R. J., and Buseck,
131 P. R.: Aerosol Optical Properties at Pasadena, CA During CalNex 2010, *Atmos Environ*, doi:
132 10.1016/j.atmosenv.2012.03.011, 2012.
133 Wang, Q., Huang, R., Zhao, Z., Cao, J., Ni, H., Tie, X., Zhu, C., Shen, Z., Wang, M., and Dai,
134 W.: Effects of photochemical oxidation on the mixing state and light absorption of black carbon
135 in the urban atmosphere of China, *Environmental Research Letters*, 12, 044012, 2017.
136 Wang, Q. Y., Huang, R. J., Cao, J. J., Han, Y. M., Wang, G. H., Li, G. H., Wang, Y. C., Dai,
137 W. T., Zhang, R. J., and Zhou, Y. Q.: Mixing State of Black Carbon Aerosol in a Heavily
138 Polluted Urban Area of China: Implications for Light Absorption Enhancement, *Aerosol. Sci.*
139 *Technol.*, 48, 689-697, doi: 10.1080/02786826.2014.917758, 2014.
140 Xu, J., Bergin, M. H., Yu, X., Liu, G., Zhao, J., Carrico, C. M., and Baumann, K.: Measurement
141 of aerosol chemical, physical and radiative properties in the Yangtze delta region of China,
142 *Atmos. Environ.*, 36, 161-173, 2002.
143 Yang, M., Howell, S. G., Zhuang, J., and Huebert, B. J.: Attribution of aerosol light absorption
144 to black carbon, brown carbon, and dust in China - interpretations of atmospheric measurements
145 during EAST-AIRE, *Atmos. Chem. Phys.*, 9, 2035-2050, 2009.

146

147

Table S1. Comparison of Mass absorption efficiency (MAE) at various locations. For literature MAE values at different wavelengths rather than 550 nm, an estimated MAE₅₅₀ is given in the brackets following equations given by Moosmuller et al. (2011) assuming AAE of 1.

Location	Type	Sampling Duration	Inlet	λ (nm)	σ_{abs} Instrument	EC determination protocol	$\sigma_{\text{abs}} \pm 1$ S.D. (Mm ⁻¹)	EC mass ($\mu\text{g m}^{-3}$)	estimated MAE _p * (m ² g ⁻¹)	observed MAE (m ² g ⁻¹)		Reference
										arithmetic mean ± 1 S.D.	Gaussian fit	
Guangzhou, China	Suburban	2012.2-2013.1	PM _{2.5}	550	AE	NIOSH_TOT	42.65±29.41	2.66±2.27	13*	18.75±6.16	16.16	This study
Shenzhen, China	Urban	2011.8-9	PM _{2.5}	532	PAS	LII	25.4±19.0	4.0±3.1	/	6.5±0.5[6.29±0.48]	/	(Lan et al., 2013)
Xi'an, China	Urban	2012.12-2013.1	PM _{2.5}	870	PAS	LII	/	8.8±7.3	7.17[11.34]	/	7.62[12.05]	(Wang et al., 2014)
Xi'an, China	Urban	2013.2	PM _{2.5}	532	PAS	LII	/	/	/	14.6±5.6	12.7	(Wang et al., 2017)
Guangzhou, China	Urban	2004.10	PM _{2.5}	532	PAS	NIOSH_TOT	91±60	7.1	7.7[7.44]	/	/	(Andreae et al., 2008)
Fresno, USA	Urban	2005.8-9	PM _{2.5}	532	PAS	IMPROVE_A_TOR	5.06	1.01	/	6.1±2.5[5.9±2.42]	/	(Chow et al., 2009)
						NIOSH_TOT	/	0.58	/	9.3±2.4[8.99±2.32]	/	
T1, Mexico city, Mexico	Suburban	2006.3	PM _{2.5}	870	PAS	NIOSH_TOT	/	/	/	9.2~9.7***[14.55~15.34]	/	(Doran et al., 2007)
Tokyo, Japan	Suburban	2005.8	PM _{2.5}	565	PSAP	IMPROVE_A_TOR	30.43±20.41	2.9±2.13	11±1	/	/	(Naoe et al., 2009)
Pasadena, USA	Urban	2010.5-6	PM _{2.5}	532	AM	NIOSH_TOT	3.8±3.4	0.6~0.7	5.7[5.51]	/	/	(Thompson et al., 2012)
Toronto, Canada	Urban	2006.12-2007.1	PM _{2.5}	760	PAS	NIOSH_TOT	/	/	6.9~9.1** [9.53~12.57]	9.3~9.9[12.85~13.68]	/	(Knox et al., 2009)
Toronto, Canada	Suburban						3~6	0.10~0.14	/	30~43[42.6~61.06]	/	
Windsor, Canada	Urban	2007.8	PM _{2.5}	781	PAS	LII	4.4±2.9	0.27±0.23	/	16±1[22.72±1.42]	/	(Chan et al., 2011)
Ottawa, Canada	Urban						26±17	1.7±0.9	/	15±3[21.3±4.26]	/	
Beijing, China	Rural	2005.3	/	550	AE	NIOSH_TOT	/	/	9.5	11.3	/	(Yang et al., 2009)
Montseny, Spin	Rural (Mediterranean)	2009.11-2010.10	PM ₁₀	637	MAAP	NIOSH_TOT	2.8±2.2	0.271±0.215	/	10.4[12.04]	/	(Pandolfi et al., 2011)
Jungfrauoch, Switzerland	Rural (high alpine)	2007.2-3	/	637	MAAP	LII	/	/	/	10.2±3.2[11.81±3.71]	/	(Liu et al., 2010)
Lin'an, China	Rural	1999.11	PM _{2.5}	550	PSAP	NIOSH_TOT	23±14	3.4±1.7	/	8.6±7.0	/	(Xu et al., 2002)
Jeju Island, Korea	Coastal Rural, (East China Sea)	2001.4	PM ₁₀	550	PSAP	NIOSH_TOT	/	/	/	12.6±2.6	/	(Chuang et al., 2003)
Maldives	Oceanic rural	1999.2-3	PM ₃	550	PSAP	EGA	62±34	2.5±1.4	6.6	8.1	/	(Mayol-Bracero et al., 2002)

*Determined by Minimum R Squared method; ** Median values;

AE: Aethalometer ; PAS photo acoustic spectrometer; MAAP: Multi Angle Absorption Photometer; PSAP: particle soot absorption photometer; AM: albedo meter; LII: Laser induced incandescence

Table S2. Statistics of monthly MAE₅₅₀.

Month	95th	75th	50th	25th	5th	Mean	Max	Min	S.D.	N
Feb-2012	31.24	22.00	18.12	15.74	13.92	19.66	47.73	11.74	5.66	529
Mar-2012	26.51	19.63	17.45	15.91	13.71	18.46	45.56	10.98	4.30	651
Apr-2012	33.06	22.66	18.24	16.11	13.85	20.21	48.29	6.01	6.23	595
May-2012	33.24	23.25	19.59	17.16	14.82	21.07	46.66	6.33	5.62	528
Jun-2012	35.52	25.86	21.28	18.57	14.99	22.95	49.07	5.62	6.66	315
Jul-2012	33.93	23.77	18.81	15.58	12.71	20.51	49.22	9.23	6.79	587
Aug-2012	40.75	27.72	21.85	16.14	12.51	23.09	49.95	9.75	8.56	545
Sep-2012	30.75	20.86	17.52	15.24	12.97	18.99	46.44	10.39	5.63	674
Oct-2012	20.72	15.84	13.95	12.60	11.18	14.70	34.09	7.34	3.21	715
Nov-2012	26.45	18.10	15.43	13.70	11.89	16.75	39.32	8.34	4.72	495
Dec-2012	28.57	19.04	15.73	13.66	11.78	17.18	47.39	9.33	5.47	585
Jan-2013	21.53	16.24	14.47	13.03	11.80	15.29	43.19	7.16	3.77	708

Table S3. Statistics of monthly AAE₄₇₀₋₆₆₀.

Month	95th	75th	50th	25th	5th	Mean	Max	Min	S.D.	N
Feb-2012	1.42	1.26	1.18	1.11	0.96	1.19	1.72	0.86	0.14	529
Mar-2012	1.33	1.18	1.10	1.02	0.93	1.10	1.50	0.65	0.12	651
Apr-2012	1.19	1.08	1.02	0.95	0.78	1.01	1.76	0.15	0.14	595
May-2012	1.13	1.05	1.00	0.94	0.84	0.99	1.24	0.39	0.10	528
Jun-2012	1.18	1.10	1.04	0.97	0.90	1.04	1.29	0.78	0.09	315
Jul-2012	1.22	1.11	1.04	0.98	0.83	1.04	1.43	0.20	0.13	587
Aug-2012	1.18	1.10	1.04	0.99	0.90	1.04	1.31	0.69	0.09	545
Sep-2012	1.23	1.13	1.06	1.00	0.91	1.07	1.40	0.64	0.11	674
Oct-2012	1.27	1.16	1.09	1.02	0.93	1.09	1.40	0.85	0.10	715
Nov-2012	1.24	1.16	1.11	1.05	0.97	1.11	1.52	0.79	0.08	495
Dec-2012	1.33	1.22	1.16	1.10	1.01	1.16	1.42	0.77	0.09	585
Jan-2013	1.38	1.27	1.18	1.12	1.01	1.19	1.66	0.93	0.11	708

Table S4. Statistics of monthly SSA₅₂₅.

Month	95th	75th	50th	25th	5th	Mean	Max	Min	S.D.	N
Feb-2012	0.91	0.89	0.87	0.84	0.79	0.86	0.94	0.65	0.04	526
Mar-2012	0.91	0.89	0.86	0.83	0.77	0.85	0.95	0.42	0.05	648
Apr-2012	0.92	0.89	0.86	0.83	0.76	0.85	0.94	0.45	0.06	552
May-2012	0.92	0.90	0.87	0.83	0.74	0.85	0.94	0.45	0.06	527
Jun-2012	0.92	0.89	0.86	0.81	0.74	0.84	0.95	0.64	0.06	310
Jul-2012	0.91	0.87	0.83	0.79	0.71	0.83	0.95	0.57	0.06	580
Aug-2012	0.94	0.92	0.89	0.85	0.79	0.88	0.96	0.67	0.05	536
Sep-2012	0.93	0.91	0.88	0.84	0.75	0.87	0.96	0.55	0.06	672
Oct-2012	0.94	0.93	0.91	0.89	0.84	0.90	0.96	0.66	0.03	715
Nov-2012	0.91	0.90	0.87	0.83	0.75	0.86	0.94	0.18	0.06	495
Dec-2012	0.91	0.89	0.86	0.82	0.74	0.85	0.94	0.66	0.05	585
Jan-2013	0.91	0.89	0.87	0.85	0.80	0.86	0.93	0.64	0.04	708

Table S5. Statistics of monthly E_{abs550}.

Month	95th	75th	50th	25th	5th	Mean	Max	Min	S.D.	N
Feb-2012	2.23	1.59	1.31	1.14	1.04	1.43	3.41	1.00	0.40	501
Mar-2012	1.76	1.30	1.15	1.07	1.02	1.24	2.83	1.00	0.26	466
Apr-2012	2.46	1.70	1.37	1.21	1.07	1.52	3.58	1.00	0.45	576
May-2012	2.48	1.73	1.45	1.28	1.12	1.57	3.46	1.02	0.41	520
Jun-2012	2.47	1.80	1.49	1.30	1.09	1.61	3.38	1.01	0.45	305
Jul-2012	2.83	1.97	1.57	1.30	1.10	1.71	4.03	1.01	0.55	568
Aug-2012	3.45	2.34	1.86	1.40	1.11	1.97	4.20	1.00	0.71	528
Sep-2012	2.36	1.62	1.36	1.20	1.05	1.48	3.54	1.00	0.42	636
Oct-2012	1.87	1.44	1.27	1.15	1.04	1.34	3.07	1.00	0.28	683
Nov-2012	2.14	1.51	1.27	1.13	1.04	1.38	3.17	1.00	0.38	461
Dec-2012	2.46	1.64	1.35	1.18	1.05	1.49	4.02	1.00	0.46	555
Jan-2013	1.85	1.39	1.24	1.12	1.03	1.31	3.66	1.00	0.32	672

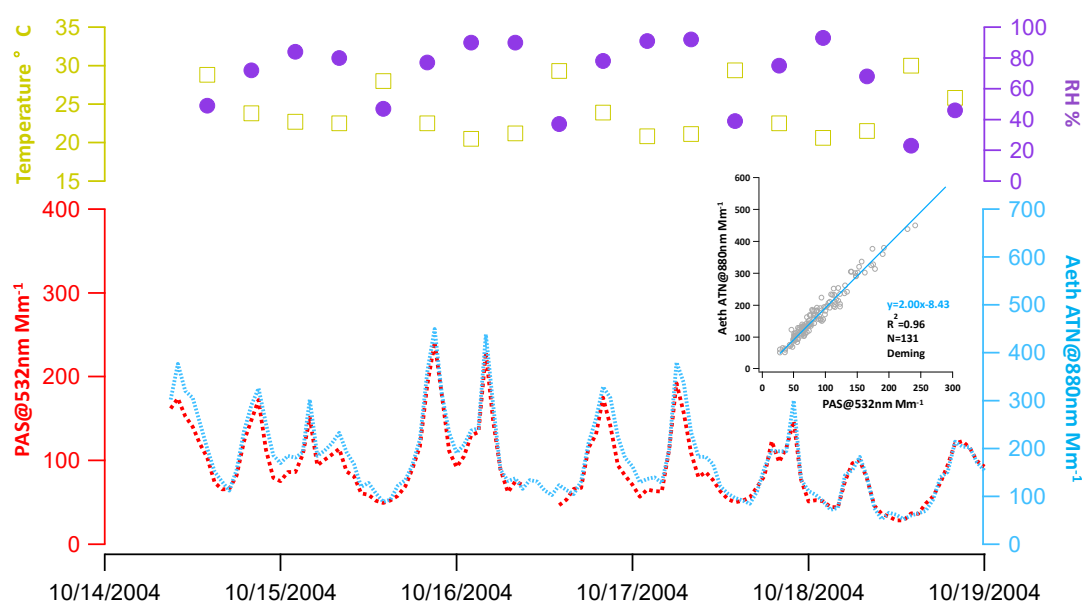


Figure S1. Comparison of collocated Aethalometer and PAS at Guangzhou (Oct 2004). Both PAS and Aethalometer (AE-16) were equipped with PM_{2.5} inlets. RH of the sampled air was controlled to be <45% for PAS. Aethalometer sampling was conducted without RH control.

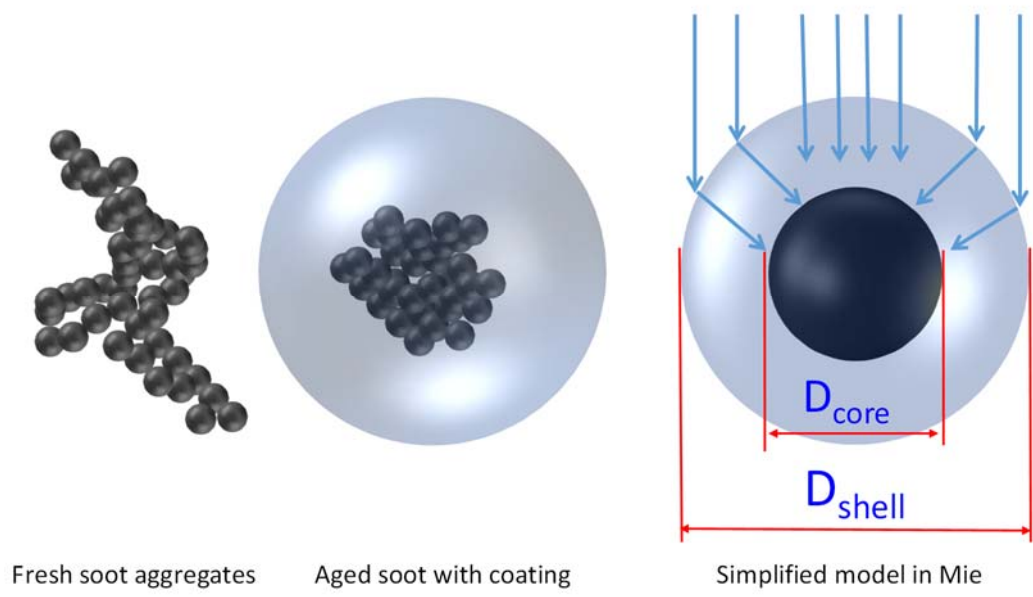


Figure S2. Schematic of the aging effect on light absorption. More light is absorbed by the soot particle core due to the lensing effect of the coating materials.

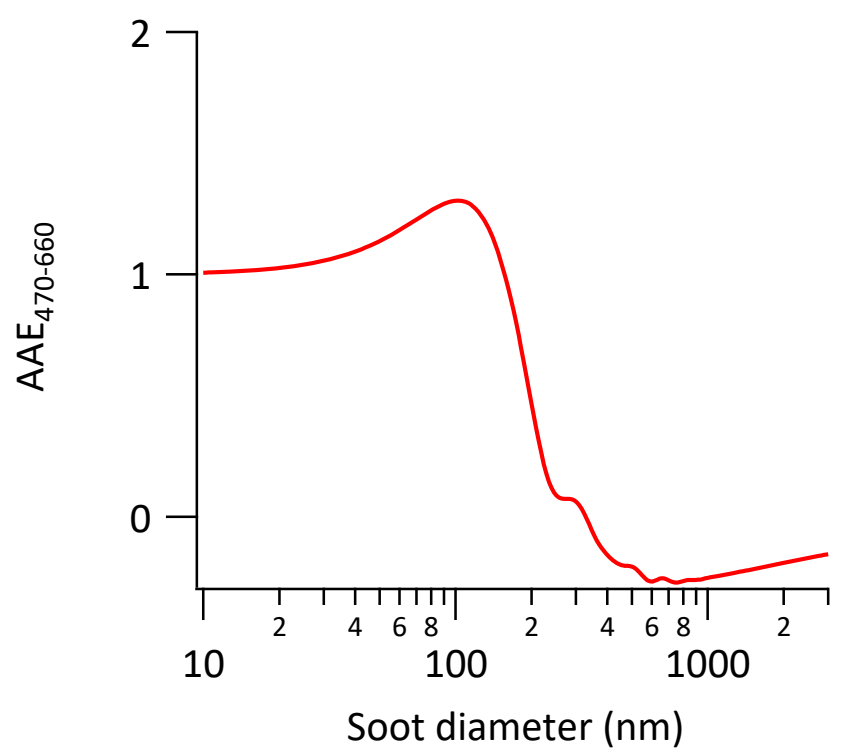


Figure S3. Mie simulated AAE₄₇₀₋₆₆₀ of a bare soot particle as a function of diameter with a Refractive index of 1.85 – 0.71i.

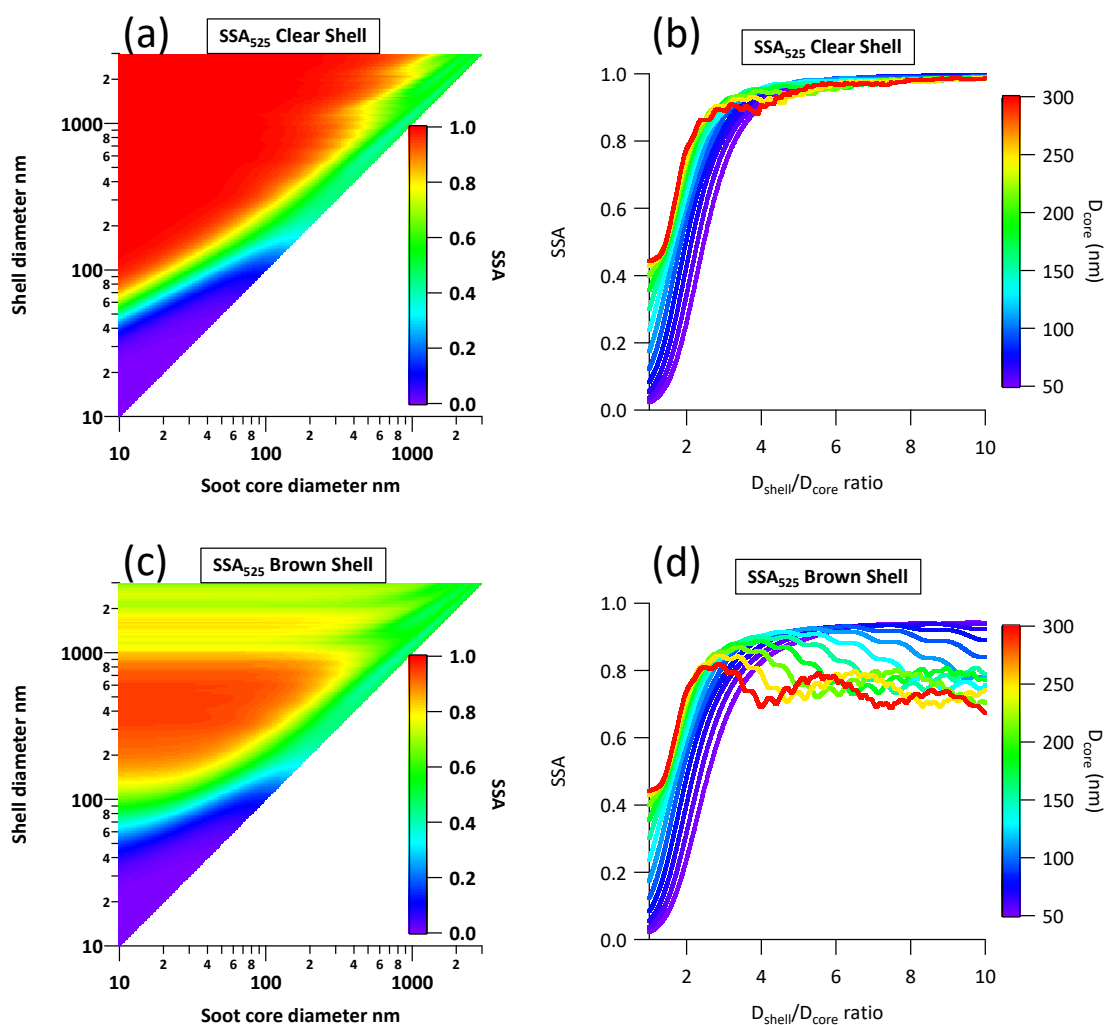


Figure S4. Mie simulated size dependency of soot particles SSA at wavelength 525 nm. (a) Combination of different clear shell (y axis) and core diameters (x axis). The color coding represents the SSA of a particle with specific core and clear shell size; (b) Cross-sections views of (a). The color coding represents different D_{core} in the range of 50 – 300 nm. (c)&(d) Similar to (a)&(b) but from the brown shell scenario.

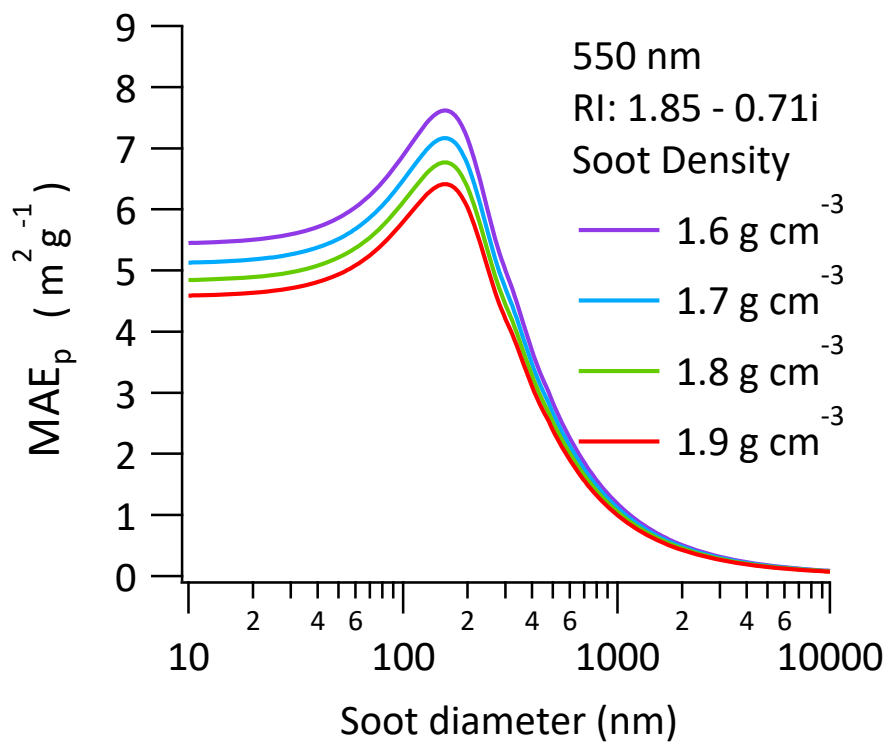


Figure S5. Mie simulated mass absorption efficiency (MAE_p) of a bare soot particle as a function of diameter at a wavelength of 550nm. Refractive index is 1.85 – 0.71i and density varied from 1.6 to 1.9 g cm⁻³.

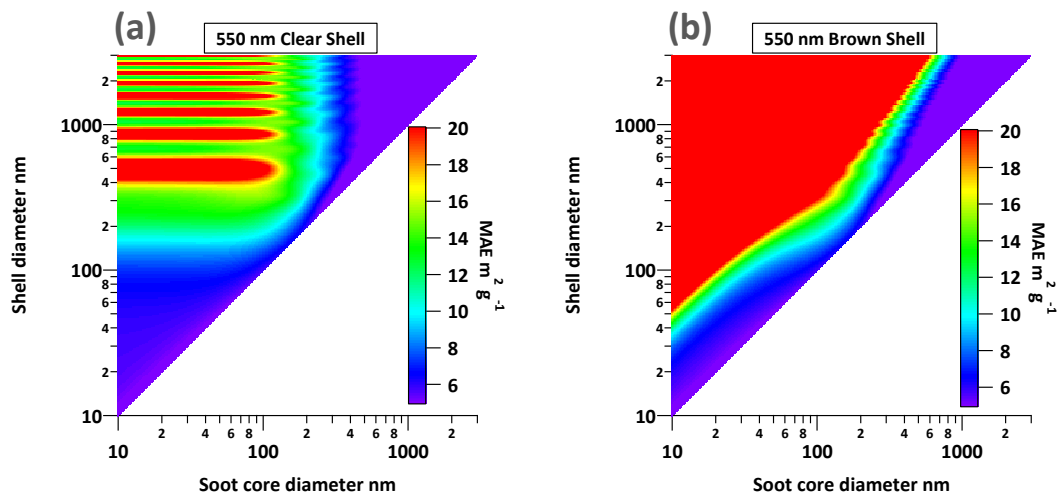


Figure S6. Mie simulated mass absorption efficiency (MAE) of a bare soot particle as a function of diameter at a wavelength of 550nm. Refractive index is $1.85 - 0.71i$ and density is 1.9 g cm^{-3} for the soot core. Refractive index for clear coating is 1.55. Refractive index for brown coating is wavelength dependent adopted from Lack and Cappa (2010).

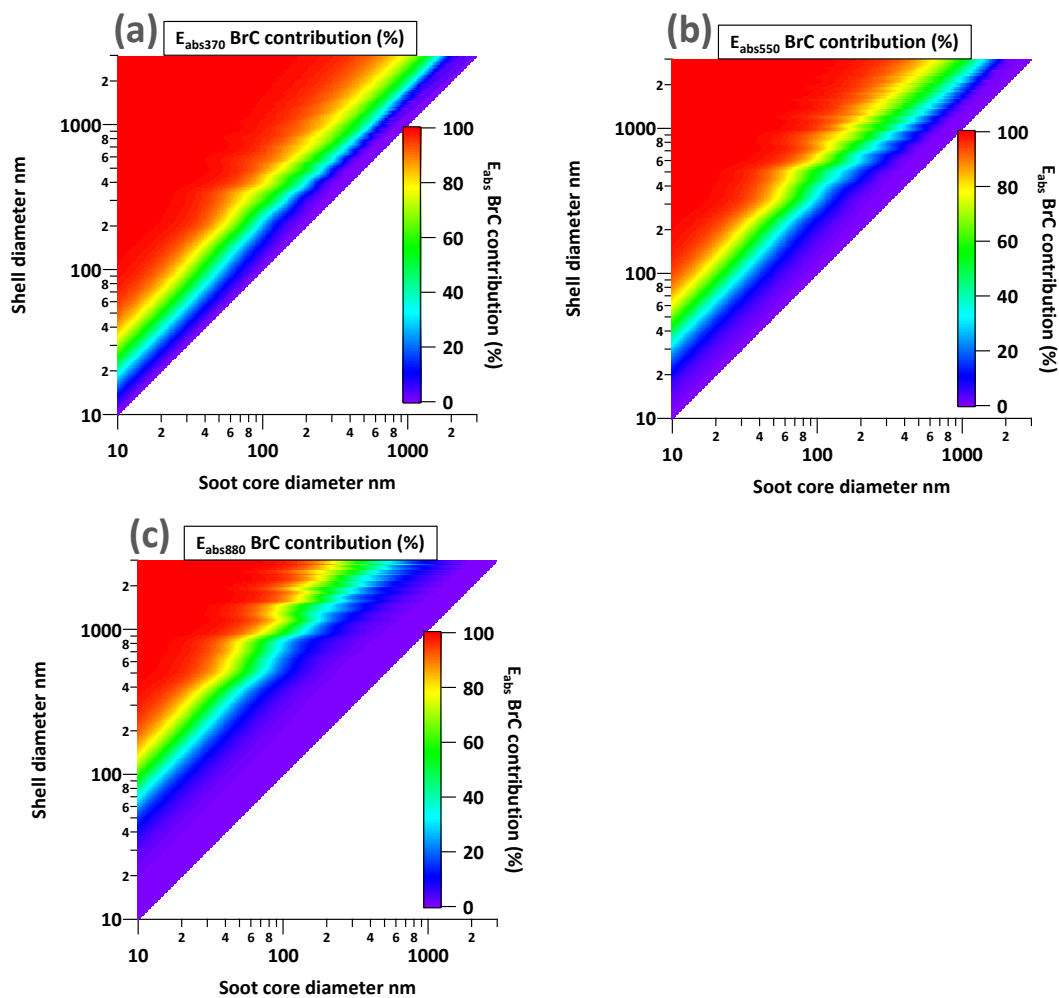


Figure S7. Mie simulated BrC absorption contribution to total E_{abs} (lensing effect + BrC absorption) in the brown shell scenario. (a) 370 nm (b) 550 nm (c) 880 nm.

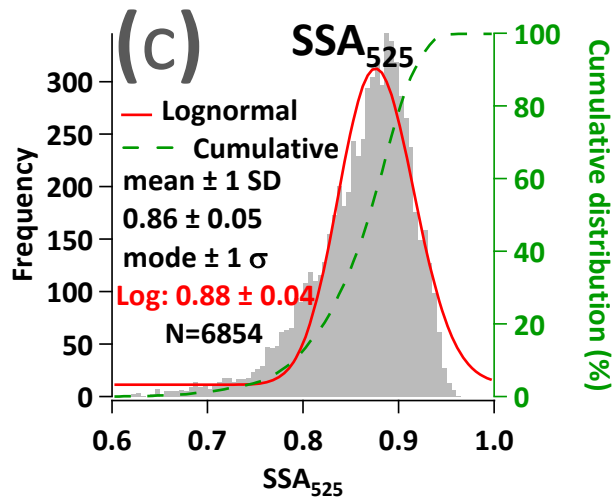
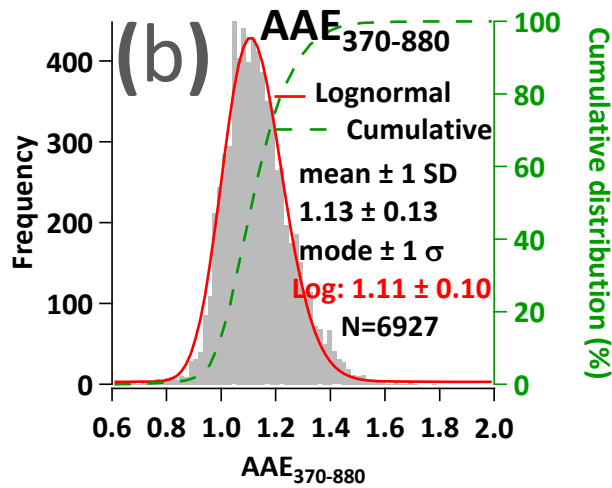
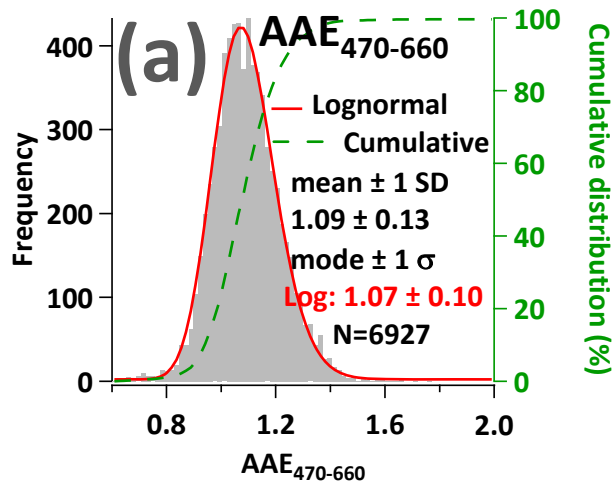


Figure S8. Measured annual statistics of AAE and SSA. (a) Annual frequency distribution of AAE₄₇₀₋₆₆₀. (b) Annual frequency distribution of AAE₃₇₀₋₈₈₀. (c) Annual frequency distribution of SSA₅₂₅. The red line represents lognormal fitting curve.

Test A

Original data

Systematically biased data

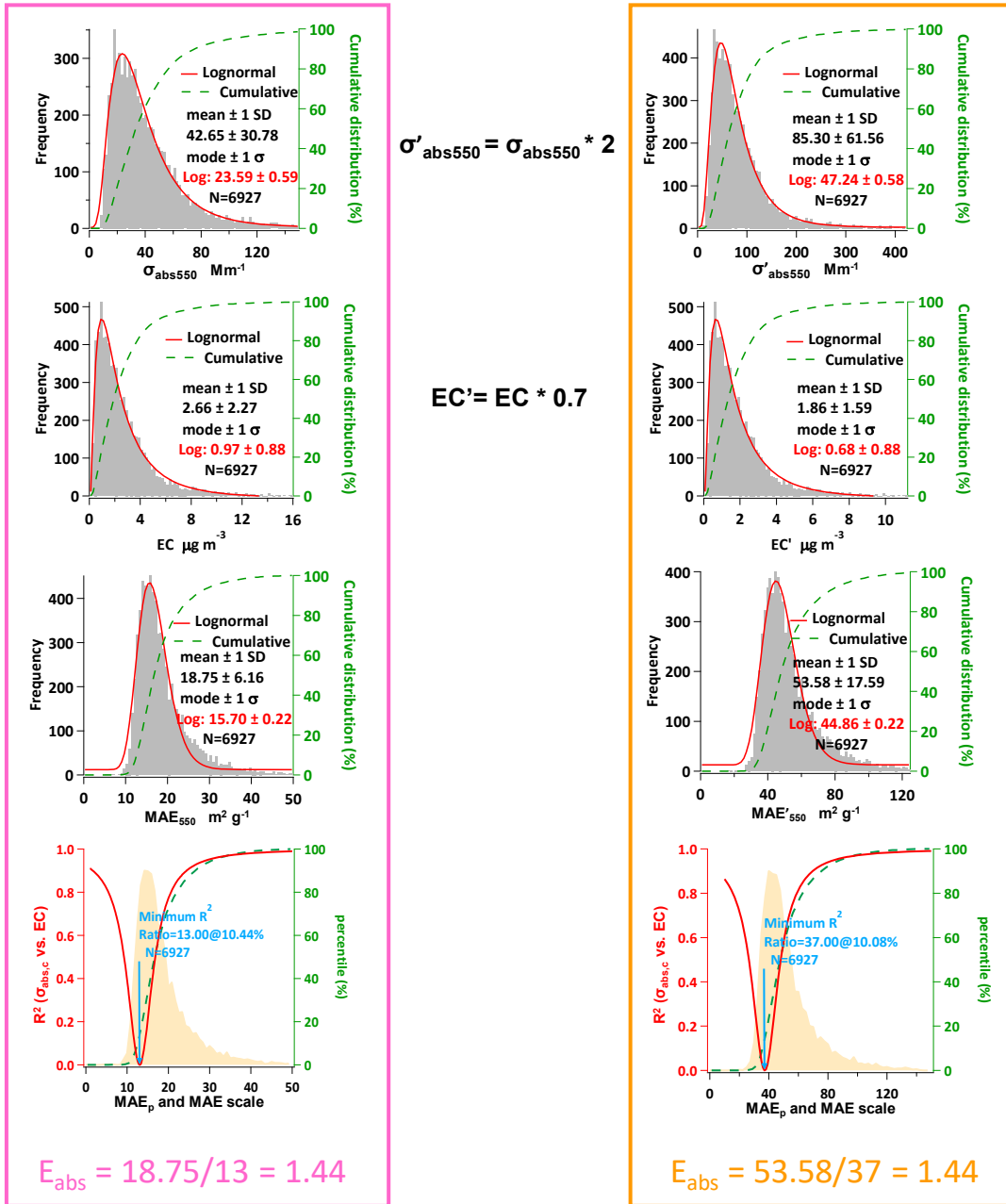


Figure S9. Comparison of E_{abs} from original data and systematically biased data (Test A). It should be noted that the E_{abs} shown here is ratio of averages, which is different from the annual average E_{abs} calculated from average of ratios.

Test B

Original data

Systematically biased data

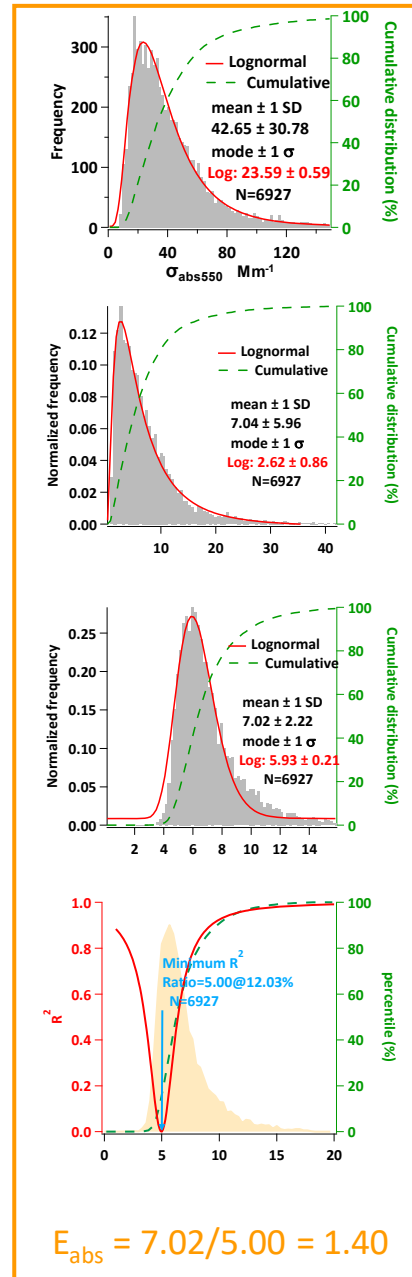
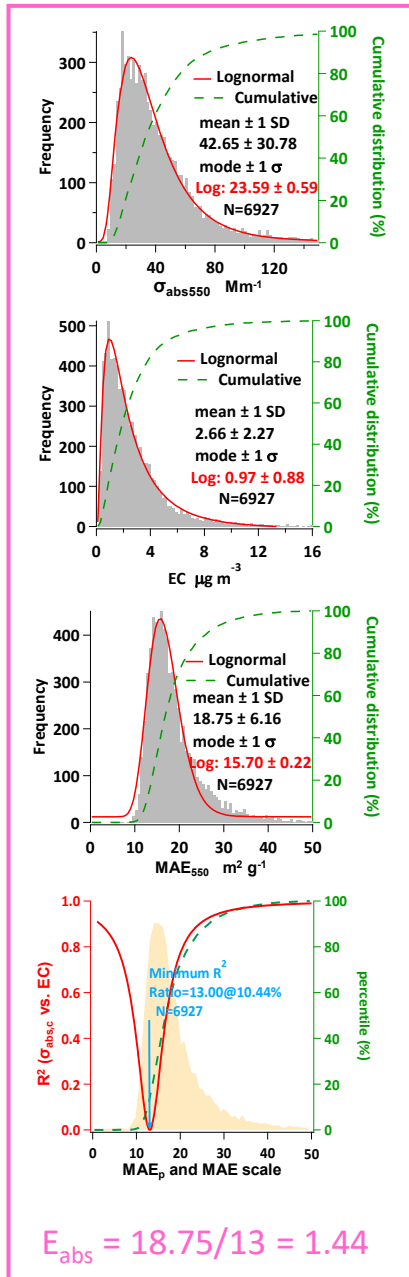
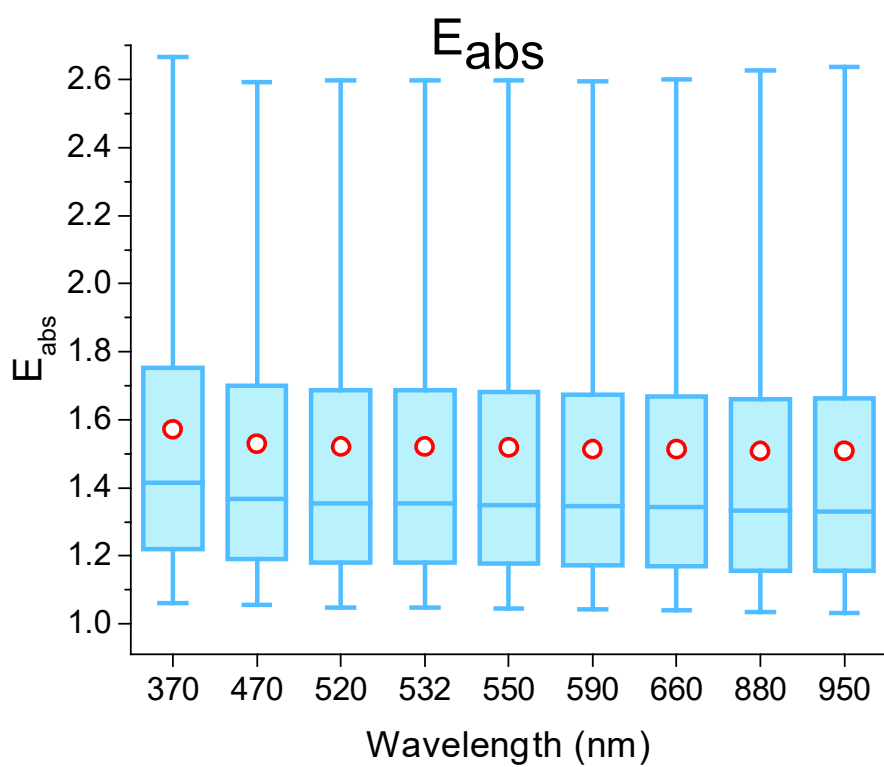


Figure S10. Comparison of E_{abs} from data using NIOSH EC and data using IMPROVE EC (Test B). It should be noted that the E_{abs} shown here is ratio of averages, which is different from the annual average E_{abs} calculated from average of ratios.



Wavelength (nm)	370	470	520	532	550	590	660	880	950
E_{abs} mean	1.55	1.51	1.50	1.50	1.50	1.49	1.49	1.48	1.49
E_{abs} S.D.	0.48	0.47	0.47	0.47	0.48	0.47	0.48	0.49	0.49

Figure S11. Spectrum annual average E_{abs} from 370 to 950 nm.

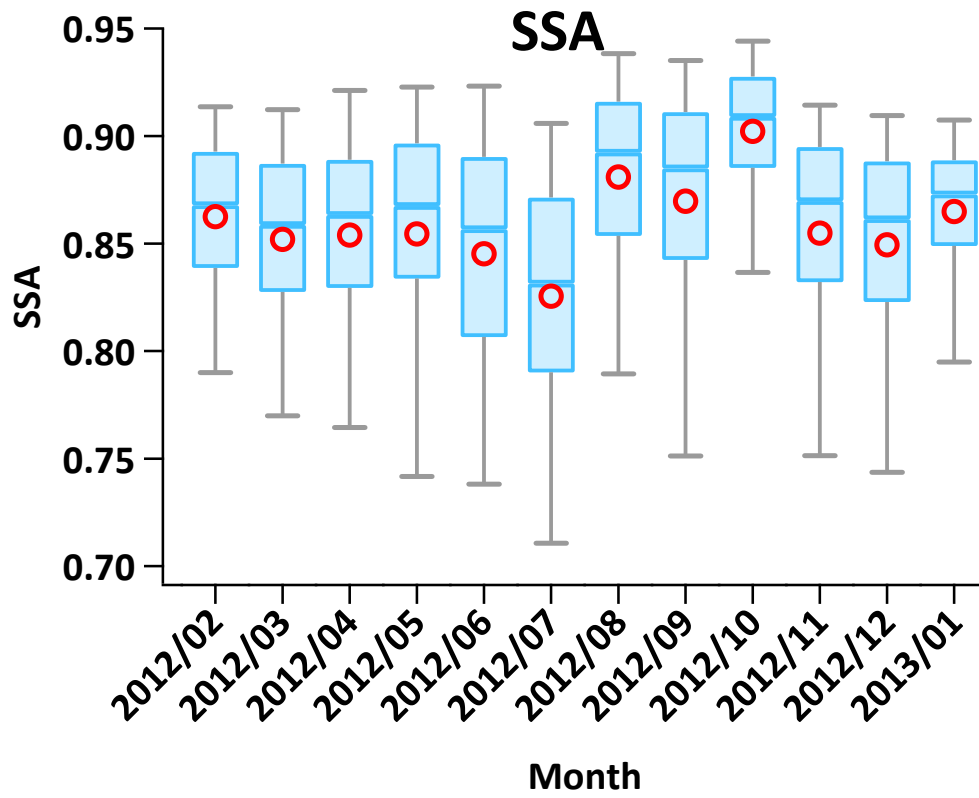


Figure S12. Measured monthly variations of SSA₅₂₅.

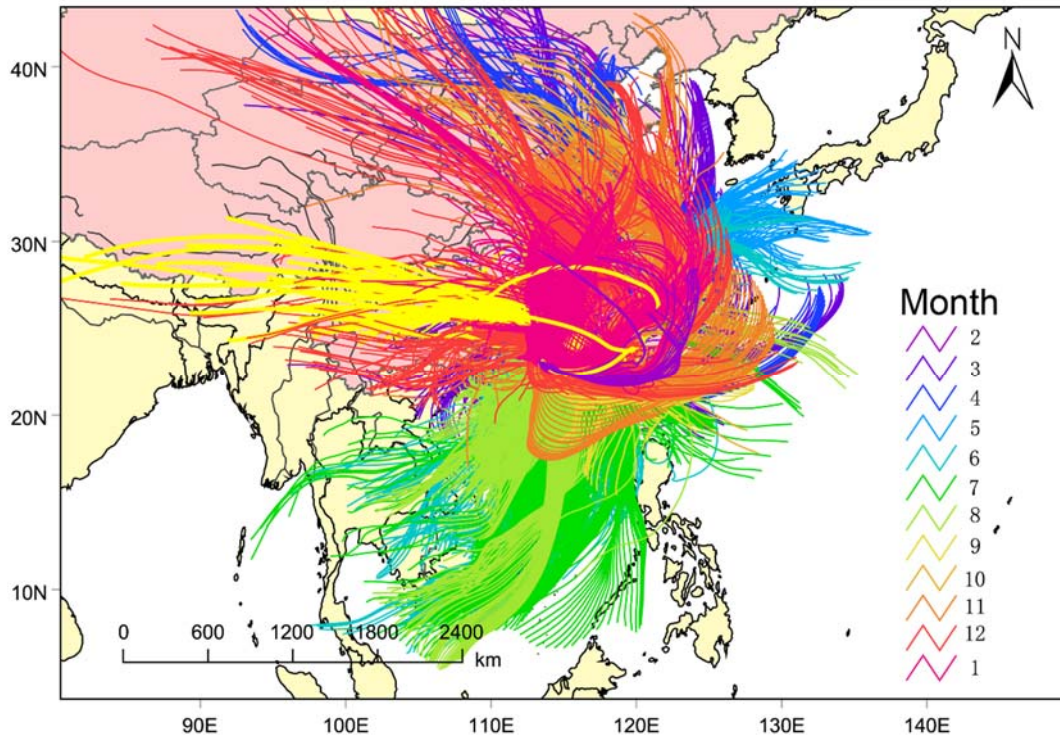


Figure S13. Hourly back trajectories for the past 72 hours calculated using NOAA's HYSPLIT model from Feb 2012 to Jan 2013. The color coding represents different months.

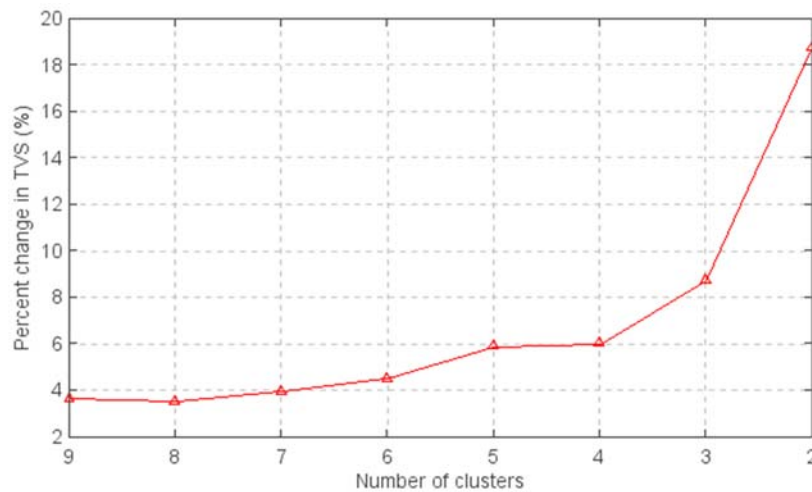


Figure S14. Total spatial variance (TSV) as a function of number of clusters in back trajectories clustering analysis.

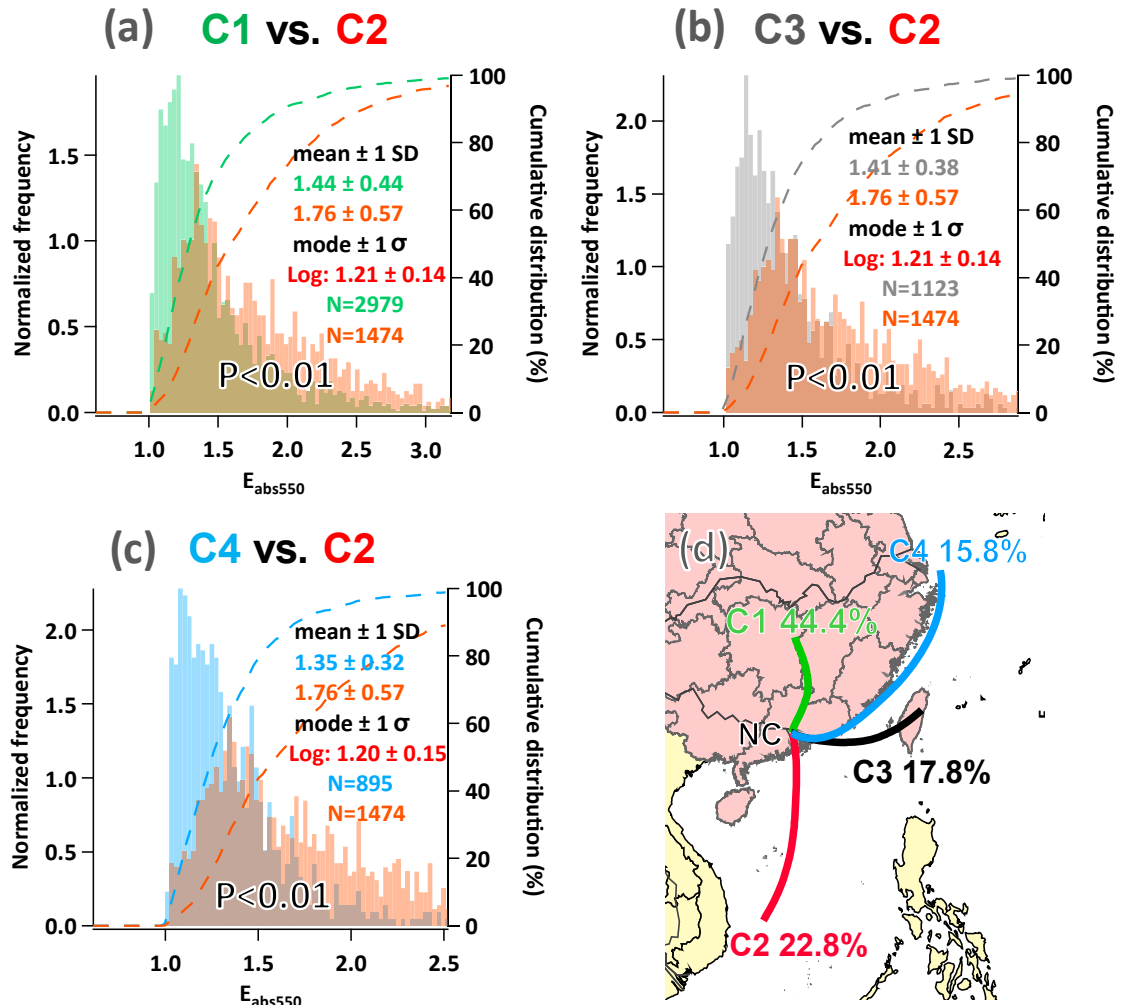
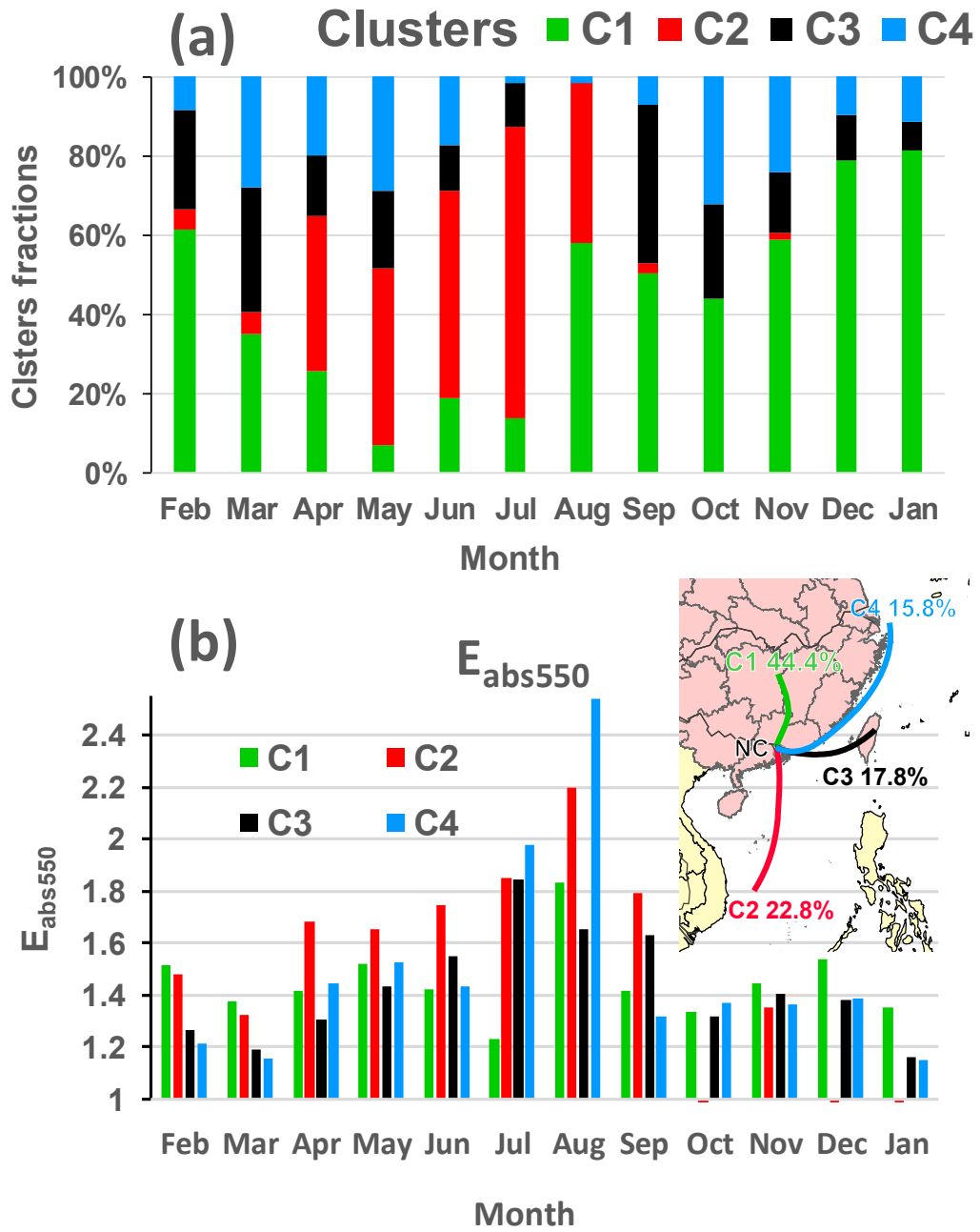


Figure S15. Frequency distributions of E_{abs550} by different air mass clusters. P is calculated by Wilcoxon-Mann-Whitney tests.



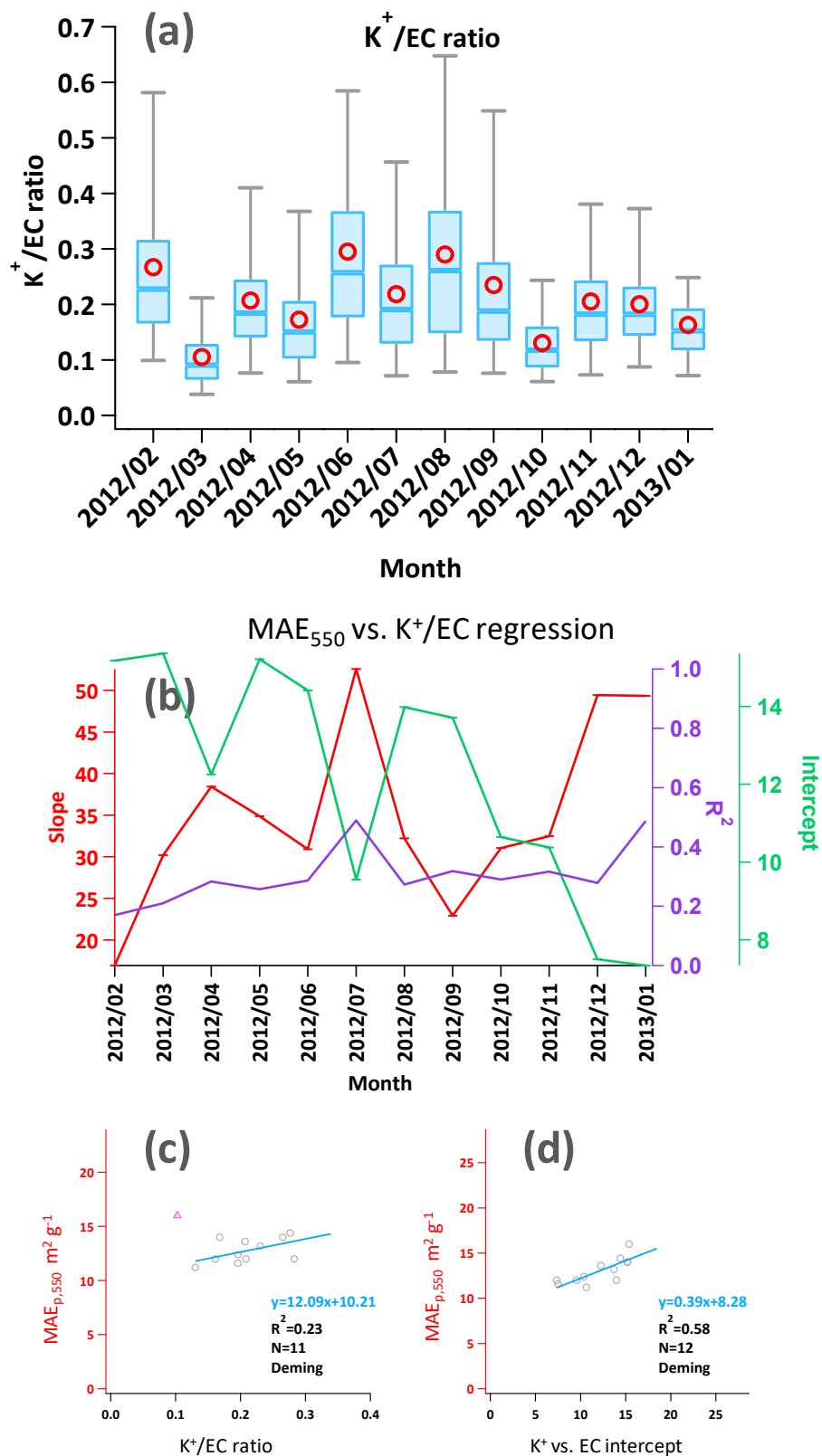


Figure S17. (a) Monthly variations of K⁺/EC ratio from 2012 Feb to 2013 Jan at NC site. (b) Monthly regressions between MAE₅₅₀ and K⁺/EC with slope in red, intercept in green and R² in purple. (c) regressions between monthly MAE_{p,550} and K⁺/EC. (d) regression between monthly MAE_{p,550} and intercepts from (b).

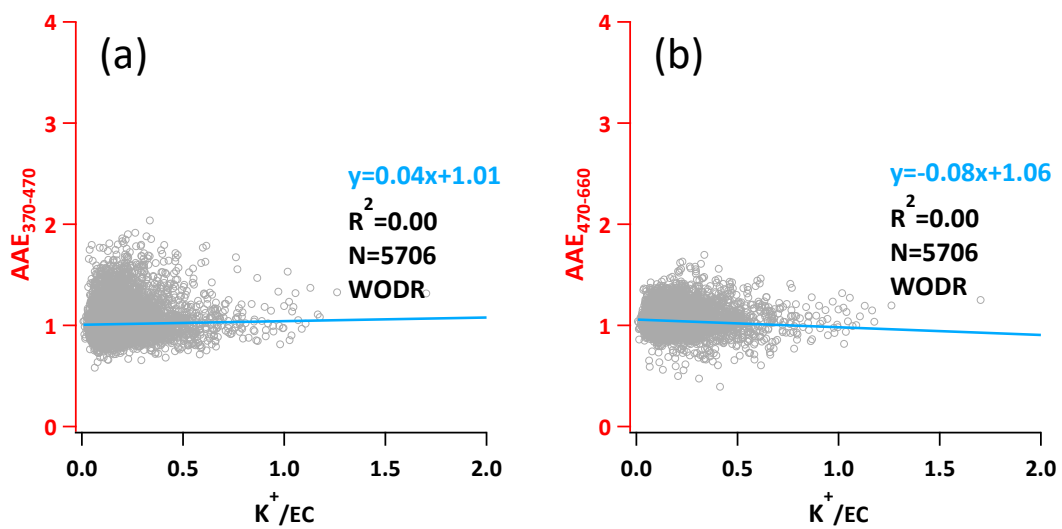


Figure S18. Correlations of AAE with K^+/EC ratio (biomass burning indicator). (a) AAE from 370 – 470 nm. (b) AAE from 470 – 660 nm.

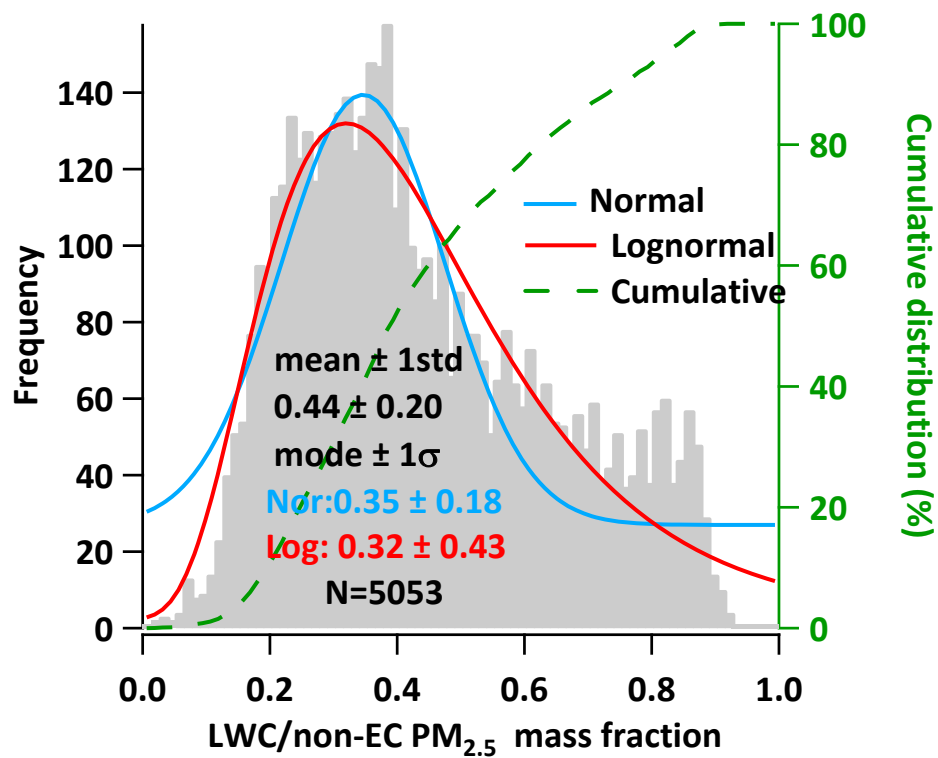


Figure S19. Annual frequency distribution of LWC/non-EC PM_{2.5} mass fraction.

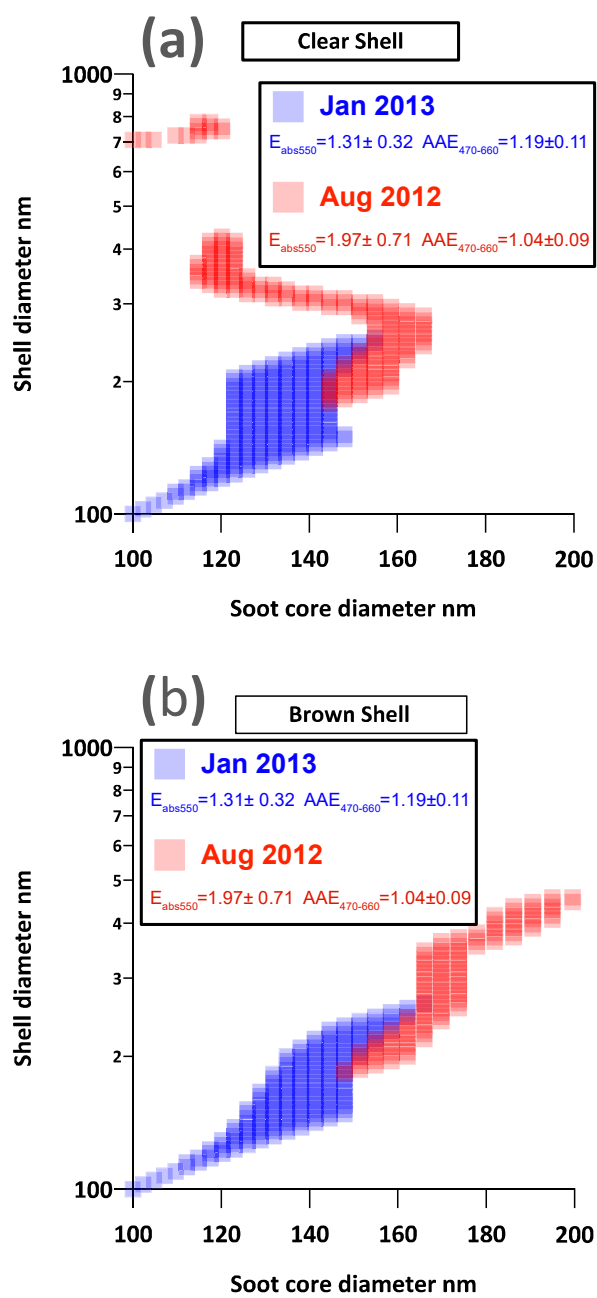


Figure S20. Size range of soot particles constrained by E_{abs} , SSA_{525} and $AAE_{470-660}$ from measurements. (a) Clear shell scenario; (b) Brown shell scenario

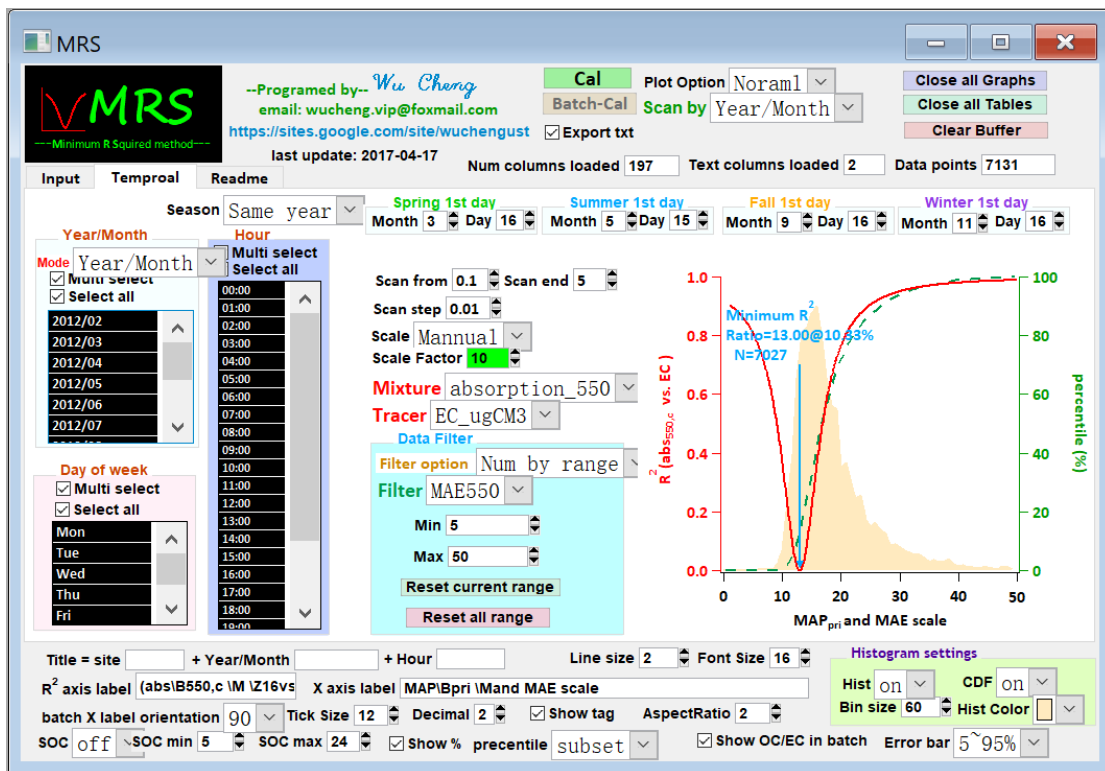
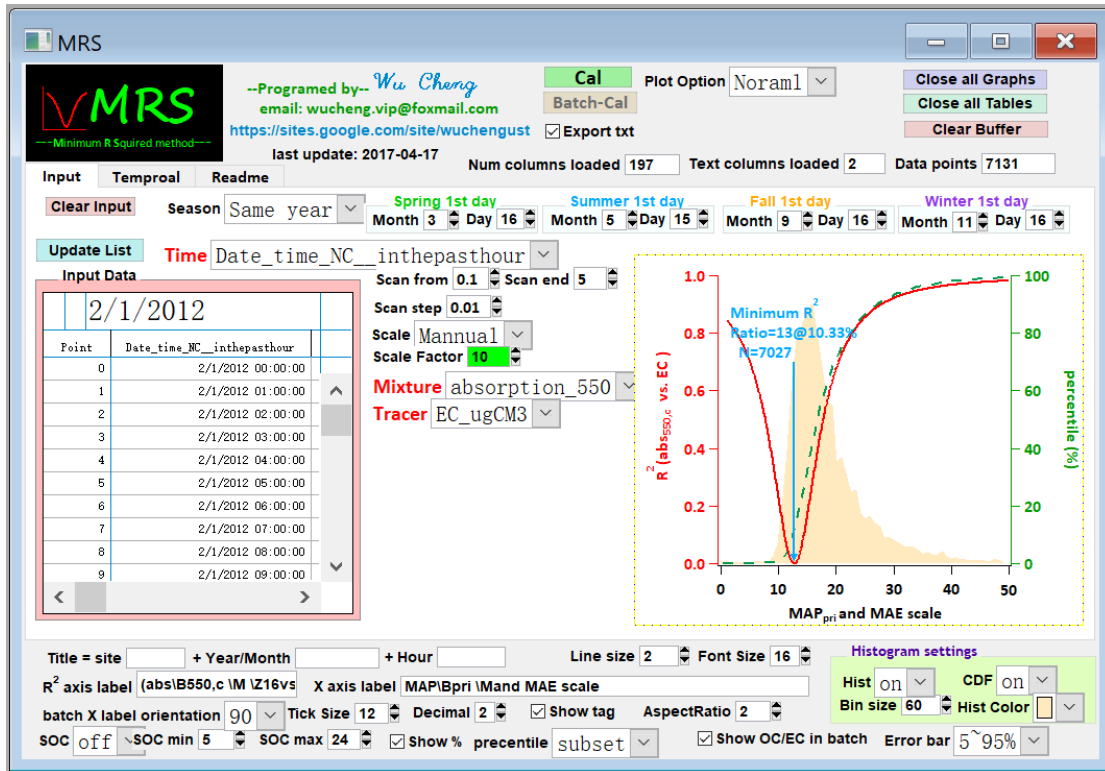


Figure S21. MRS program written in Igr Pro (WaveMetrics, Inc. Lake Oswego, OR, USA). Available from <https://sites.google.com/site/wuchengust>.

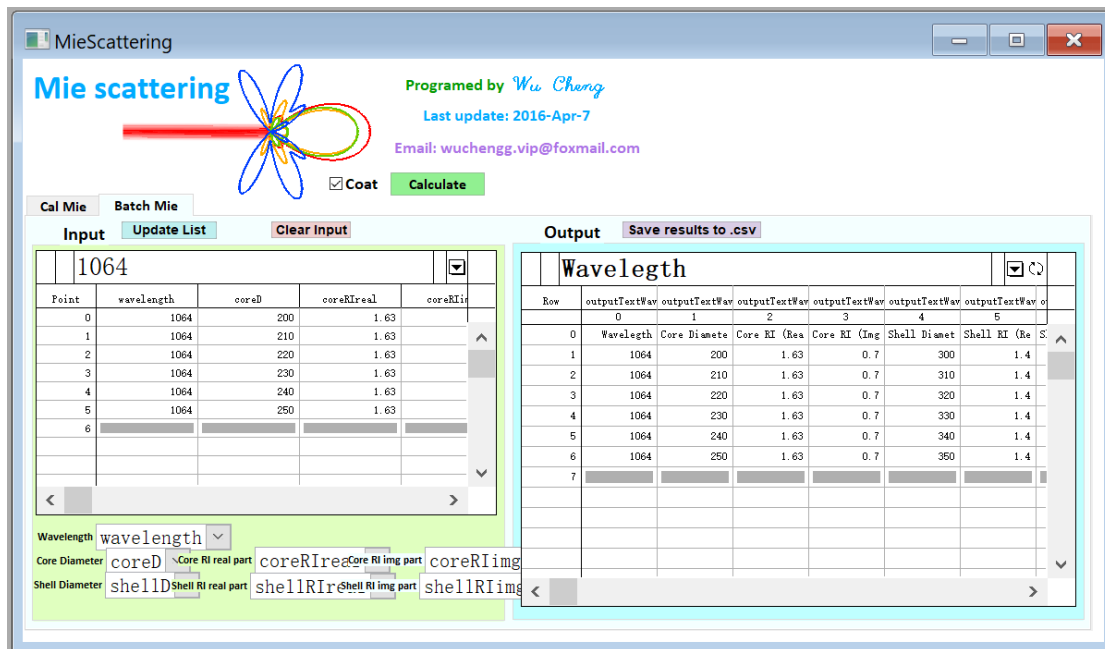
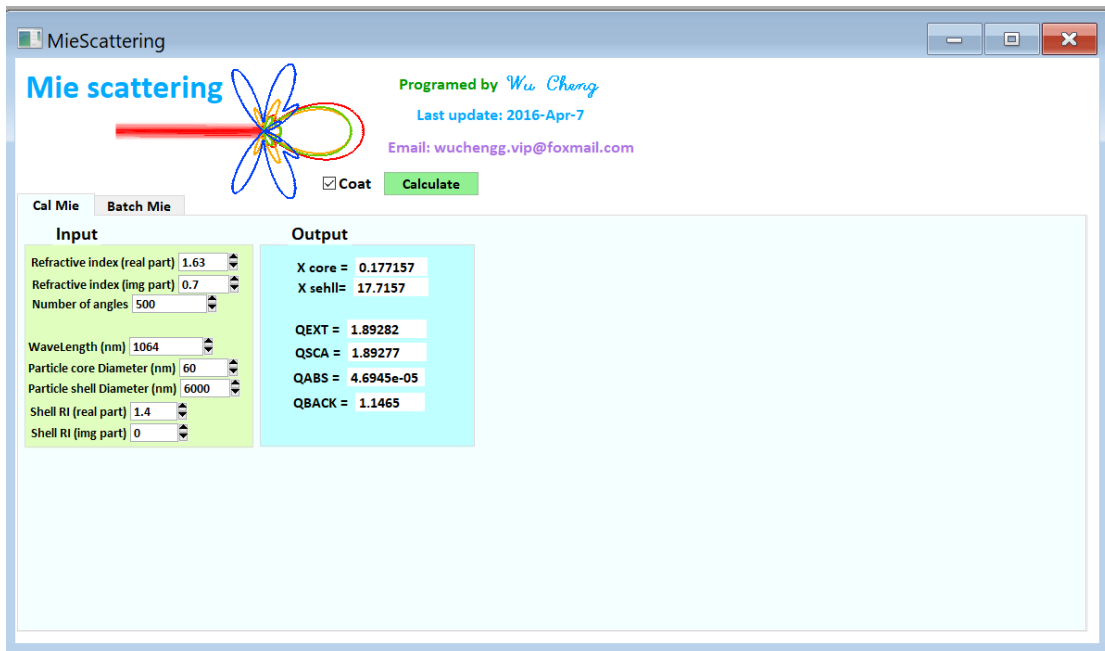


Figure S22. Mie program written in Igro Pro (WaveMetrics, Inc. Lake Oswego, OR, USA). Available from <https://sites.google.com/site/wuchengust>.

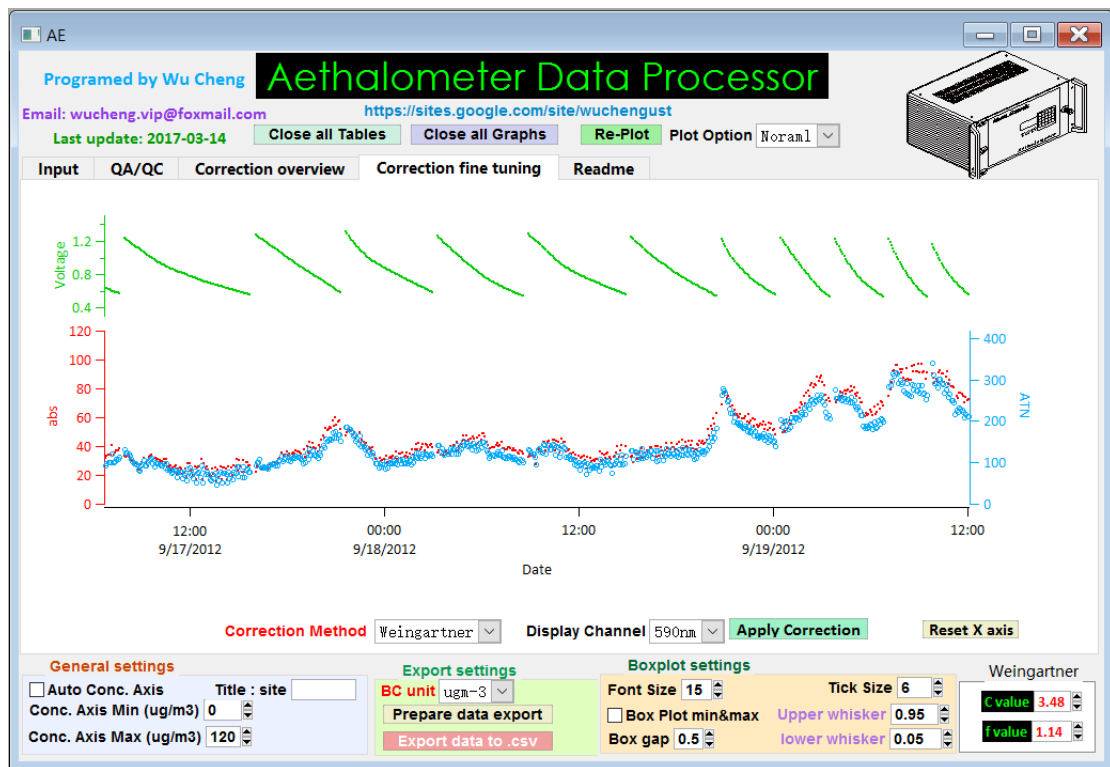
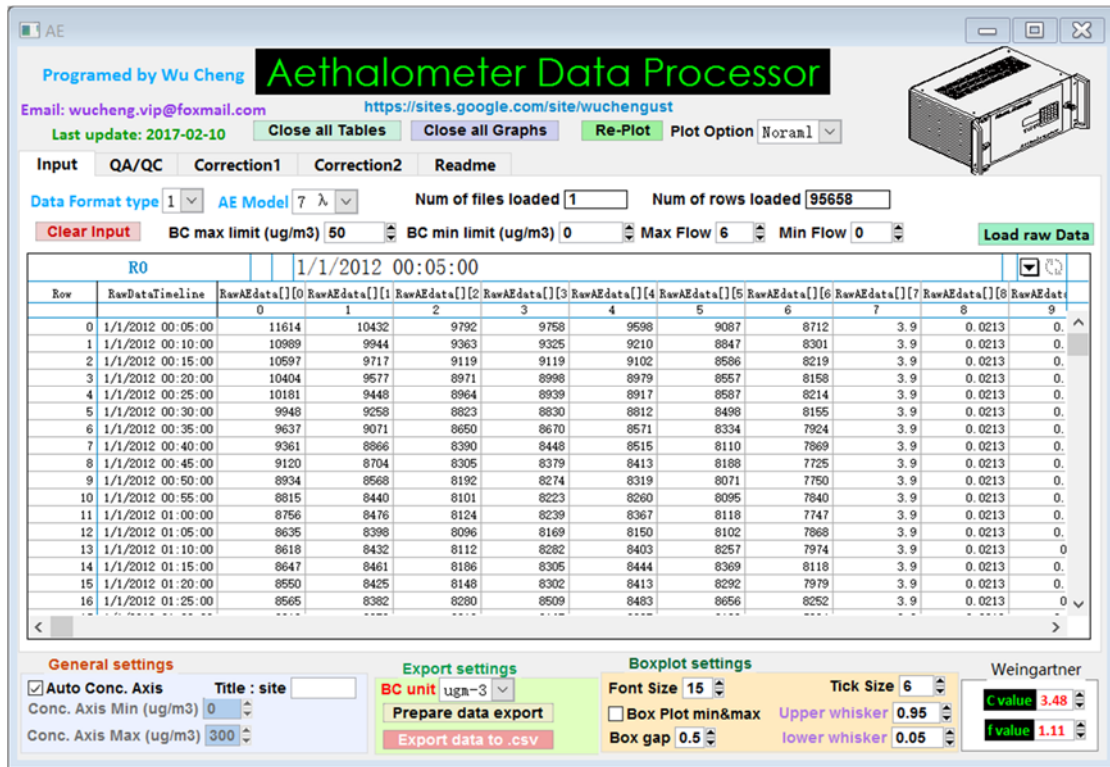


Figure S23. Aethalometer data processing program written in Igro Pro (WaveMetrics, Inc. Lake Oswego, OR, USA). Available from <https://sites.google.com/site/wuchengust>.

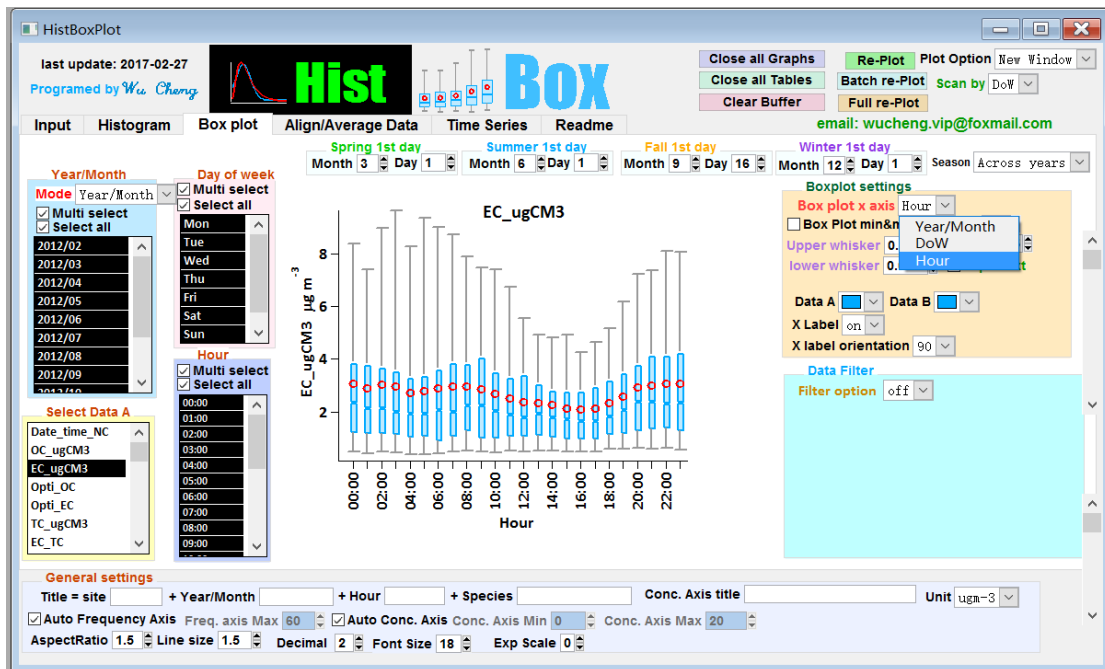
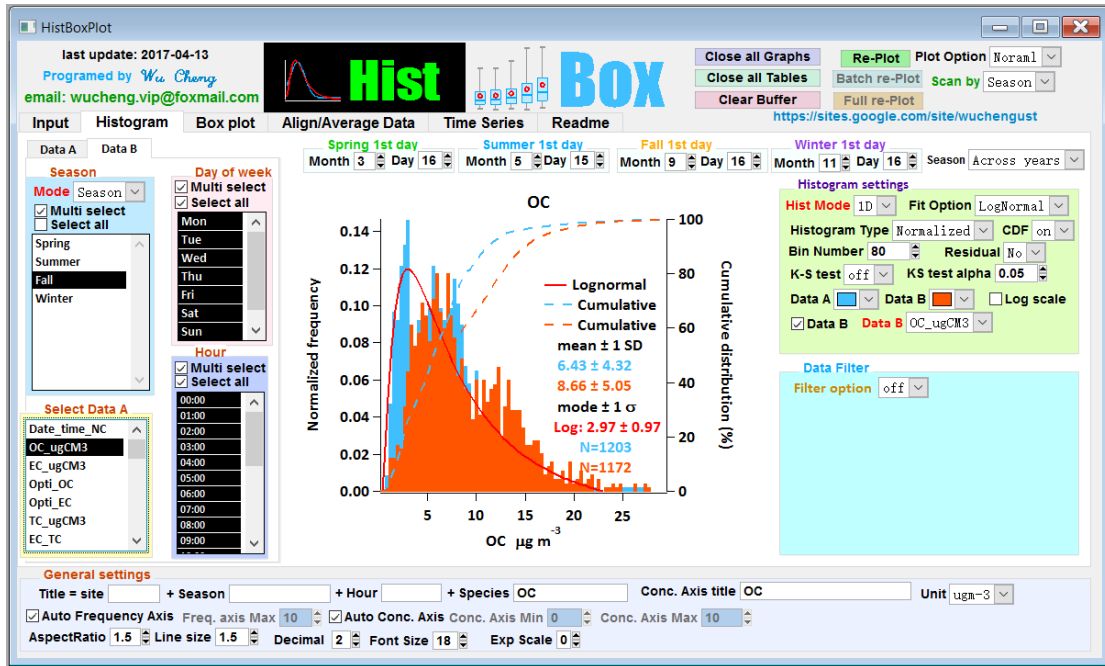


Figure S24. Histbox program written in Igro Pro (WaveMetrics, Inc. Lake Oswego, OR, USA). Available from <https://sites.google.com/site/wuchengust>.

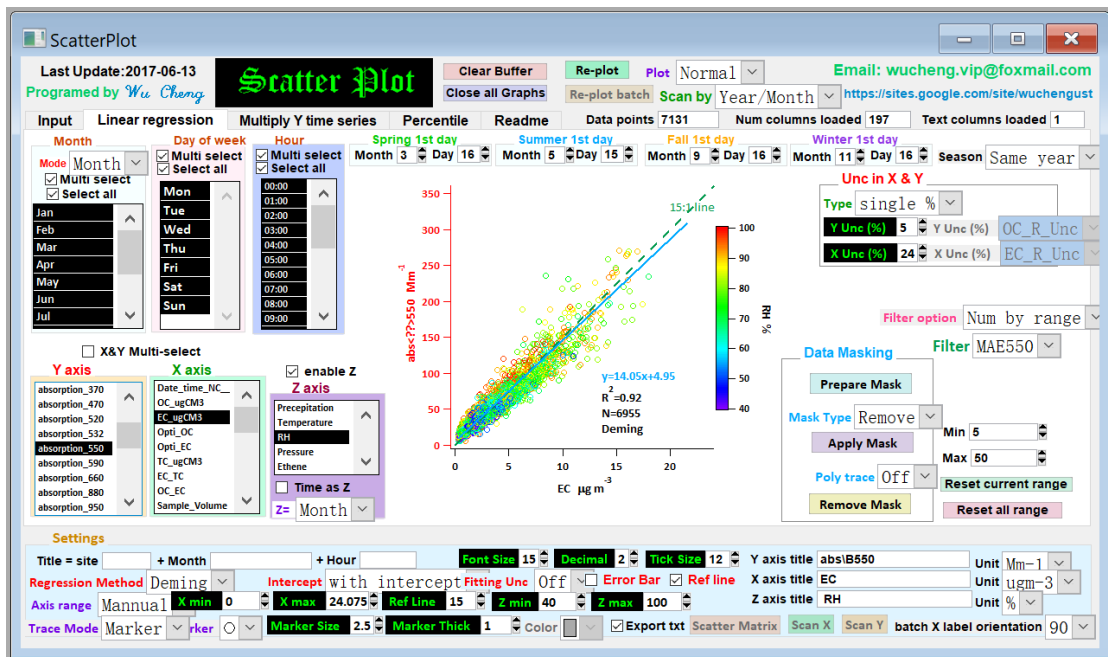
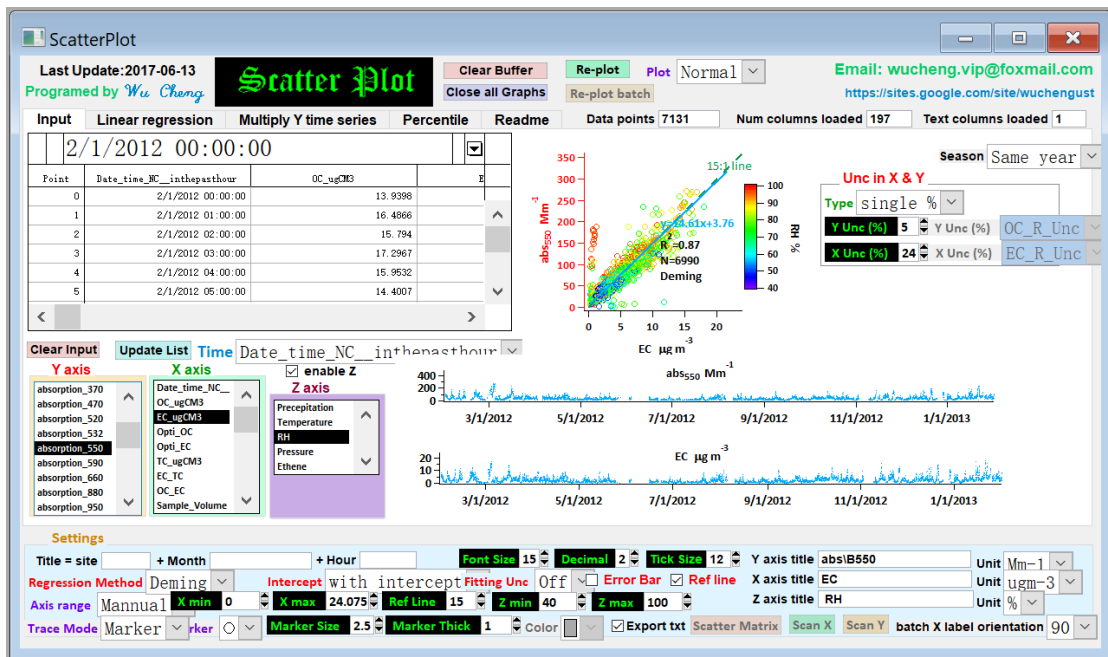


Figure S25. Scatter plot program written in Igro Pro (WaveMetrics, Inc. Lake Oswego, OR, USA). Available from <https://sites.google.com/site/wuchengust>.